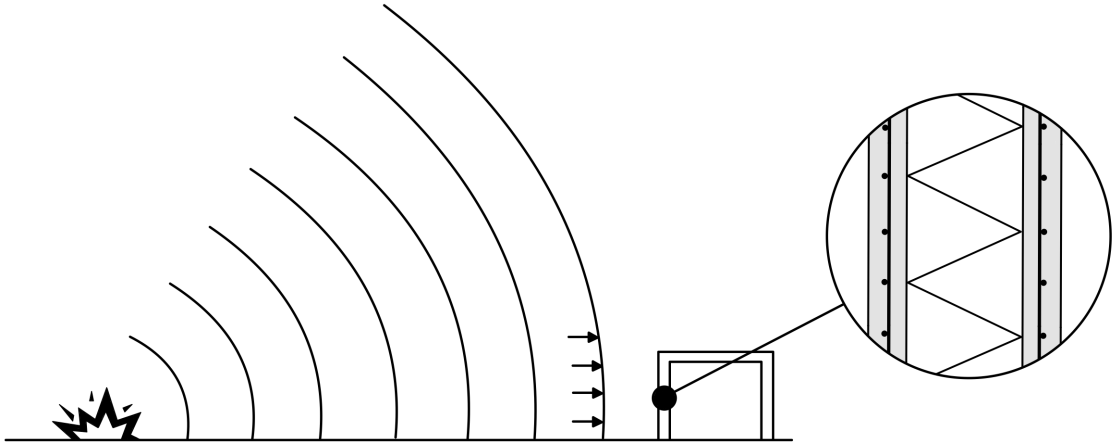

Parametric study of concrete sandwich walls subjected to impulse loading

A study to evaluate the important properties of a blast loaded concrete sandwich wall

Master's thesis in Master's Program Structural Engineering and Building Technology

JAKOB BRINKMANN
ALEXANDER LUNDH

DEPARTMENT OF ARCHITECTURE AND CIVIL ENGINEERING
DIVISION OF STRUCTURAL ENGINEERING

CHALMERS UNIVERSITY OF TECHNOLOGY
Master's thesis ACEX30
Gothenburg, Sweden 2024

Master's thesis ACEX30

Parametric study of concrete sandwich walls subjected to impulse loading

A study to evaluate the important properties of a blast loaded concrete sandwich wall

JAKOB BRINKMANN
ALEXANDER LUNDH

CHALMERS
UNIVERSITY OF TECHNOLOGY

Department of Architecture and Civil Engineering
Division of Structural engineering
Chalmers University of Technology
Gothenburg, Sweden 2024

Parametric study of concrete sandwich walls subjected to impulse loading
A study to evaluate the important properties of a blast loaded concrete sandwich wall

JAKOB BRINKMANN
ALEXANDER LUNDH

Supervisor: Peder Bodén & Erik Johansson, ELU
Examiner: Senior Lecturer Joosef Leppänen, Department of Architecture and Civil Engineering

Department of Architecture and Civil Engineering
Division of Structural engineering
Chalmers University of Technology
SE-412 96 Gothenburg
Telephone +46 31 772 1000

Cover: Illustration of propagating blast wave when the source is at ground level

Department of Architecture and Civil Engineering
Gothenburg, Sweden 2024

Parametric study of concrete sandwich walls subjected to impulse loading
A study to evaluate the important properties of a blast loaded concrete sandwich wall

JAKOB BRINKMANN
ALEXANDER LUNDH
Department of Architecture and Civil Engineering
Division of Structural Engineering
Chalmers University of Technology

Abstract

Energetic materials in densely built environments possess a high risk in the case of ignition. It is therefore of interest to understand the response of surrounding structures subjected to blast loading. One common wall structure is the concrete sandwich wall, composed of two reinforced concrete layers separated by an intermediate layer of insulation. This thesis describes the response of such a wall composition subjected to an impulse load. Additionally, the effect of the intermediate insulation layer is investigated to emphasise its potential energy-absorbing effect.

Different models were developed to describe the behaviour of a concrete sandwich wall: two simplified mass-spring models (SDOF and MDOF) and one 2D Finite element model. The models were compared to highlight their strengths and weaknesses. A parametric study, including material properties and geometry, investigated the favourable effects and potential benefits of the intermediate layer.

All models display a similar response when studying deflections, energy distribution and load transfer. The MDOF and FE model can describe the response of the wall composition in more detail. The parametric study found that the intermediate layer has an energy-absorbing effect, reducing the deflection. The yield stress of the intermediate layer greatly influences the structural response. Various factors, such as wall geometry, load magnitude, and insulation thickness, influence the optimal yield stress.

Utilizing optimized parameters of the intermediate layer can be beneficial when designing walls subjected to severe loading. However, implementation can be difficult since the favourable effect depends on numerous factors. Additionally, some simplifications must be investigated further, such as the effect of shear connectors connecting the outer and inner panels.

Keywords: Concrete sandwich wall, Impulse loading, SDOF, MDOF, Parametric study

Parametrisk studie av sandwich-väggar i betong utsatta för impulsbelastning
En studie för att utvärdera de viktiga egenskaperna hos en explosionsbelastad sandwich-vägg i betong
JAKOB BRINKMANN
ALEXANDER LUNDH
Avdelningen för Konstruktionsteknik
Chalmers Tekniska Högskola

Sammanfattning

Energirika ämnen i tätbebyggda miljöer utgör en stor risk vid potentiell antändning. Det är därför viktigt att ha förståelse för hur omgivande strukturer svarar vid explosionsbelastning. En vanligt förekommande väggkonstruktion är sandwichväggen, som består av två armerade betongskikt och ett mellanliggande isoleringsskikt. Denna rapport beskriver responsen hos en sådan väggkonstruktion när den utsätts för impulsbelastning. Dessutom undersöks effekten av det mellanliggande skiktet för att betona dess energiabsorberande effekt.

Olika modeller har utvecklats för att beskriva beteendet: två förenklade massa-fjäder-modeller (SDOF och MDOF) och en 2D finita-element-modell. Modellerna jämförs för att lyfta fram dess styrkor och svagheter. En parametrisk studie som innefattar materialegenskaper och geometri, undersöker de gynnsamma effekterna samt potentiella fördelar med det mellanliggande skiktet.

Alla modeller ger en liknande respons vid analys av utböjning, energifördelning samt lastöverföring. MDOF- och FE-modellen kan beskriva den strukturella responsen mer detaljerat. Den parametriska studien påvisar att det mellanliggande lagret har en energiabsorberande effekt, vilket märkbart minskar nedböjningen. Det mellanliggande skiktets sträckgräns påverkar den strukturella responsen till hög grad. Olika faktorer såsom geometri, laststorlek samt isoleringstjocklek, påverkar den optimala sträckgränsen.

Att använda optimerade materialparametrar för det mellanliggande skiktet kan vara fördelaktigt vid design av tungt belastade väggar. Det kan däremot vara svårt att implementera då många parametrar påverkar den gynnsamma effekten. En del av de förenklingar som gjorts undersöks med fördel vidare, såsom effekten av skjuv-stag som förbinder betongskikten.

Nyckelord: Sandwichvägg i betong, Impulsbelastning, SDOF, MDOF, Parametrisk studie

Acknowledgements

We would like to thank our supervisors Erik Johansson and Peder Bodén at ELU for their support and guidance. We would also like to extend our gratitude to Morgan Johansson for helping us and sharing his expertise on the subject. Special thanks are due to Joosef Leppänen at Chalmers for his engagement and support throughout the project. Additionally, we want to thank everyone at ELU for welcoming us and sharing their workspace during the spring.

Jakob Brinkmann & Alexander Lundh, Gothenburg, June 2024

Contents

1
Introduction

1.1 Background

Energetic materials in densely built environments possess a high risk with severe consequences in case of ignition. Therefore, it is of interest to investigate the effects of blast loading on surrounding structures. A structure exposed to rapid loading is expected to behave differently compared to a static load case. For instance, a wall designed to have a high load-bearing capacity regarding static loading, may have a different response when exposed to an explosion (Johansson & Laine, 2012b). Consequently, it is of interest to investigate what properties make a building behave in a suitable manner when subjected to an explosion.

One commonly used wall structure is a concrete sandwich wall, with outer layers of concrete and an intermediate layer of insulation. This layer can for instance consist of expanded polystyrene insulation (EPS) or extruded polystyrene insulation (XPS). Precast concrete sandwich wall panels are commonly used in residential and commercial buildings (Anand & Singhal, 2023). The wall composition aims to provide a reduced usage of concrete, high energy performance and fast construction. The insulation layer has a positive effect on energy performance and is expected to influence the structure's response when exposed to transverse impulse loading.

The insulating layer has a damping, energy absorbing effect, hence reducing the response caused by an impulse (Johansson & Laine, 2012b). However, this effect depends on several factors such as the stiffness and thickness of the concrete and insulation layer. The objective of the thesis is to evaluate how the properties of the insulating layer affect the response of a concrete sandwich wall. Additionally, the thesis aims to find optimal properties that provide the most favourable effect when subjected to impulse loading.

1.2 Aim and objective

The thesis aims to describe the response of a concrete sandwich wall subjected to an explosion. In addition, different wall configurations were analysed and compared to find the properties resulting in the most favourable response. The following objectives were treated:

- Find simplified models that describe the dynamic behaviour of a concrete sandwich wall.
- Describe the response of the wall structure using FE-modeling in Abaqus.
- Compare models to highlight differences and find when they are accurate and applicable.
- Conduct a parametric study to evaluate the importance of the material properties of the intermediate layer.

1.3 Limitations

The analysis is limited to studying one strip of a wall section, i.e. not a global structure. Furthermore, the study does not treat normal forces and moments from second order effects. Additionally, only blast waves in the air are considered. Effects from fragment impact and shock waves in the ground are disregarded. The effect of strain rate is not included in the scope of the thesis.

1.4 Method

The work was performed in three phases, where the first phase included information gathering and a literature survey. The survey includes a description of the wall structure, characteristics of an explosion, the material response and a condensed way to model a wall using a mass-spring system.

The gathered information was incorporated and adapted to describe the response of a sandwich panel, using two simplified models with varying complexity. Additionally, the same wall structure was modelled using finite element analysis in Abaqus.

The second phase consisted of a comparison of simplified models and the FE-model. Different wall configurations, subjected to varying load magnitudes, were compared to find differences and similarities between the models. The purpose of the comparison was to evaluate when each model is applicable and able to capture the dynamic response of the structure. The effects of simplifications and varying complexity were visualised and highlighted by comparing displacements, energy distribution and load transfer through the structure.

Lastly, the developed simplified models were utilized to describe the effect of the intermediate insulation layer. Properties such as yield strength and modulus of elasticity were analysed for varying geometries and load magnitudes. The optimized structure was then compared to a non-optimized wall configuration to highlight the significance of a properly designed intermediate layer.

1.5 Social, ethical, and ecological aspects

One aspect to consider regarding blast loaded structures is the safety of people in the vicinity. A wall designed to withstand an explosion should be able to mitigate risks. Not only should the load bearing capacity be fulfilled, but also the risk of fragments from materials should be avoided. It is therefore essential to know the behaviour of the structure when it is subjected to an explosion.

There are few ethical and ecological aspects connected to the work. The findings of the thesis are intended to provide an improved understanding of the behaviour of a structure when subjected to impulse loading. This can help to design and build structures that provide safety even in the case of an explosion.

The thesis will not focus on the ecological benefits of using concrete sandwich walls, but instead on the structural behaviour of the structure. Despite this, an increased knowledge of the structure can help to design efficient structures where the material can be used resourcefully. Hence, reducing the ecological footprint.

2
Theory

This chapter covers the essential theory used throughout the thesis. This includes a description of concrete sandwich walls, basic concepts in dynamics and a detailed description of impulse loads. Additionally, the theory behind analytical models is covered to obtain a model that describes the response during blast loading.

2.1 Precast concrete sandwich wall

One commonly used wall structure is a precast concrete sandwich wall panel, consisting of an inner layer of load bearing reinforced concrete, an intermediate layer of insulation and an outer facade layer of concrete, see Figure 2.1. The insulating layer can vary between materials such as EPS, XPS or similar. The main purpose of this layer is to provide thermal insulation and high thermal performance (Anand & Singhal, 2023). This is especially important for walls separating indoor and outdoor environments. In addition, this layer can have a favourable energy absorbing effect, reducing the response during transverse impulse loading.

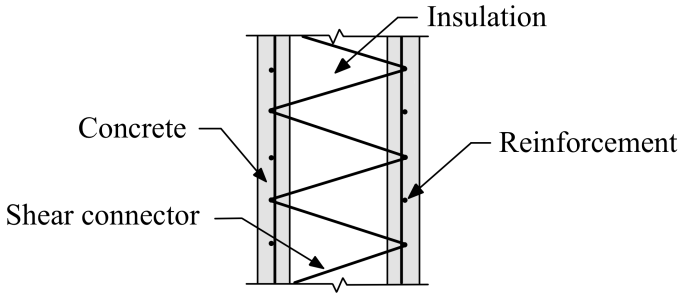

Figure 2.1: Illustration of precast concrete sandwich wall panel with truss-shaped shear connectors. Based on (Huang et al., 2020).

2.1.1 Shear connectors and composite action

The shear connectors between the layers of concrete can be made of different materials and arranged in different configurations (Anand & Singhal, 2023). Shear connectors are commonly made of steel pins, steel bars, fibre-reinforced pins or fibre-reinforced meshes. Fibre-reinforced connections provide good thermal performance since thermal bridges are avoided due to the low conductivity of the material.

Different arrangements of shear connectors will affect the response of the wall structure. Some examples of shear connectors are summarized in Figure 2.2, where the arrangement and material influence the degree of composite action. A truss-like pattern provides a higher composite action compared to straight connecting pins (Tawil et al., 2022).

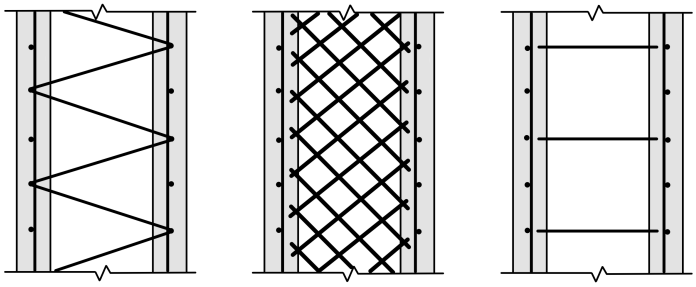

Figure 2.2: Different types of shear connectors. Left: truss-like pattern. Middle: mesh arrangement. Right: pins. Based on (Huang et al., 2020).

The stress distribution of a wall with non-composite and fully composite action is illustrated in Figure 2.3. A wall with a composite cross-section is expected to be stiffer compared to a section where each element acts independently.

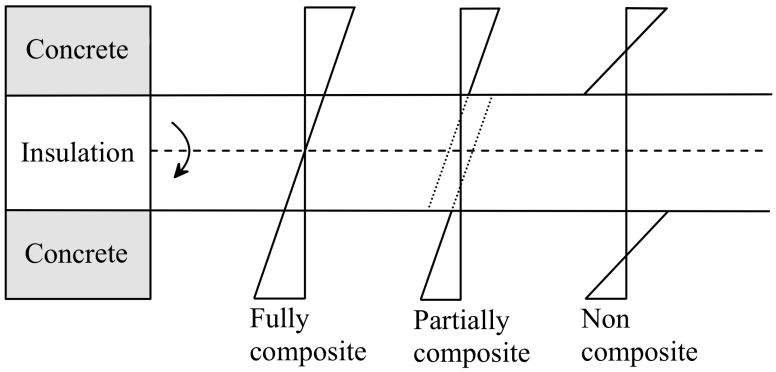

Figure 2.3: Fully composite, partially composite and non-composite action of cross-section subjected to bending moment. Based on (Tawil et al., 2022).

2.2 Basic concepts in dynamics

Basic knowledge of physical concepts such as momentum, impulse and work is essential to understanding the dynamic response of a structure. This section aims to describe these fundamental concepts used in later chapters. The theory is based on material presented in Ekengren et al. (2005).

2.2.1 Momentum

The momentum, p, of an object can be described by its mass, m, and velocity, v, according to Equation 2.1.

$$p = m \cdot v \tag{2.1}$$

Newton's second law relates the external force, F, to the acceleration, a, of a mass. Applying an external force will give rise to an acceleration of the mass, causing a rate of change in momentum according to Equation 2.2.

$$F = m \cdot a = \frac{dp}{dt} \tag{2.2}$$

2.2.2 Impulse

An impulse, I, describes the change in momentum of an object. The impulse can arise from an applied external force and is expressed as in Equation 2.3.

$$I = p - p_0 = \int_{t_0}^{t_1} F(t)\ dt \tag{2.3}$$

The force is expressed as a pressure, P, acting on an area, A. Equation 2.3 is rewritten and impulse density, i, is introduced as the pressure integrated over time, see Equation 2.4.

$$I = A \int_{t_0}^{t_1} P(t)\ dt = A \cdot i \tag{2.4}$$

From the equations, it is evident that the applied load will change the velocity of an object with constant mass. The magnitude and duration of the force determine the size of the impulse.

2.2.3 Kinetic energy

Changing the momentum of an object with constant mass will change its velocity. Hence affecting the kinematic energy, E_k, of the object. The kinematic energy can be described by the mass and velocity of the object, see Equation 2.5.

$$E_k = \frac{m \cdot v^2}{2} \tag{2.5}$$

2.2.4 Work

Work, W, is a concept that relates the energy required to cause a displacement by an acting force. The external work is described according to Equation 2.6. Kinetic energy and work are related through the work-energy theorem, where the work corresponds to the change of kinetic energy of an object.

$$W_{ext} = \int_0^u F(x)\ dx \tag{2.6}$$

2.2.5 Structural dynamic equation

The structural dynamic equation can be used to describe the motion of a mass that is subjected to an external force. The acting force causes internal resistance that can be divided into a static and a dynamic component (Johansson & Laine, 2012b). Newton's second law, Equation 2.2, states that force can be expressed as the ability to accelerate a mass. The resultant of the forces acting on the free body diagram illustrated in Figure 2.4 will therefore cause an acceleration of the mass.

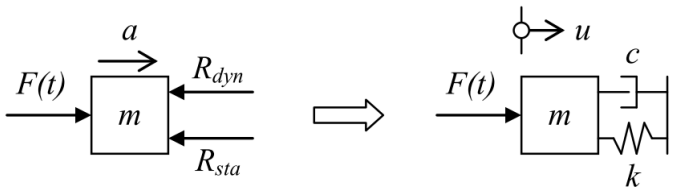

Figure 2.4: Forces acting on an accelerating mass, from (Johansson & Laine, 2012b).

The static resisting force, R_{sta}, can in the elastic range be expressed by the spring stiffness, k, and the displacement, u. While the dynamic resisting force, R_{dyn}, is expressed using the damping, c, and velocity, $\dot{u}$. The structural dynamic equation is expressed in Equation 2.8 and is based on the force balance in Equation 2.7.

$$F(t) - (R_{dyn} + R_{sta}) = m\ddot{u} \tag{2.7}$$

$$m\ddot{u} + c\dot{u} + ku = F(t) \tag{2.8}$$

In the expression, $\ddot{u}$ represents the acceleration as the second derivative of the displacement. A detailed presentation of how the internal response R_{sta} is expressed for an elastic, plastic and elastic-plastic case is presented in Section 2.6.

2.3 Dynamic impulse load

Many possible sources can lead to a blast load in urban areas. For instance transportation of energetic materials, intentional detonations, or accidents in industrial areas (Johansson & Laine, 2012a). There are different ways for the load to reach and affect nearby buildings. The load can travel directly through a blast wave or phenomena such as reflection and diffraction. This means that the geometry and properties of the surroundings play a significant role in the characteristics of the load reaching the building.

2.3.1 Characteristics of a blast wave

In the event of an explosion, the energetic material expands to a larger volume instantaneously, triggering a blast wave that propagates away from the blast source (Mlakar & Barker, 2010). This is a chemical change of state where potential energy is transformed to mechanical work since the surrounding air particles are forced outwards due to the created pressure difference. When the blast wave reaches an object the wave is reflected, increasing applied pressure. An illustration of this phenomenon can be seen in Figure 2.5, where the source of the blast is located at the ground surface. This will result in an increased blast load, compared to an air burst, due to the instant ground reflection. A conservative assumption is to assume full reflection, corresponding to a doubling of the charge weight for a spherical free-propagated blast.

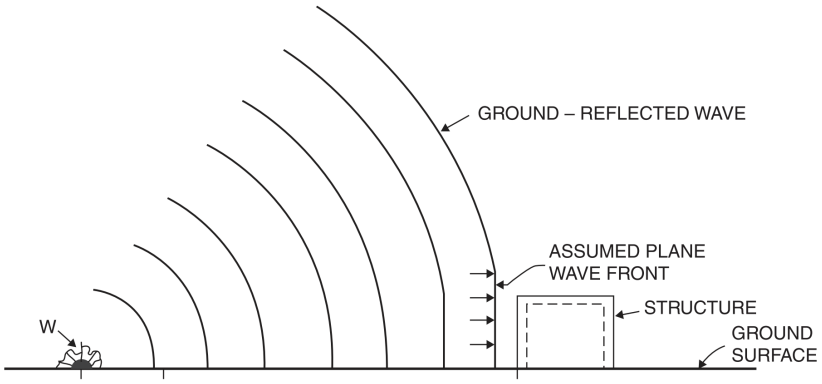

Figure 2.5: Propagating blast wave when the source is at ground level, from (Mlakar & Barker, 2010).

The type of blast wave depends on the amount of overpressure produced and the velocity at which the wave moves forward (Mlakar & Barker, 2010). When the blast wave propagates at supersonic speeds with high pressure, it is characterised as a shock wave. When the velocity instead is below the speed of sound with smaller pressure, it is characterised as a pressure wave. The period between pressure increase and decay varies between the two, where the shock wave displays a more instantaneous and shorter time span.

How the blast wave propagates depends on several factors such as travel distance and amount of energy discharged at the blast source. The pressure caused by an explosion has an initial positive phase with an instant increase in pressure above the ambient pressure, see Figure 2.6. The time until the pressure is back at ambient is a few milliseconds. The positive phase is followed by a negative phase with a longer period and smaller intensity. The area under the curve is defined as the impulse density, this parameter is used to describe the magnitude of the applied load.

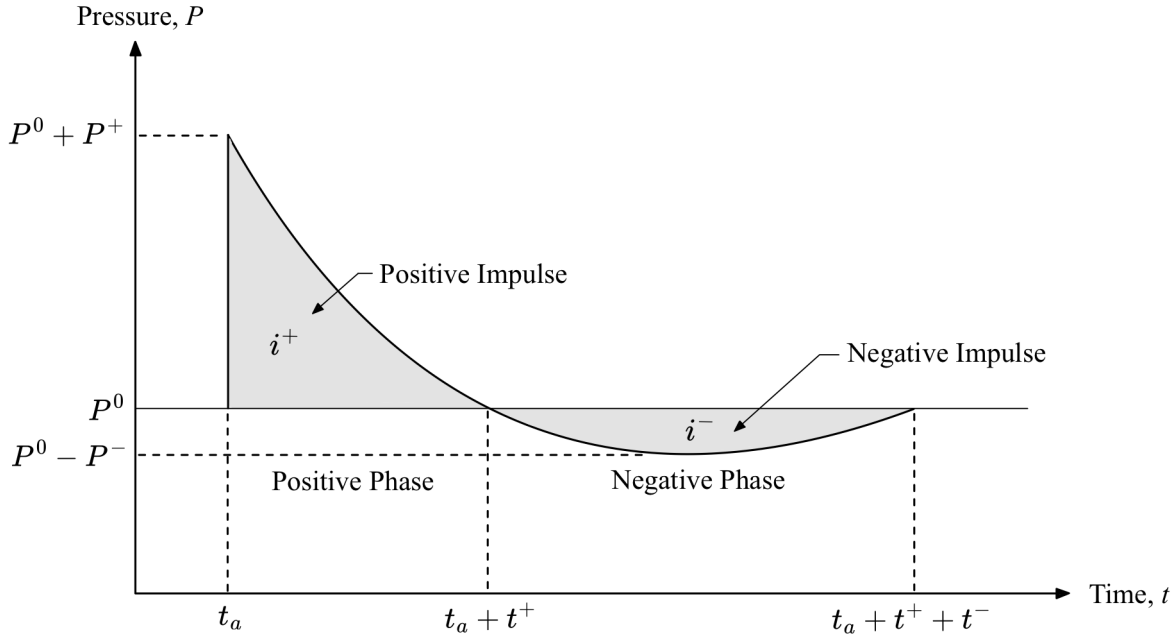

Figure 2.6: How pressure is related to time for a blast wave. Based on (Mlakar & Barker, 2010).

2.3.2 Scaling laws

The characteristics of a blast wave mainly depend on the amount of discharged energy and travel distance. Scaling laws have been developed from experimental observations to compare the effect of different sized explosions with varying distances (Ekengren et al., 2005). They enable data from experimental tests to be used for similar cases regardless of charge weight and distance. One of these is Hopkinson's law, expressed as

$$Z = \frac{R}{W^{1/3}} \tag{2.9}$$

Where Z is defined as the scaled distance, R is the real distance in meters and W is the amount of discharged energy in the explosion, which usually is expressed in kilograms of TNT. Equation 2.9 states that two different explosions with varying distances R are expected to produce an equally large blast wave when the scaled distance is the same (Ekengren et al., 2005). The equation assumes spherical and free propagation in all directions, hence the cubic root of W in the Equation 2.9. If the

explosion instead occurs in an enclosed space such as a tunnel, the blast propagation will be limited to one direction whereas the scaled distance is calculated as

$$Z = \frac{R}{W} \tag{2.10}$$

This means that an explosion occurring in a tunnel has a drastically smaller scaled distance compared to a blast with free spherical propagation. Hence, an explosion in a tunnel is far more serious since it keeps its high magnitude at longer distances. This also means that care must be taken when analysing different sources of explosions, since the surrounding environment has a significant role in blast characteristics.

2.3.3 Simplified impulse curve

It is beneficial to describe a blast load in a simplified manner to facilitate calculations. This can be done by expressing the overpressure by a linear decreasing curve, meaning that the positive impulse density is described by a triangle in the curve relating pressure and time as shown in Figure 2.6 (Johansson & Laine, 2012a). With a given overpressure P^+ and impulse density i^+, an approximate time span can be expressed as in Equation 2.11. The simplified curve is visualized in Figure 2.7.

$$t_\Delta^+ = \frac{2i^+}{P^+} \tag{2.11}$$

The negative phase in Figure 2.6 is neglected due to the relatively low pressure amplitude. The values of P^+, i^+ and t^+ can be determined by empirical expressions, based on the scaled distance Z described in 2.3.2. Worth noting is that the scaled distance is calculated by assuming free propagation in all directions, i.e. no reflections. The empirical expressions make it possible to describe the magnitude of a blast load, for different explosive charges at arbitrary distances.

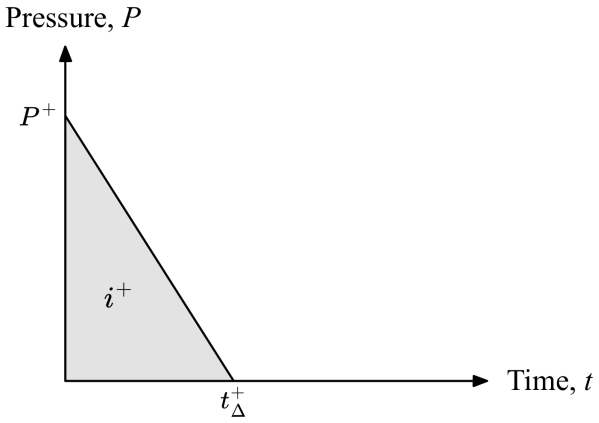

Figure 2.7: Simplified pressure-time curve for impulse load.

2.4 Material response

The response during blast exposure is highly dependent on the structure's material properties. This section describes the response of each material individually and of the composite reinforced concrete. Furthermore, the dissipation of energy in materials and the effects of strain rates are presented.

2.4.1 Concrete

Concrete is characterized by its high compressive strength and low tensile strength. The material is composed of several ingredients such as aggregates and cement paste. Both aggregates and cement paste possess a brittle failure when tested separately (Mehta & Monteiro, 2014). The combined mixture in concrete can however provide a ductile material response in compression, see Figure 2.8. The tensile strength of concrete is low and brittle, plain concrete is therefore often regarded as a brittle material. When combined with reinforcement, the ductility of concrete in compression can be significant and a desired property.

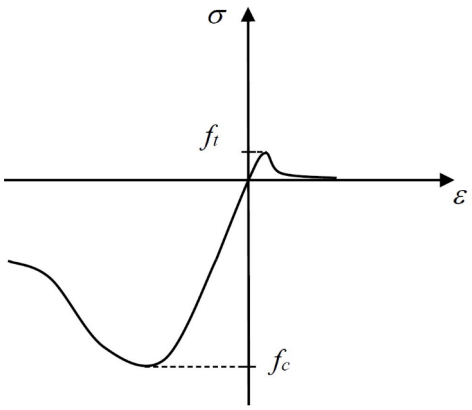

Figure 2.8: Stress-strain relation for concrete, from (Munther & Runebrant, 2018).

2.4.2 Reinforcing steel

Steel is an alloy containing iron, carbon and other elements (Al-Emrani et al., 2019). The iron ore is treated for the material to get the desirable properties. A blast furnace is used to transform the iron ore into pig iron. Pig iron usually contains a high carbon content of 3-5%, making the material brittle and with low workability, the material is therefore treated to reduce the carbon content by oxidation. Different steel properties can be achieved by regulating the oxidation process. Steel has similar properties in tension and compression, a schematic illustration of the material stress-strain-curve is illustrated in Figure 2.9.

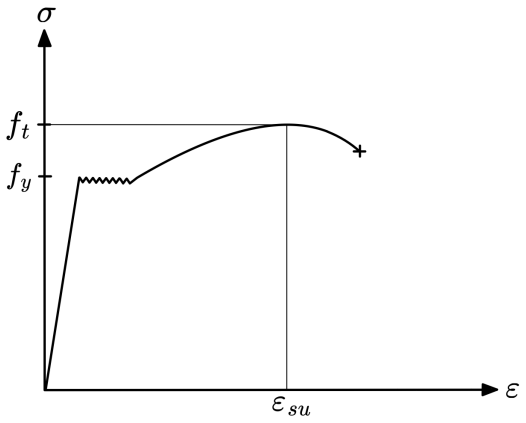

Figure 2.9: Typical stress-strain curve for reinforcing steel.

Steel has an elastic range, followed by yielding, hardening and failure. During yielding, deformations increase for a constant load giving the material a ductile behaviour. The rate at which strain is applied to reinforcing steel affects its tensile properties (International Federation for Structural Concrete, 2013). A faster strain application results in an increased capacity. Impulse loading is typically characterised by a fast strain rate, resulting in an increased yield and ultimate capacity of the steel. However, the modulus of elasticity is not affected by the strain rate.

2.4.3 Reinforced concrete

Reinforced concrete is a composite that utilizes each material's benefits, where the high compressive strength of concrete is combined with the high tensile strength of steel. Since plain concrete is characterised by a brittle behaviour when loaded in tension, the reinforcement properties greatly influence the ductility of the composite (Al-Emrani et al., 2019). The response of reinforced concrete during bending is illustrated in Figure 2.10.

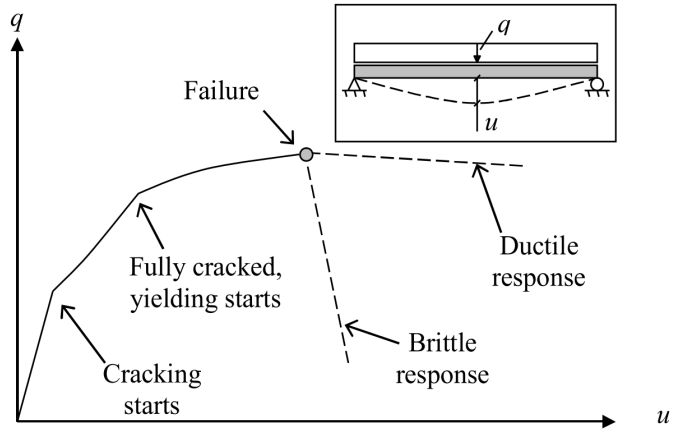

Figure 2.10: Structural behaviour of reinforced concrete, from (Munther & Runebrant, 2018).

During the first part of the response, the entire element is uncracked and characterised by high stiffness (Al-Emrani et al., 2019). The concrete acts in both tension and compression while deformations increase linearly with increasing load.

When the tensile strength of concrete is reached in the most loaded section, a crack will form and start propagating (Al-Emrani et al., 2019). The flexural rigidity drastically decreases in this section and the reinforcement has a significant role in ensuring global equilibrium. The surrounding sections subjected to lower moments are still uncracked. It is noticeable in Figure 2.10 that the global deformations barely is affected. However, a distinct gradient change in response can be observed. As the load is increased, more sections will start to crack and the deformation once again increases linearly.

At some point, the reinforcement will start to yield and the response becomes plastic. The failure of the structure highly depends on the ductility and arrangement of the reinforcement in the section. Failure is reached as the load can no longer be increased.

2.4.4 Polymeric foam insulation

Polymeric foams such as EPS and XPS are lightweight materials that possess a high energy absorbing effect (Rahimidehgolan & Altenhof, 2023). Polymeric foams are divided into several classes depending on their mechanical behaviour. Foams used in structures such as sandwich panels are characterized by either elastic-plastic or elastic-brittle response. The response of foam materials can typically be divided into an elastic part and two plastic regions with different characteristics, see Figure 2.11. The material behaves elastically for small deformations, followed by a plateau region for intermediate strains and a compacting region with increased strength for larger strains.

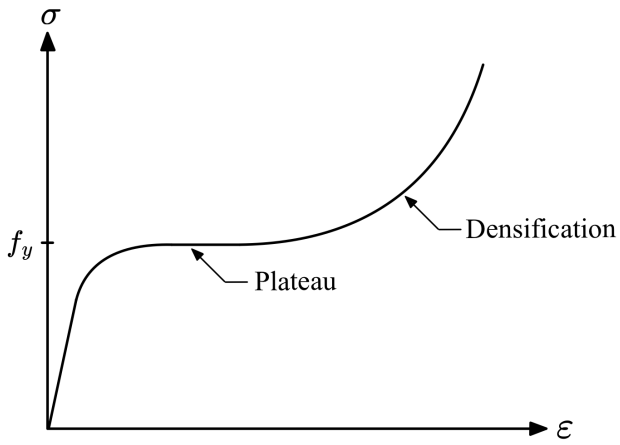

Figure 2.11: Response of polymeric foam material, based on (Rahimidehgolan & Altenhof, 2023).

The densification and rapid increase of strength is initiated as the pores and cell walls of the foam material structure start to cave in (Rahimidehgolan & Altenhof, 2023). The material experiences an increase in strength as the material gets less porous. A typical range for the densification of EPS is approximately 70-90 % (Krundaeva et al., 2016). The engineering strain at which densification occurs depends on material properties, temperature and strain rate.

2.4.5 Dissipation of energy

Energy absorption or dissipation is desired when a structure is exposed to severe loading. When a load is applied to a material, mechanical work is transformed into internal strain energy in the material structure (Runesson & Larsson, n.d.). The total internal strain energy contains stored free energy, ψ, and dissipated energy, D. The stored free energy is recoverable and accumulated in the elastic response of the material. The total internal strain energy, e, can be expressed as in Equation 2.12.

$$e = \int_0^{\varepsilon} \sigma \, d\varepsilon \tag{2.12}$$

The strain energy can be interpreted from the stress-strain curve (Runesson & Larsson, n.d.), as shown in Figure 2.12. The figure illustrates the dissipated energy of material after experiencing plastic deformations from loading and unloading. The dissipated energy is expressed according to Equation 2.13.

$$D = e - \psi \tag{2.13}$$

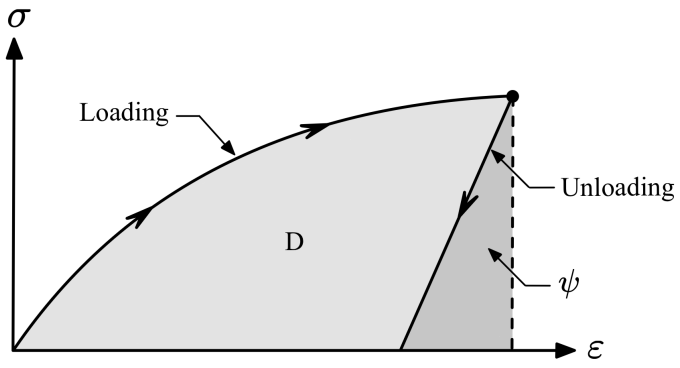

Figure 2.12: Illustration of stored free energy, ψ, and dissipated energy, D, based on (Runesson & Larsson, n.d.)

From Figure 2.12 one can conclude that a material that allows high stresses and large strains can store large amounts of energy. A material with a ductile behaviour, dominated by plastic strains, will allow for dissipation of energy when loaded beyond the elastic range. Ductile materials can therefore be suitable to absorb energy caused by external loads.

2.4.6 Effects of strain rate and triaxial stress

The strain rate between a static and dynamic load case can vary significantly. For a blast load the rate is typically in the ranges of 10^2 to 10^3 s^{-1}, while a static load is around 10^{-5} s^{-1}, see Figure 2.13. Low strain rates with long duration characterize long-term effects such as creep, while blasts are characterized by high strain rates during short periods.

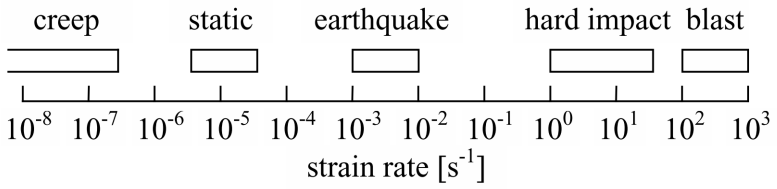

Figure 2.13: Typical strain rates for different load cases, from (Johansson, 2000).

The rate of material straining for concrete and reinforcement influences their mechanical properties (Johansson, 2000). The ratio between dynamic and static strength for concrete and varying strain rates is schematically shown in Figure 2.14, where the transition zone indicates a sudden increase in dynamic strength. Reinforcing steel exhibits a similar increase in strength, without a distinct transition zone. The ratio between the dynamic and static strength is commonly referred to as the Dynamic Increase Factor.

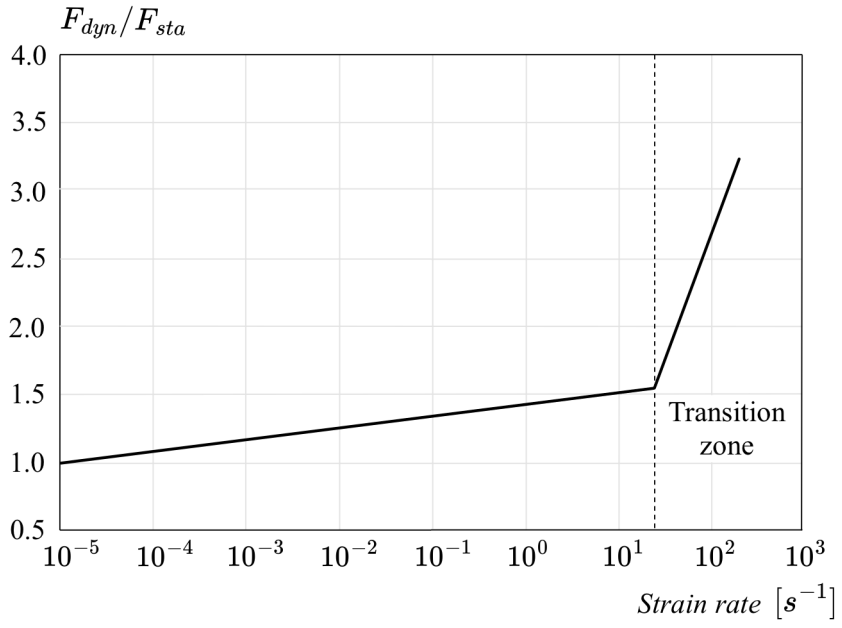

Figure 2.14: Schematic illustration of strain rate effects in concrete, based on (Johansson, 2000).

The increase in concrete material strength after the transition zone is caused by multiple phenomena in the material structure. The observed increase is partly caused by internal confining stresses and effects on crack propagation (Bischoff & Perry,

1991). Figure 2.15 illustrates an object subjected to both an impact and a static compressive load. As the structure is loaded vertically, it expands in the lateral direction for static load. When loaded rapidly, the inertia of the material will cause a delay in lateral movement, resulting in confinement stresses. These stresses increase the material strength since the material is stronger when loaded tri-axially, compared to uni-axially (Sfer et al., 2002).

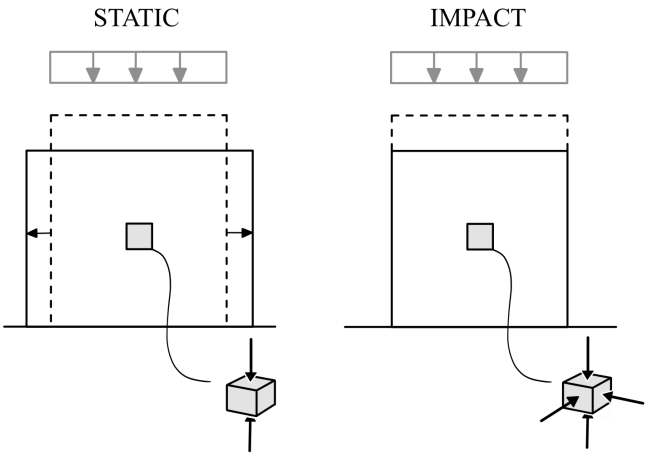

Figure 2.15: Illustration of confining stresses caused by rapid loading.

Concrete reaches its material strength as micro-cracks propagate through the material, this applies in tension and compression (Bischoff & Perry, 1991). As the material is loaded rapidly, the cracks may form through regions with high resistance, for instance by splitting through aggregates in the concrete. Crack propagation for static and impact loading is illustrated in Figure 2.16. The amount of micro-cracks required to reach failure is higher for high strain rates relative to static loading, further increasing the dynamic strength of the material.

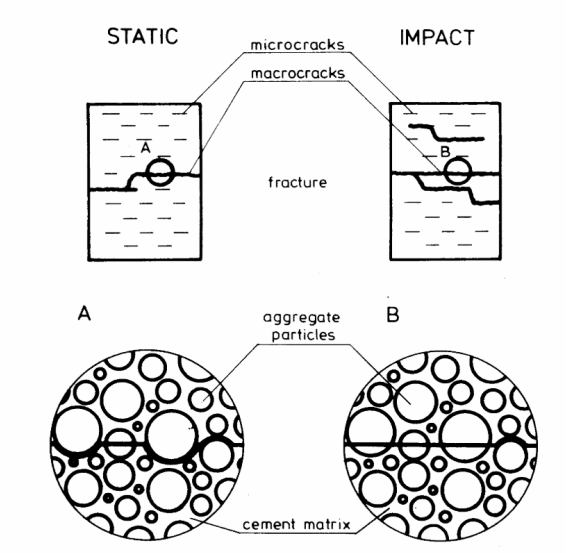

Figure 2.16: Crack propagation of specimen loaded in tension for static and impact loading, from (Zielinski, 1982).

According to Bischoff & Perry (1991) the material experiences an increase in the critical strain for fast straining. This effect combined with the increased dynamic strength implies an increase in the material's capacity to dissipate energy, as described in Section 2.4.5. The energy absorbing capacity in compression for concrete can according to Bischoff & Perry increase up to 40 % compared to the static capacity.

2.5 SDOF systems

There are various ways to describe the response of a structure subjected to an impulse load. Before complex finite element methods were developed, single-degree-of-freedom (SDOF) models were used for the structural design (Smilowitz & Tennant, 2010). An SDOF model can describe the response in a simplified manner by representing the system with a single mass, spring and viscous damper, as depicted in Figure 2.17. The system can be used to describe the displacement u, velocity $\dot{u}$ and acceleration $\ddot{u}$ caused by the external force $F(t)$ acting on the mass m. Motion of the mass will cause internal resisting forces $R(u)$ in the spring together with viscous damping $c(\dot{u})$ (Johansson & Laine, 2012b).

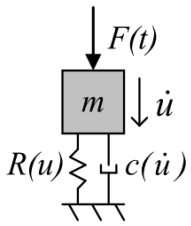

Figure 2.17: Illustration of an SDOF system with mass m, viscous damping $c(\dot{u})$ and resisting force $R(u)$, from (Johansson & Laine, 2012b).

SDOF systems are ideal for fast analyses where a small deviation in accuracy is permitted (Biggs, 1964). Both the acting load and structure must be facilitated to use these models. The load can be idealized as described in Section 2.3.3, while the transformation from global structure to SDOF system is described in the following sections.

2.5.1 Transformation to an SDOF model

The response of a structure is solved by the structural dynamic equation, Equation 2.14. The mass, stiffness and damping properties of the system are reflected in m, k and c.

$$m\ddot{u}(t) + c\dot{u}(t) + ku(t) = F(t) \tag{2.14}$$

where:

k : stiffness of system
m : mass of system
c : damping of system

An SDOF model describes the response of a single point in a system. The mass, stiffness and damping are transformed to describe the characteristics at one specific point, u_s (Johansson & Laine, 2012b). This transformation is illustrated in Figure 2.18.

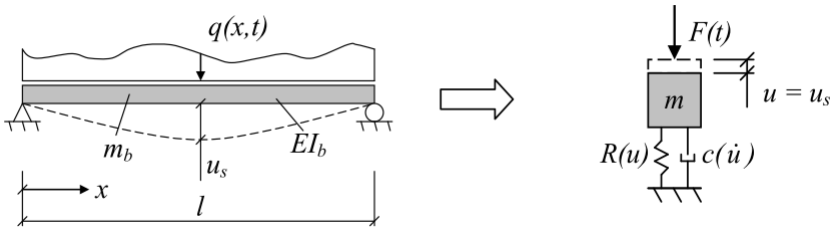

Figure 2.18: Transformation from beam to SDOF system for studied point u_s, from (Johansson & Laine, 2012b).

The mass m_b, sectional constant EI_b and load $q(x,t)$ of the original system are transformed and connected to the mass m, viscous damping $c(\dot{u})$, resisting force $R(u)$ and external force $F(t)$ in the SDOF system, see Figure 2.18. The transformation from wall segment to SDOF system is made with transformation factors, κ (Johansson & Laine, 2012b). The properties of the wall are transformed with its specific transformation factor as shown below.

$$m = \kappa_m m_b \tag{2.15}$$

$$c = \kappa_c c_b \tag{2.16}$$

$$k = \kappa_k k_b \tag{2.17}$$

$$F = \kappa_F F_b \tag{2.18}$$

According to Smilowitz & Tennant (2010) the effects of damping are small compared to the total structural response during impulse loading and can therefore be neglected. The structural dynamic equation is rewritten with the transformation factors in Equation 2.19.

$$\kappa_m m_b \ddot{u}(t) + \kappa_k R_b(u) = \kappa_F F_b(t) \tag{2.19}$$

where:

$$F_b = \int_{x=0}^{x=l} q(x)\,dx = ql$$

$$R_b(u) = k_b u(t)$$

The resistance response, $R_b(u)$, is further described in Section 2.6 for both an elastic- and inelastic case.

2.5.2 Transformation factors

The transformation factors have to be assigned in a correct way for the SDOF system to accurately represent the original system. The transformation factors are assigned to each parameter in the structural dynamic equation, according to Equation 2.19. The factors are governed by the deformed shape of the structure (Biggs, 1964). Therefore, these factors depend on boundary conditions, applied load and stiffness distribution of the element. The deformed shape of the structure also varies when loaded elastically, compared to plastic loading. An illustration of the assumed deformation shapes for a wall element loaded by a uniform transversal load is shown in Figure 2.19.

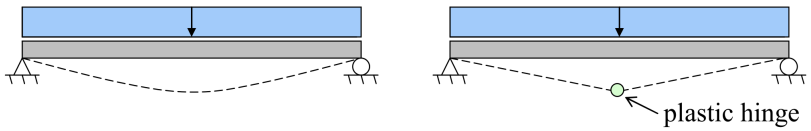

Figure 2.19: Deformed shape of a uniformly loaded wall segment. Left: elastic response, Right: plastic response (Johansson & Laine, 2019).

The deformed shape is essential in the derivation of transformation factors. The work performed by the external force, the kinetic energy and internal work should be adjusted to describe the system accurately. Utilizing the full mass of the structure and combining it with the movement of the described midpoint would overestimate the kinetic energy and the external work, since there is less displacement at the supports compared to the midpoint. Transformation factor κ_k is according to Biggs (1964) equal to κ_F, the structural dynamic equation can therefore be rewritten according to Equation 2.20. A full description and derivation of each transformation factor is described by Johansson & Laine (2012b).

$$\frac{\kappa_m}{\kappa_F} m_b \ddot{u}(t) + R_b(u) = F_b(t) \tag{2.20}$$

The transformation factors for a beam or one-way slab are calculated and tabulated by Biggs (1964) and summarized in Table 2.1. The factor κ_{mF} is introduced and defined as the fraction of κ_m and κ_F.

Table 2.1: κ_m, κ_F and κ_{mF} for plastic and elastic response of a simply supported beam subjected to uniform impulse load.

Transformation factors			
	κ_m	κ_F	κ_{mF}
Elastic response	0.504	0.640	0.787
Plastic response	0.333	0.500	0.667

2.6 Resistance response

The resistance response of an element can have multiple shapes, depending on the geometry and material of the structure (Biggs, 1964). The response can be brittle, ductile, or where the material loses resistance for large deformations, Figure 2.20. A reinforced concrete element in bending has a response similar to curve B. A simplified way to describe the response of such structures is to use a bi-linear function, where the response is divided into an elastic and a plastic range.

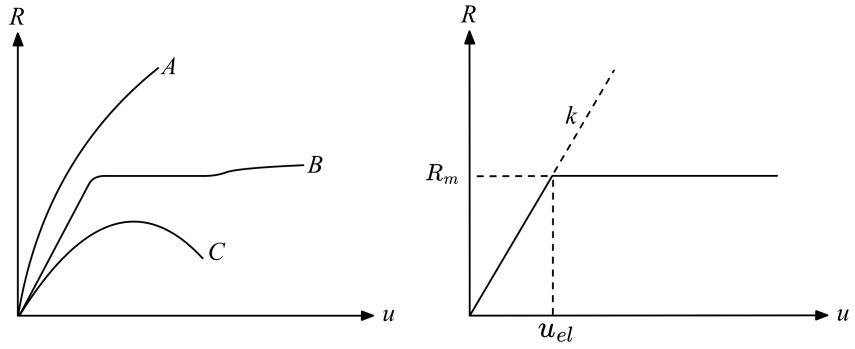

Figure 2.20: *Left:* Structure with, A: brittle response, B: ductile response, C: loss of strength for large deformations, *Right :* simplified bi-linear response. Based on (Biggs, 1964).

According to Biggs (1964), "*The resistance of an element is the internal force tending to restore the element to its unloaded static position*" (p. 203). For an elastic behaviour, the full displacement can be restored, while a plastic response will result in remaining displacements.

The resistance response can be derived by utilizing the condition of energy balance (Johansson & Laine, 2012b). The energy balance requires equilibrium between the work performed by the applied external force and the work performed by the internal resisting forces, Equation 2.21. The applied load can be expressed by the concepts of momentum, impulse and work described in Section 2.2, yielding the expression in Equation 2.22. I_k is the characteristic impulse for an ideal impulse load, which is a load with infinitely high pressure and infinitesimal duration. For loads that resemble

an ideal impulse, the expressions in Equation 2.22 can be utilized to describe the external work.

$$W_{ext} = W_{int} \tag{2.21}$$

$$W_{ext} = E_k = \frac{I_k^2}{2m} \tag{2.22}$$

The internal work, W_{int}, caused by the resisting force is derived for an elastic, plastic and elastic-plastic case in the following sections. The derivation is based on the description given by Johansson & Laine (2012b).

2.6.1 Elastic response

For an elastic case the resistance, R, is linearly dependent on the stiffness, k, as illustrated in Figure 2.21 and described by Equation 2.23.

$$R(u) = ku \tag{2.23}$$

The internal work performed by the resisting force can be derived using Equation 2.23. The internal work is equal to the integral of the response with respect to the displacement, illustrated as the area below the graph in Figure 2.21 and expressed in Equation 2.24.

$$W_{int} = \int_0^{u_{el}} R(u)\, du = \frac{ku^2}{2} \tag{2.24}$$

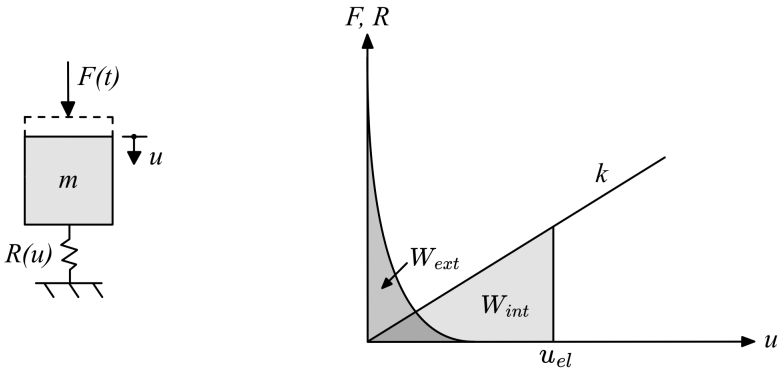

Figure 2.21: Internal and external work in the elastic case, based on (Johansson & Laine, 2012b).

The condition of energy balance is used to express the elastic displacement required for the internal work to be equal to the applied external work, see Equation 2.25.

$$\frac{I_k^2}{2m} = \frac{ku^2}{2} \rightarrow u_{el} = \frac{I_k}{m}\sqrt{\frac{m}{k}} \tag{2.25}$$

2.6.2 Plastic response

In the case of a perfectly plastic response, the resisting force is not dependent on the displacement (Johansson & Laine, 2012b). Instead, it is constant as illustrated in Figure 2.22. The internal work performed by the resisting force can be expressed using Equation 2.26.

$$W_{int} = R_m u \tag{2.26}$$

The plastic displacement required to reach an equilibrium between internal and external work is found by combining Equation 2.22 and 2.26.

$$\frac{I_k^2}{2m} = R_m u \rightarrow u_{pl} = \frac{I_k^2}{2mR_m} \tag{2.27}$$

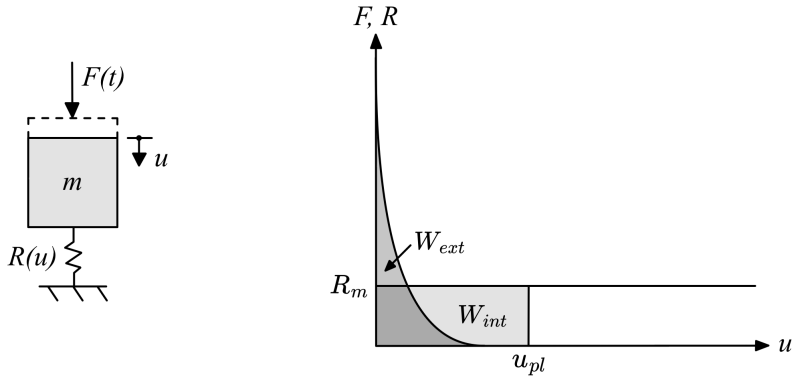

Figure 2.22: Internal and external work in the plastic case, based on (Johansson & Laine, 2012b).

2.6.3 Elastic-plastic response

The elastic-plastic response consists of an elastic part followed by a plastic part. The transition from elastic to plastic response occurs as the displacement exceeds the elastic limit, u_{el} (Johansson & Laine, 2012b). The elastic limit represents the displacement required to reach the maximum resistance, R_m, as presented in Equation 2.28.

$$u_{el} = \frac{R_m}{k} \tag{2.28}$$

The resistance response can be described by Equation 2.29.

$$R(u) = \begin{cases} ku & \text{if } u \leq u_{el} \\ R_m & \text{if } u > u_{el} \end{cases} \tag{2.29}$$

Energy balance must be fulfilled similarly to the elastic and plastic case. The internal work can be expressed using the total deformation, u_{tot}, and the elastic limit according to Equation 2.30.

$$W_{int} = R_m(u_{tot} - \frac{u_{el}}{2}) \tag{2.30}$$

The required total deformation is found using Equation 2.22 and 2.30.

$$\frac{I_k^2}{2m} = R_m(u_{tot} - \frac{u_{el}}{2}) \rightarrow u_{tot} = \frac{I_k^2}{2mR_m} + \frac{u_{el}}{2} \tag{2.31}$$

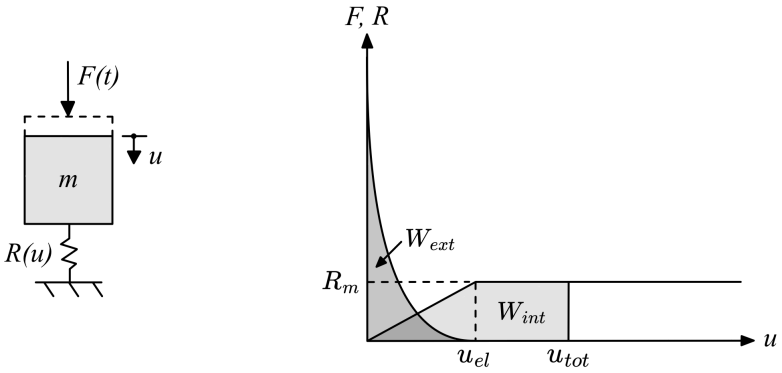

Figure 2.23: Internal and external work in the elastic-plastic case, based on (Johansson & Laine, 2012b).

2.6.4 Implementing response functions

The stiffness k_b and maximum resistance R_m of the system have to be determined to describe the response function of the structure. The case of a uniformly loaded, simply supported beam element is described in the following sections. Expressions for other boundary conditions and load cases are tabulated by Biggs (1964).

2.6.4.1 Elastic Stiffness, k_b

For a beam element in the elastic range, it is possible to express the resistance response using the stiffness k_b, which is derived using Bernoulli's beam theory combined with Hooke's law. The deflection of a beam with constant stiffness is derived from Equation 2.32.

$$EI_b\frac{d^4u}{dx^4} = q(x) \tag{2.32}$$

For a simply supported beam subjected to a uniform load, the mid displacement δ can be expressed according to Equation 2.33.

$$u = \frac{5ql^4}{384EI_b} \tag{2.33}$$

Utilizing Equation 2.33, it is possible to link the deflection to the total applied load using Hooke's law. The stiffness k_b, can be derived as:

$$k_b = F_b/u = \frac{384EI_b}{5l^3} \tag{2.34}$$

where:

F_b : total applied load according to Equation 2.19

u : displacement according to Equation 2.33

The stiffness is used in Equation 2.35 to express the resistance response for the elastic range.

$$R(u) = \kappa_k k_b u \tag{2.35}$$

2.6.4.2 Maximum resistance, R_m

The resisting force, R_m, corresponds to the load applied to cause yielding of the cross-section. In the case of a simply supported beam subjected to uniform load, R_m is calculated according to Equation 2.36.

$$R_m = ql = \frac{8M_{Rd}}{l} \tag{2.36}$$

Where q is calculated from the moment capacity of the beam section, M_{Rd}.

$$q = \frac{8M_{Rd}}{l^2} \tag{2.37}$$

2.6.4.3 Secant stiffness

One can utilise secant stiffness to describe loading and unloading during a nonlinear response. The secant stiffness relates the displacement to the nonlinear resistance, as illustrated in Figure 2.24 (Johansson & Laine, 2012b). The method can be used in the numerical solution method presented in Section 2.7 and is implemented using the resistance response and displacement from the previous loading step, see Equation 2.38. The stiffness is continuously updated using the information from previous time steps in the calculation procedure.

$$k_t = \frac{R_{t-\Delta t}}{u_{t-\Delta t}} \tag{2.38}$$

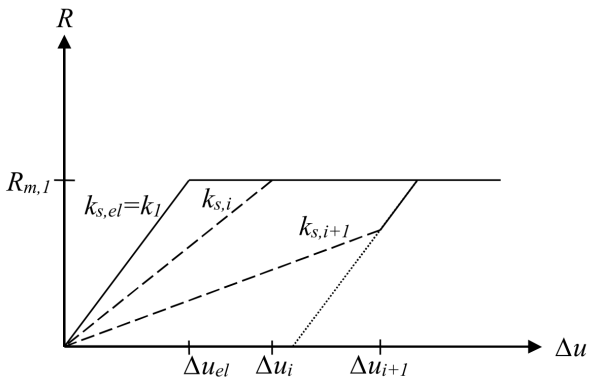

Figure 2.24: Secant stiffness relating resisting force and displacement (Munther & Runebrant, 2018).

2.7 Numerical solution methods

Using an analytical approach to solve the structural dynamic equation is not viable when the response is nonlinear and applied force varies in time (Cimellaro & Marasco, 2018). In such cases, numerical time-stepping methods can be used in analysis involving dynamic loading.

A numerical solution method that requires information from previous time steps to obtain equilibrium, is called an *explicit* solution method (Cimellaro & Marasco, 2018). If solely information from the current time step is needed, the numerical method is called *implicit*. With a discretized time domain, it is essential to ensure a stable and accurate solution that converges. Stable implies that errors do not increase with time, accuracy evaluates how close the solution is to the real solution and convergence implies that the error tends to zero as the number of time steps are increased.

Two examples of closely related numerical solution methods are the *Central Difference Method* and *Newmark's* method. The former is an explicit method while the latter is implicit. Both are suitable for describing the nonlinear response of a system, whereas Newmark's method is used in this thesis. A short presentation of the key takeaways of Newmark's method is presented in the following text. The calculations are presented for an SDOF system but can be implemented for systems with multiple degrees of freedom, by expanding the problem into multiple equations. The stiffness, mass and damping of the system are then expressed in matrices and the response is summarized in vectors as described in Section 2.8.

2.7.1 Newmark's method

Newmark's method utilizes the known acceleration, velocity and displacement to estimate the motion of the system at the next time step. The current time step is denoted with subscript, t, and the calculated next step is denoted $t+\Delta t$. According to Abrahamsson (2019), Equations 2.39 to 2.41 are used to describe the motion of the system. The solution method can be used to solve a system with one or multiple degrees of freedom by inserting scalars to m, k and c or matrices M, C and K respectively. Nonlinear structural behaviour can be implemented in the model by updating the stiffness. This is done by using secant stiffness as described in Section 2.6.4.3. The stiffness is recalculated each time step to account for the non-linearity.

$$\ddot{u}_{t+\Delta t} = \bar{M}^{-1}[F_{t+\Delta t} - c[\dot{u}_t + (1-\gamma)\Delta t\ddot{u}_t] - k[u_t + \Delta t\dot{u}_t + (0.5-\beta)\Delta t^2\ddot{u}_t]] \quad (2.39)$$

$$\dot{u}_{t+\Delta t} = \dot{u}_t + [(1-\gamma)\ddot{u}_t + \gamma\ddot{u}_{t+\Delta t}]\,\Delta t \quad (2.40)$$

$$u_{t+\Delta t} = u_t + \dot{u}_t\Delta t + [(0.5-\beta)\ddot{u}_t + \beta\ddot{u}_{t+\Delta t}]\,\Delta t^2 \quad (2.41)$$

where:

$$\bar{M}^{-1} = \left[m + \gamma\Delta t c + \beta\Delta t^2 k\right]^{-1} \tag{2.42}$$

β and γ are parameters that affect the stability and accuracy of the integration. According to Abrahamsson (2019), $\beta = 0.25$ and $\gamma = 0.5$ is recommended since it results in a stable integration. Biggs (1964) suggests that β should be chosen between 1/6 to 1/4. To ensure a converging solution, Δt should be chosen between 1/6 to 1/5 of the shortest natural period. The natural period is calculated according to Equation 2.43.

$$T = \frac{2\pi}{\omega_0} = 2\pi\sqrt{m/k} \tag{2.43}$$

For a system at rest, without initial movement, the initial conditions are as follows.

$$u_0 = 0 \tag{2.44}$$

$$\dot{u}_0 = 0 \tag{2.45}$$

$$\ddot{u}_0 = \bar{M}^{-1}[F_0] \tag{2.46}$$

By utilizing the equations, one can calculate the acceleration, velocity and displacement in a step-wise manner. The response can hence be calculated for a given period.

2.8 MDOF systems

A multi-degree-of-freedom (MDOF) system can capture the response of multiple points in a system (Biggs, 1964). An example of a simple MDOF system, i.e. a 2DOF system, is illustrated in Figure 2.25. In this example, mass m_1 is connected to mass m_2 through spring k_1. The MDOF system can hence capture the interaction between different nodes and points. An MDOF system can be used to increase the complexity and capture a more detailed behaviour of a structure.

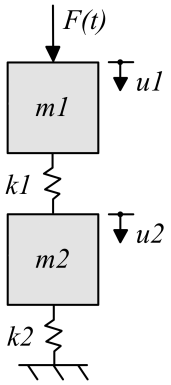

Figure 2.25: Illustration of a 2DOF-system.

The response of an MDOF system is calculated similarly as for SDOF systems (Biggs, 1964). The structural dynamic equation is utilized, where the mass, stiffness

and damping are expressed for multiple nodes. Matrices are introduced to structure and solve the system of equations. Each degree of freedom (DOF) will introduce one additional equation. The mass matrix, M, stiffness matrix, K, and damping matrix, C, are introduced and inserted in the structural dynamic equation, see Equation 2.47. Additionally, the acceleration, velocity and displacements of the nodes are summarized in vectors $\ddot{u}$, $\dot{u}$, u respectively.

$$M\ddot{u}(t) + C\dot{u}(t) + Ku(t) = F(t) \tag{2.47}$$

where:

$$\begin{aligned} M, C, K &: \text{n}\times\text{n matrices} \\ \ddot{u}, \dot{u}, u &: \text{n}\times 1 \text{ vectors} \\ F(t) &: \text{n}\times 1 \text{ load vector} \\ n &: \text{DOFs of system} \end{aligned}$$

The dependency of different movements is established through the stiffness and damping matrix. The stiffness of the spring and damping of the viscous damper is represented by a 2×2 matrix, connecting two DOFs, Equation 2.48.

$$K_e = k\begin{bmatrix} 1 & -1 \\ -1 & 1 \end{bmatrix} \quad C_e = c\begin{bmatrix} 1 & -1 \\ -1 & 1 \end{bmatrix} \tag{2.48}$$

where:

$$\begin{aligned} K_e &: \text{Element stiffness matrix} \\ C_e &: \text{Element damping matrix} \\ k &: \text{Stiffness of the spring} \\ c &: \text{Damping coefficient of the damper} \end{aligned}$$

Each spring, mass and damper has to be assembled into the global system to represent their connection to the specific DOFs. The mass of each DOF is inserted in the diagonal of the global mass-matrix, as illustrated in Equation 2.49.

$$M = \begin{bmatrix} m_1 & 0 & 0 & \dots & 0 \\ 0 & m_2 & 0 & \dots & 0 \\ \vdots & \vdots & \ddots & \vdots & \vdots \\ 0 & 0 & \dots & m_{n-1} & 0 \\ 0 & 0 & \dots & 0 & m_n \end{bmatrix} \tag{2.49}$$

An explicit solution method can be used to solve the structural dynamic equation and to find the response, $\ddot{u}$, $\dot{u}$, u. One commonly used solution method is Newmark's method described in Section 2.7.1.

3
Method

Two simplified models using mass-spring systems and one finite element model were constructed to describe the response of a simply supported sandwich wall subjected to impulse loading. This chapter describes modelling techniques, assumptions and simplifications of the respective model. The models captured the response differently and were compared to highlight their strengths and weaknesses. The structural response, energy distribution and load transfer were compared using each modelling technique. Additionally, a parametric study was conducted to evaluate the effects of the intermediate insulation layer. Different material properties and layer thicknesses were analysed. The methodology used for the comparison and the parametric study is described in Section 3.5 and 3.6.

3.1 Analysed sections

A sandwich panel can be constructed in various ways, with varying material thicknesses, reinforcement arrangements and material properties. A schematic illustration of a sandwich panel is shown in Figure 3.1. The wall was simplified in the analysis to a one-meter wide strip with one-way action. Adhesion between layers was not considered and the shear connectors were excluded, resulting in a wall with non-composite action.

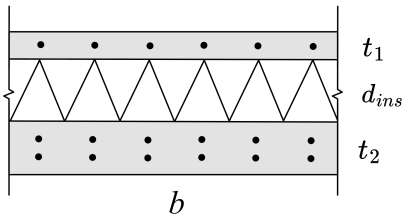

Figure 3.1: Cross-section of general sandwich panel. t_1: outer facade layer thickness. d_{ins}: insulation thickness. t_2: inner concrete layer thickness.

Three cross-sections with varying concrete dimensions were studied, see Figure 3.2. All configurations have a total concrete thickness of 200 mm, distributed between the outer and inner layers. The illustrated cross-sections are additionally provided with the reinforcement layout shown in Figure 3.1.

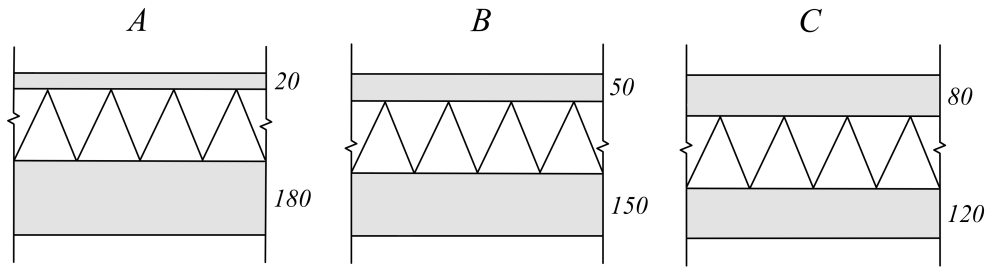

Figure 3.2: Cross-sections, A: thin facade layer, B: intermediate facade thickness, C: thick facade layer. Thicknesses in millimetres.

The geometry of the wall configurations was chosen to capture the response of structures with varying stiffness and mass distribution. The geometry of the analysed wall configurations is summarized in Table 3.1.

Table 3.1: Geometry of cross-section.

Geometry of CS			
b	1000	mm	Width of panel
l	2700	mm	Length of panel
ϕ_i	10	mm	Rebar diameter
s	200	mm	Rebar spacing horizontally
t_1	20/50/80	mm	Outer layer thickness
t_2	180/150/120	mm	Inner layer thickness
t_c	25	mm	Inner layer cover thickness
d_{ins}	200	mm	Insulation thickness

Each material has defined properties such as elastic modulus E, yield stress/strength f and density ρ. Table 3.2 summarizes the assigned properties of the concrete and reinforcement. The table also provides a common span for the properties of the insulating layer, used as a basis in the parametric study presented in Section 3.6. The reinforced concrete layers in the presented wall configurations were assigned constant material properties.

Polystyrene foams such as EPS are often used as insulation. These have a relatively high lower limit of compressive strength. A common span for EPS insulation is approximately 60-400 kPa, corresponding to a modulus of elasticity of 1.5-10 MPa (Sundolitt, 2019). Since good blast mitigation is associated with large plastic straining, a lower yield limit of 10 kPa was investigated. This limit was chosen to include the potential benefits of softer insulation. The lower limit may be associated with other polymers such as polyurethane or polyethylene.

Table 3.2: Material properties with common ranges.

Material Properties			
Concrete C25/30			
E_c	31	GPa	Modulus of Elasticity
f_{ck}	25	MPa	Compressive Strength
ρ_c	2500	kg/m^3	Density
Reinforcement B500C			
E_s	200	GPa	Modulus of Elasticity
$f_{y,s}$	500	MPa	Yield Stress
ρ_s	7850	kg/m^3	Density
Insulation			
E_{ins}	1-10	MPa	Modulus of Elasticity
$f_{\text{y,ins}}$	10-1000	kPa	Compressive Yield Stress

3.2 Load characteristics

Three different load magnitudes were investigated, to highlight the response as the structure is loaded lightly (L1), moderately (L2) and severely (L3). The impulse density, peak pressure and corresponding load duration for a linearly decreasing load are summarized in Table 3.3. L1 corresponds to the reflected pressure from a hemispherical charge of 75 kg TNT, detonating at a distance of 25 meters. L2 and L3 have the same travel distance but correspond to 150 kg and 400 kg TNT respectively. The charge was assumed to take place at ground level, hence the presented charge weights were doubled to account for ground reflection. The calculation of loads was based on the material presented by Johansson & Laine (2012a) and are found in Appendix A.

Table 3.3: Characteristics of loads.

Load characteristics			
	i_r^+	P_r^+	$t_{\Delta,r}^+$
L1	425 Pas	80 kPa	10.6 ms
L2	800 Pas	150 kPa	10.7 ms
L3	1500 Pas	300 kPa	10.0 ms

3.3 Simplified models

Two simplified models were developed to predict the response of a simply supported wall panel subjected to impulse loading, an SDOF and an MDOF model. The SDOF model is the simplest and does not account for the thickness and properties of the insulating layer. Therefore, a 2DOF model was proposed to account for the concrete layers' separate motion and the insulation's energy-absorbing effect. A finite element model was assembled in Abaqus to compare with the simplified models. Each model is described in the following sections.

3.3.1 SDOF model

The SDOF model is the simplest system where the structure is described by a mass and a spring. It considers the total concrete mass and the stiffness of the main inner layer, see Figure 3.3. The model does not account for the influence of the insulation and neglects the stiffness of the outer concrete layer. Hence, the simplified SDOF model cannot capture the effects of different insulation properties.

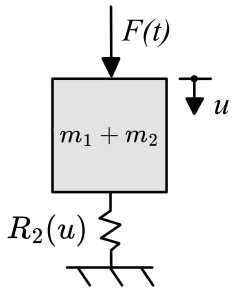

Figure 3.3: SDOF model of sandwich panel. $m_1 + m_2$: Total mass of concrete. $R_2(u)$: Response function of main concrete layer. $F(t)$: Applied external load.

Neglecting the stiffness of the outermost layer is presumed justified since it is thin compared to the main inner layer. The bending stiffness of the outer layer is considerably smaller since it is proportional to the cube of the layer thickness. For instance, in a sandwich wall with a main layer of 100 mm and a facade layer of 50 mm, the uncracked stiffness of the facade layer will account for approximately 1/8 of the stiffness of the main layer. On the contrary, the mass of the thinner layer accounts for 1/3 of the total mass. The model therefore accounts for the mass while it neglects the stiffness. The assumed stress distribution is illustrated in Figure 3.4.

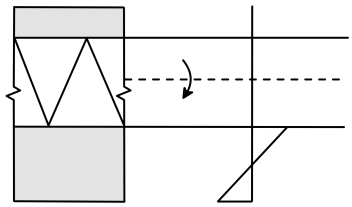

Figure 3.4: Assumed stress distribution of cross-section.

The resistance response of the SDOF model assumes the bi-linear behaviour presented in Section 2.6. Where the elastic response corresponds to the stiffness of the inner layer. The elastic stiffness is calculated according to Equation 2.34, utilizing the moment of inertia for stage II. The maximum resisting force is calculated using the bending moment capacity of the inner layer. The structural dynamic equation for the SDOF model is written as follows:

$$\kappa_{mF}(m_1 + m_2)\ddot{u} + k_2 u = F(t) \tag{3.1}$$

The response of the structure is solved by Equation 3.1. The response function, $R_2(u)$, is described by continuously updating the stiffness, k_2, using the secant stiffness described in Section 2.6.4.3. Using this method enabled a description of both the elastic and the plastic behaviour.

3.3.2 MDOF model

Utilizing an additional degree of freedom increases the complexity of the model, by accounting for the movement of two nodes. The MDOF model in Figure 3.5 can describe the movement of both the inner and outer layer. It describes the effects of the intermediate insulation and captures the interaction between the concrete layers. Unlike the SDOF model, the mass of the inner and outer layer are described separately and connected by a spring representing the insulation. The stiffness of the outer layer is neglected and the assumed stress distribution is illustrated in Figure 3.4. The mass of the insulation is disregarded since it is small relative to the concrete mass.

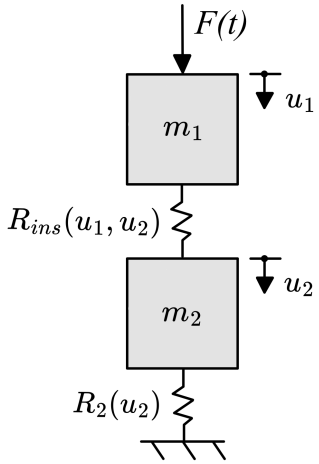

Figure 3.5: MDOF model of sandwich panel. m_1 & m_2: Mass of concrete layers. $R_{ins}(u_1, u_2)$ & $R_2(u_2)$: Response function of insulation and inner concrete layer respectively. $F(t)$: Applied external load.

The Structural dynamic equation is solved using matrices as described in Section 2.8. The matrices are expressed and inserted into the structural dynamic equation as shown in Equation 3.2. The damping effects are disregarded since they are small compared to the total structural response during impulse loading (Smilowitz & Tennant, 2010). Hence, damping matrix C is not included in the expression.

$$\kappa_{mF} \begin{bmatrix} m_1 & 0 \\ 0 & m_2 \end{bmatrix} \begin{bmatrix} \ddot{u}_1 \\ \ddot{u}_2 \end{bmatrix} + \begin{bmatrix} k_{ins} & -k_{ins} \\ -k_{ins} & k_2 + k_{ins} \end{bmatrix} \begin{bmatrix} u_1 \\ u_2 \end{bmatrix} = \begin{bmatrix} F(t) \\ 0 \end{bmatrix} \tag{3.2}$$

Similar to the SDOF model, the secant stiffness is implemented to capture the nonlinear behaviour of the structure. The model considers the effect of the insulation by the stiffness k_{ins}, connecting the masses of the inner and outer concrete layer. The response function for the insulation is described in the following section.

3.3.2.1 Insulation response function

The load is applied to the external layer and transferred through the insulation to the stiff inner layer. Equation 3.3 describes the elastic stiffness of the insulation, where E_{ins}, A_{ins} and d_{ins} is the modulus of elasticity, wall panel area and thickness of the insulation respectively.

$$k_{ins} = \frac{E_{ins} A_{ins}}{d_{ins}} \tag{3.3}$$

The maximum resistance, R_m, is described by the yield stress of the material as shown in Equation 3.4. The expression assumes a uniform compression of the insulation along the panel.

$$R_m = A_{ins} \cdot f_{y,ins} \tag{3.4}$$

The response function of the insulation is implemented according to Section 2.6.4. The insulation is assumed to follow a bi-linear response up to the moment when the concrete layers collide, see Figure 3.6. This is estimated to occur when the insulation is compressed to 80 % of its original volume. The assumption is based on the material behaviour presented by Rahimidehgolan & Altenhof (2023). At this strain, a direct transfer of force between layers is assumed. This occurs as Δu exceeds the limit u_{col} as described in Equation 3.5.

$$R_{ins}(u) = \begin{cases} k_{ins} \Delta u & \text{if } \Delta u \leq u_{el} \\ R_m & \text{if } u_{el} < \Delta u < u_{col} \end{cases} \tag{3.5}$$

where:

$$u_{col} = 0.8 \cdot d_{ins}$$

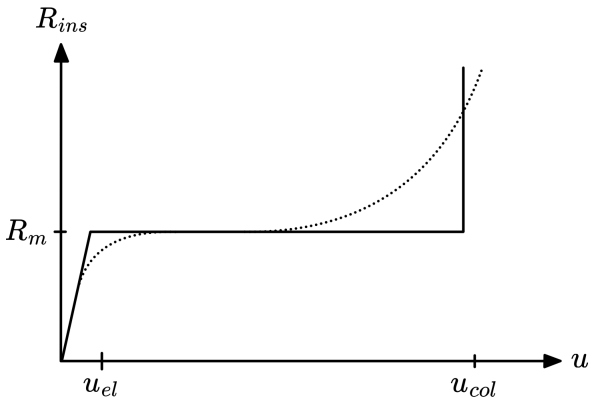

Figure 3.6: Simplified response of foam material.

3.3.2.2 Collision of concrete layers

If the intermediate layer is too soft relative to the applied load, the concrete layers will collide and transfer the load directly through impact. This is considered in the MDOF model where the momentum of each mass is transferred to the total mass of both layers when colliding. Both layers are assumed to move with the same velocity, v_{col}, after impact. Hence, the velocity of the combined mass is calculated according to Equation 3.6.

$$m_1 v_1 + m_2 v_2 = v_{col}(m_1 + m_2) \rightarrow v_{col} = \frac{m_1 v_1 + m_2 v_2}{m_1 + m_2} \tag{3.6}$$

The increase in strength and stiffness caused by densification is assumed sufficient for the material to directly transfer the load. The response of the material is therefore simplified as illustrated in Figure 3.6.

3.4 Finite Element Model

A 2D finite element model of the sandwich wall was constructed in Abaqus. The model is described in the following sections, where choices of element types, material models, boundary conditions and the solution method are presented. An illustration of the FEM model is shown in Figure 3.7. The solid horizontal lines symbolise beam elements, while the dashed lines indicate the thickness of the respective concrete layer. The insulation is illustrated by springs.

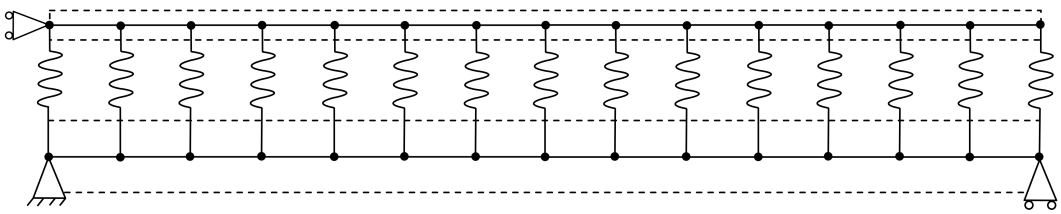

Figure 3.7: Illustration of 2D Finite Element Model.

3.4.1 Elements

The reinforced concrete layers are modelled using 2D beam elements, denoted *B21* in Abaqus. These elements are designed to model thin structures accurately (Simulia, 2006). Another benefit of using beam elements is the compatibility with large deformations. The intermediate insulation layer is modelled using *Connector elements*. These are similar to springs but are in addition able to account for the nonlinear behaviour. This is used to describe the plastic plateau region of the foam material. Each element in the FEM model represents a one meter wide panel, meaning the beam and connector elements are assigned the characteristics corresponding to one meter.

3.4.2 Material models

The behaviour of reinforced concrete, see Section 2.4.3, is simplified to a bi-linear function. The elastic range is described by an equivalent modulus of elasticity, E_{eq}. This accounts for the different material properties in the combined concrete section, see Figure 3.8. The equivalent modulus of elasticity is calculated as shown in Equation 3.7. The cross-section in Abaqus does not account for the change in inertia caused by cracking. Instead, the uncracked rectangular cross-section is considered in I_{FEM}. The material's modulus of elasticity is therefore reduced.

$$E_{eq}I_{FEM} = E_{cm}I_{II} \rightarrow E_{eq} = \frac{E_{cm}I_{II}}{I_{FEM}} \tag{3.7}$$

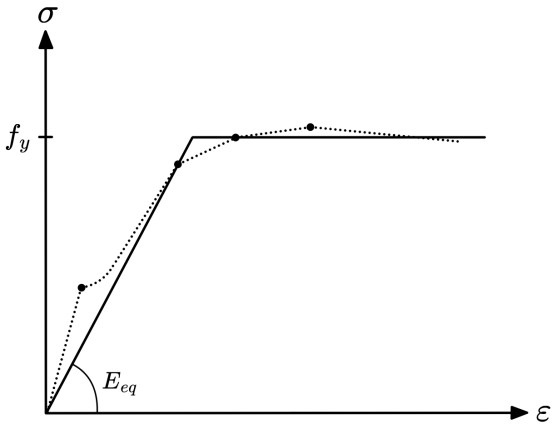

Figure 3.8: Bi-linear material model with an equivalent modulus of elasticity.

The material is assumed to be perfectly plastic after yielding, where the yield stress, f_y, is calculated from the ultimate bending capacity of the cross-section, M_{Rd}. The fictional yield stress is calculated as shown in Equation 3.8.

$$f_y = \frac{M_{Rd}}{W_{pl}} \qquad W_{pl} = \frac{bt^2}{4} \tag{3.8}$$

The plastic section modulus, W_{pl}, is used in Equation 3.8 to account for the number of integration points in Abaqus. The default number is five across the height of the beam, making the sectional stress distribution resemble a plastic cross-section as in Figure 3.9. This could be an issue since it is difficult to interpret an exact stress distribution from Abaqus. However, since the verification in Section 3.4.5 indicates a good correlation in results, this approach is considered reasonable. Utilizing three integration points would theoretically result in a more controlled response since the stress distribution is known and treated as linear. However, according to Simulia (2006) the minimum number of integration points must be equal to five when using a rectangular beam section in the analysis. Utilizing three integration points would instead be combined with the elastic section modulus, W_{el}.

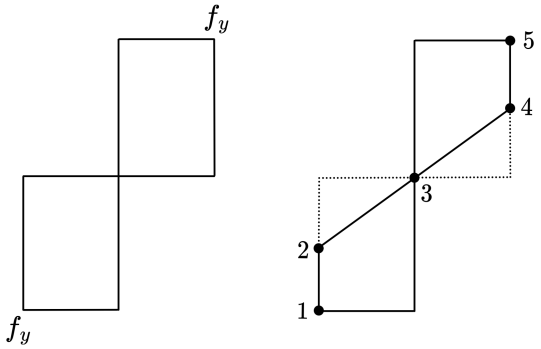

Figure 3.9: Assumed plastic stress distribution and interpreted stress distribution in Abaqus.

The equivalent modulus of elasticity and yield stress for the analysed concrete sections is presented in Table 3.4. Complete calculations of the input data for Abaqus are found in Appendix B.

Table 3.4: Equivalent modulus of elasticity and yield stress for each configuration.

Abaqus material data				
Inner concrete layer	A	B	C	
E_{eq}	3.063	3.352	3.641	GPa
f_y	3.660	4.223	4.961	MPa
Outer concrete layer				
E_{eq}	4.883	2.655	1.862	GPa
f_y	11.715	6.587	4.414	MPa

The response of the insulating layer is implemented using connector elements. The stiffness of each element is calculated according to Equation 3.9, where d_{ins} and E_{ins} correspond to the thickness and modulus of elasticity of the insulation layer. The effective area, A_{eff}, depends on the mesh element length, $l_{element}$, and the width of the panel, b, according to Equation 3.10.

$$k_{ins} = \frac{E_{ins} A_{eff}}{d_{ins}} \tag{3.9}$$

$$A_{eff} = b \cdot l_{element} \tag{3.10}$$

The yielding force is calculated using the compressive yield stress of the insulation, see Equation 3.11. k_{ins} and F_y are inserted in Abaqus when assigning the element behaviour.

$$F_y = f_{y,ins} \cdot A_{eff} \tag{3.11}$$

3.4.3 Boundary conditions and applied load

The wall strip is modelled as a simply supported element, shown in Figure 3.10. The boundary conditions are implemented on the inner layer, by restricting movement along the vertical axis at each support and horizontally at one side. Since the connectors/springs only carry axial loads, the outer layer has additional restraint in the horizontal direction. The boundary conditions of both edges are illustrated in Figure 3.10.

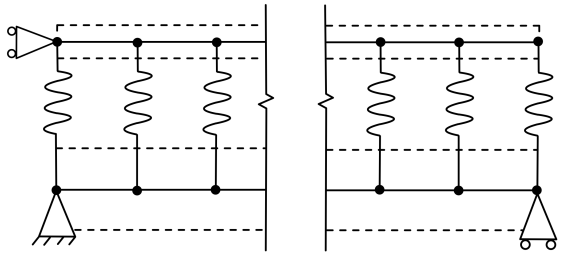

Figure 3.10: Schematic illustration of boundary conditions.

Similarly to the simplified models, the load is modelled as described in Section 2.3.3. The load is implemented as a line load acting on the outer edge of the exterior concrete layer. The line load corresponds to the pressure on a one meter wide wall segment.

3.4.4 Solution method and mesh convergence

Solution method *Abaqus/Explicit* is used in the analyses since it is well suited for dynamic events, such as impulse loading (Simulia, 2006). It utilizes an explicit time integration scheme, making it computationally efficient compared to *Abaqus/Standard*. The standard solution method utilizes implicit time integration which is more computationally demanding, since iteration is required within every time step.

A sufficient number of elements is needed to find an accurate solution to the structural response. The mesh size is determined by a sensitivity study performed on the inner load-bearing layer of wall configuration B. The layer is loaded by an impulse corresponding to load L2, and the maximum deflection is compared for a varying

number of elements, see Figure 3.11. The graph indicates that 54 elements are sufficient, equivalent to a mesh size of 50 mm.

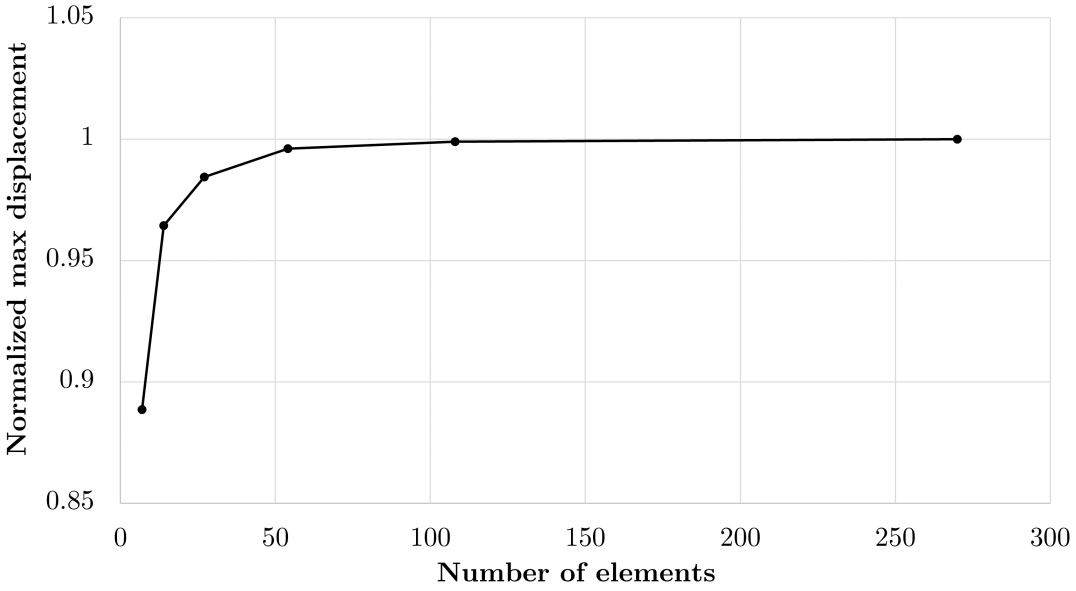

Figure 3.11: Mesh sensitivity performed on the inner load-bearing layer.

3.4.5 Model verification

The FE model is verified against hand calculations to ensure the model works as intended. Only the inner concrete layer of wall configuration B is considered to facilitate hand calculations. The simple version of the model is subjected to a static pressure of 15 kPa, to get an elastic response. Additionally, the plastic ultimate load is calculated and compared to Abaqus. The results from the static verification are summarized in Table 3.5 and calculations are found in Appendix C. The verification assures the material models, boundary conditions and loads are applied correctly.

Table 3.5: Static response of the inner layer of Wall B.

Static Response			
	Analytical	FEM	Correlation [%]
Elastic Displacement	11.0 mm	11.1 mm	99 %
Plastic Ultimate Load	26.1 kN/m	26.5 kN/m	98 %

The same model is also subjected to an impulse corresponding to load L2, where the dynamic response is compared to analytic theory. The analytical calculations, based on the theory given in Section 2.6.3, indicate similarities to the results obtained from Abaqus with subtle differences. The results from the dynamic comparison are summarized in Table 3.6. This verification assures that the model works for both static and impulse loading.

Table 3.6: Dynamic response of the inner layer of Wall B.

Dynamic Response			
	Analytical	FEM	Correlation [%]
Elastic Displacement	39.9 mm	39.2 mm	98 %
Elastic-Plastic Displacement	58.6 mm	57.0 mm	97 %

3.5 Comparison of models

The comparison of models was limited to fixed concrete material properties, where only the cross-section geometry varied. The comparison aimed to visualize and highlight each model's limitations and find when they are applicable. The insulation was modelled using a modulus of elasticity of 2 MPa and yield stress of 50 kPa if nothing else is stated. The values were chosen to get both an elastic and plastic response of the intermediate layer, as the wall configurations are loaded with load L1, L2 and L3. The comparison of models covers the structural response of the wall segment, energy distribution and load transfer using each model.

3.5.1 Structural response

The structural response using all three models was investigated regarding mid displacement over time, displacement along the element and sectional forces/moments. The effects of varying insulation properties were additionally studied by analyzing boundary cases.

3.5.1.1 Mid displacements

The maximum displacement of the inner layer was evaluated using the models described in Section 3.3 and 3.4. The response of wall configurations A, B and C were evaluated when subjected to loads L1, L2 and L3. The concrete material parameters were assigned according to Table 3.2.

The comparison aimed to visualize the correlation between the FE model and simplified models, for varying wall geometries and applied loads. The plastic rotation of the inner concrete layer determines the allowed deformation of each wall configuration. The allowed plastic rotations are summarized in Table 3.7 and calculations are found in Appendix D. Load L3 caused displacements above the rotational capacity, but was included to differentiate the models when loaded severely.

Table 3.7: Rotational capacity of inner concrete layer for each wall configuration.

Cross-section capacity			
Eurocode 2	A	B	C
θ_{pl} [rad]	0.046	0.063	0.070
u_{rd} [mm]	62.1	84.5	94.0

3.5.1.2 Displacement along the element

The displacement along the length of the element was determined for Wall B subjected to load L1 and L2. When loaded with L1 the response was assumed elastic while L2 assumed an elasto-plastic response. The deformation shape along the length of the element was determined and compared for the MDOF and the Abaqus model. The simplified models were constructed assuming a deformation shape for the elastic and plastic response, described in Section 2.5.2. The assumed displacement along the length was calculated using the following equations.

$$q(t) = R_2(u)/l \tag{3.12}$$

$$\text{Elastic:} \quad u(x,t) = \frac{q(t)x}{24EI_{II}} \cdot \left(l^3 - 2lx^2 + x^3\right) \quad \text{for} \quad 0 < x < \frac{l}{2} \tag{3.13}$$

$$\text{Plastic:} \quad u(x,t) = u_s(t) \cdot \frac{2x}{l} \quad \text{for} \quad 0 < x < \frac{l}{2} \tag{3.14}$$

The assumed deformation shape of the simplified model was compared to the findings of the Abaqus model at equal time steps. The deflections along the element were analysed for the initial phase of the deformation.

3.5.1.3 Effects of insulation layer

Boundary cases of the insulation were tested to analyse the impact on the response using each model. The boundary values of elastic modulus and yield stress presented in Table 3.2 were combined in four cases: low and high stiffness with low and high compressive yield stress. The mid displacement for the inner layer of Wall B was studied when subjected to load L2.

3.5.1.4 Moment and Shear force

Bending moments and shear forces across the length of the model were studied using both MDOF and Abaqus. The analysis used elastic material properties while the structure was subjected to load L1. The moment and shear distribution were compared for the MDOF and the Abaqus model at 5 ms, 10 ms and 15 ms. The following expressions were used to determine the distribution along the wall element. The distribution is dependent on the assumed deflection when deriving the transformation factor. The moment and shear distributions are parabolic and linear for the moment and shear respectively.

$$\text{Bending Moment:} \quad M(x,t) = \frac{q(t)}{2} \cdot \left(lx - x^2\right) \tag{3.15}$$

$$\text{Shear Force:} \quad V(x,t) = q(t) \cdot \left(\frac{l}{2} - x\right) \tag{3.16}$$

The bending moment and shear forces were extracted for the same time steps using Abaqus and compared to the results from the simplified models.

3.5.2 Energy distribution

The energy distribution was investigated using the SDOF, MDOF and Abaqus model. The total external work introduced to the system was analysed using each model. Additionally, the potential, dissipated and kinetic energy were calculated to visualize the energy distribution during and after loading.

The work performed by the applied load on the outer concrete layer should equal the sum of internal energy from all parts. This is expressed by Equation 3.17, where E_p is the potential energy, D is the dissipated energy and E_k is the kinetic energy. The external work is evaluated using Equation 2.6.

$$W_{ext} = E_p + D + E_k \tag{3.17}$$

The response was calculated utilising Equation 2.19, instead of the simplified expression shown in Equation 2.20. This was made to account for the different contributions to the energy balance correctly, where all transformation factors are included. For the bi-linear response, dissipated energy was calculated using Equation 3.18, where the energy dissipation arises from plastic deformation in each layer.

$$D = R_m \cdot u_{pl} \tag{3.18}$$

The kinetic energy was calculated as described in Section 2.2 and the potential energy was evaluated as the remaining energy. The energy balance must be fulfilled for the entire structure and for individual layers. The energy of each layer was calculated by integrating the response function, $R(u)$. This was utilized to describe the energy in the inner load-bearing concrete layer.

3.5.3 Transferred impulse

Applying the load on the outer concrete layer will initiate a reaction in the structure. The impulse will be transferred through each layer until it reaches the supports. The characteristics of the impulse might change as it propagates. The applied impulse was calculated according to Equation 2.3. The impulse in different parts of the structure was similarly found by integrating the response-time functions.

A similar analysis was made in Abaqus where the total applied load, load in the connector elements and reaction forces were compared. The load transfer was analysed for Wall B when subjected to load L2. The insulation layer was assigned the material properties described in Section 3.5.

3.6 Parametric study

A parametric study was performed to evaluate the effects of optimized material properties. The mid displacement was used to determine the properties resulting in the most favourable response. The parametric study was limited to analysing the effect of varying properties and thicknesses of the intermediate layer. The MDOF model described in Section 3.3 was utilized to find the optimized material properties.

3.6.1 Varying insulation properties

The effect of varying insulation yield stress was investigated by analysing the mid displacement of each wall configuration. The intermediate layer was assigned varying yield stress, combined with a modulus of elasticity of 2 MPa. The value resulting in the smallest deflection was considered the optimal value. A nonlinear program solver in MATLAB called *fminsearch* was then implemented to find the optimal yield stress for different load intensities. The load duration was set to 10 ms independently of the impulse density.

A similar procedure was made when studying the modulus of elasticity. The wall configurations were analysed for varying modulus of elasticity when subjected to load L2. The yield stress was assigned to 50 kPa.

The effect of the insulation thickness was investigated. The optimal yield stress for different thicknesses was calculated and the displacement of the optimized structures was compared for varying thicknesses. The wall configurations were subjected to load L2 and the modulus of elasticity was assigned to 2 MPa.

3.6.2 Effects of optimized material properties

The effects of the optimized values were studied by re-analysing wall configuration B when subjected to load L2. The mid displacement, energy balance and transferred impulse were studied and compared to the analysis in Chapter 4. Additionally, the optimized analysis using the MDOF model was compared to the analysis with the SDOF model to highlight the effect of considering the insulation layer when analyzing a concrete sandwich wall.

4
Comparison of models

This chapter consists of a comparison between the SDOF, MDOF and Abaqus model, performed according to the method described in Section 3.5. The structural response, energy distribution and load transfer are studied using each modelling technique.

4.1 Structural response

Mid displacements, displacements along the wall element and sectional forces are studied in the following sections. The methodology for this section is presented in Section 3.5.1.

4.1.1 Mid displacements

The response of each wall configuration is analysed when subjected to loads L1, L2 and L3. The mid displacement of the inner layer using the SDOF, MDOF and Abaqus model are presented in Figure 4.1, 4.2 and 4.3.

The response of Wall A is shown in Figure 4.1. Load L1 causes a mainly elastic response where all three models illustrate similar behaviour. Increasing the load to L2 yields an increase in displacement and a response that is both elastic and plastic. Similar to load L1, all models display a similar response in maximum displacement. MDOF and Abaqus indicate a delay in the movement of the inner concrete layer, while SDOF initiates movement directly after the load is applied to the element.

Further increasing the load to L3 results in large displacements, where the response is dominated by plastic displacement. The high load combined with the specific wall configuration, result in a collision of concrete layers. This phenomenon is shown in Figure 4.1, where the MDOF and Abaqus model exhibits a rapid increase in displacement at 10 ms. The SDOF model is not able to capture this behaviour. Using Eurocode to determine the plastic rotational capacity, the severe load case yields displacements that exceed the capacity, see Table 3.7.

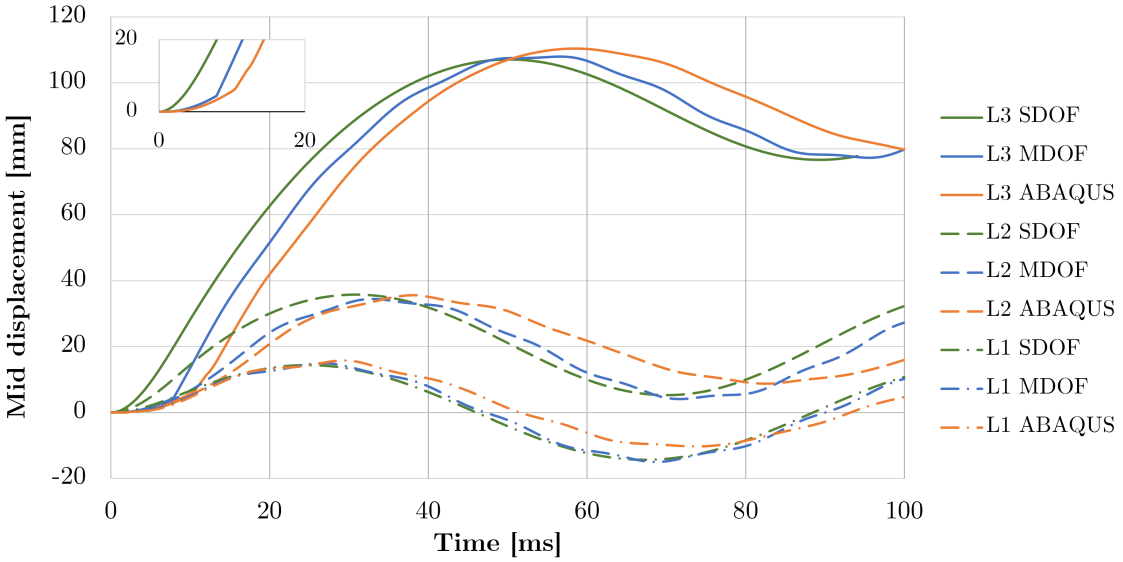

Figure 4.1: Response of Wall A subjected to Load L1, L2 and L3.

All models capture the response similarly. The elastic displacement, plastic displacement and peak response are calculated in the same range. The response of Wall B is illustrated in Figure 4.2. The results indicate similar behaviour to Wall A. However, the concrete layers do not collide as Wall B is subjected to load L3. The peak response obtained with MDOF and Abaqus is considerably lower when compared to the SDOF model for this load. The MDOF and Abaqus models have a pronounced delay in movement of the inner layer when subjected to severe loading.

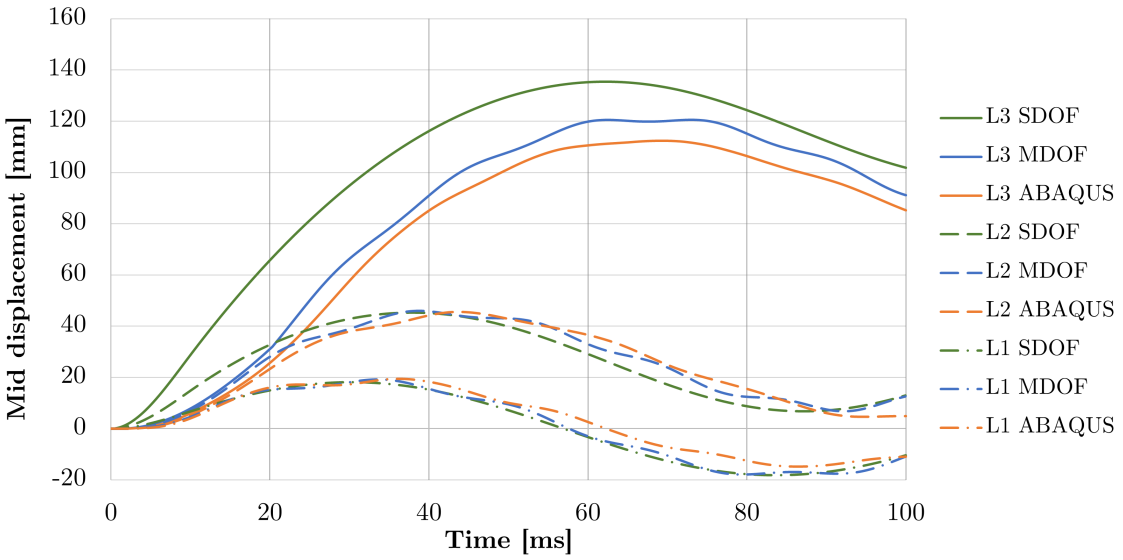

Figure 4.2: Response of Wall B subjected to Load L1, L2 and L3.

For wall configuration C there are more noticeable differences in the response, where Abaqus yield lower displacements compared to SDOF and MDOF, see Figure 4.3. This is more apparent for load L2 and L3 compared to lower loading.

It is also observed that the frequency of oscillations decreases as the inner layer becomes thinner. Wall A has a thick inner layer resulting in a higher frequency, while Wall C has a thinner inner layer generating a lower frequency. The frequency is related to the structural stiffness where a high stiffness is associated with a high frequency.

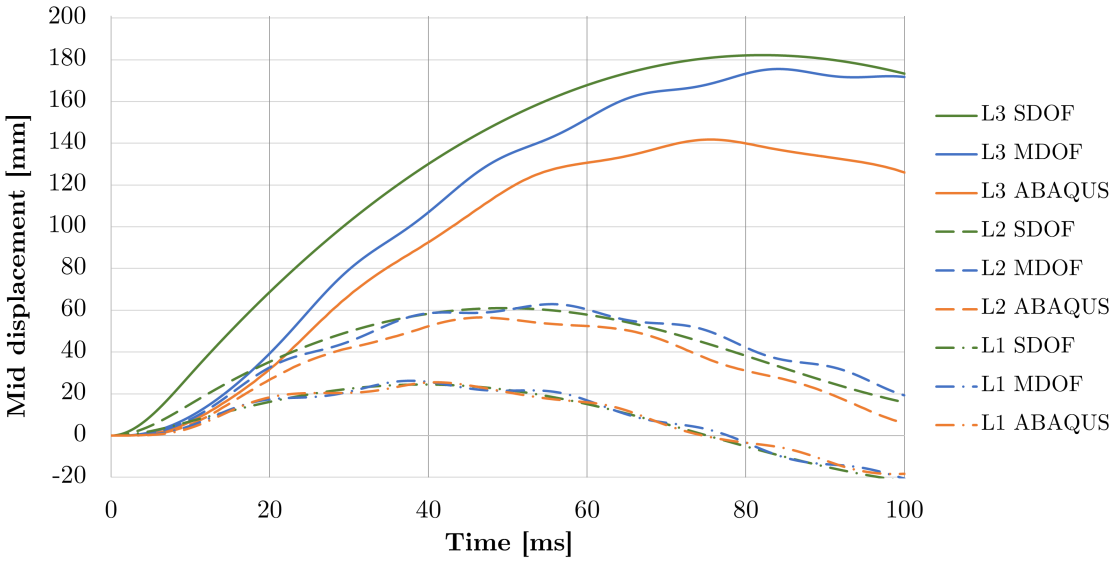

Figure 4.3: Response of Wall C subjected to Load L1, L2 and L3.

The maximum midpoint deflection for each wall configuration utilizing different modelling techniques is summarized in Table 4.1. The correlation between models is further tabulated in Table 4.2. It is observed that SDOF and MDOF correlate well and yield similar maximum displacements, while Abaqus deviates more. Abaqus correlate better with the MDOF model compared to the SDOF model.

Table 4.1: Maximum deflection of inner concrete layer for varying wall cross-section and applied load.

Maximum deflections [mm]				
		A	B	C
L1	SDOF	14.4	18.2	24.5
	MDOF	14.9	19.2	26.3
	ABAQUS	15.8	19.5	24.6
L2	SDOF	35.7	45.3	61.1
	MDOF	34.4	46.0	63.0
	ABAQUS	35.6	45.6	54.1
L3	SDOF	107.1	135.5	182.2
	MDOF	108.0	120.6	175.6
	ABAQUS	110.4	112.4	131.7

Table 4.2: Correlation of max deflection using different modelling techniques.

Correlation		A		B		C	
		SDOF	MDOF	SDOF	MDOF	SDOF	MDOF
L1	MDOF	96%		94%		93%	
	ABAQUS	91%	95%	93%	99%	96%	97%
L2	MDOF	96%		98%		97%	
	ABAQUS	100%	97%	99%	99%	93%	90%
L3	MDOF	99%		89%		96%	
	ABAQUS	97%	98%	83%	93%	78%	81%

Average		SDOF	MDOF
	MDOF	96%	
	ABAQUS	92%	94%

The modelling techniques display the least deviation for Wall B subjected to load L2. According to Table 4.2 the models deviate extensively for Wall C with an outer layer corresponding to a large portion of the total concrete thickness. In this case, Abaqus yield lower maximum deflections compared to the simplified models. Overall, the models display a high correlation for the studied wall geometries combined with the material properties of the insulation.

4.1.2 Displacement along the element

The displacements are further analysed by studying the displacements along the wall segment. The elastic and plastic behaviour of the initial phase of the response are compared for the inner load bearing layer. The elastic response is illustrated in Figure 4.4 and the elastic-plastic response is illustrated in Figure 4.5.

The assumed deformation shape in the simplified model does not capture the more complex behaviour seen in Abaqus. This is because Abaqus accounts for several bending modes while the MDOF model only considers the first fundamental bending mode. Figure 4.4 presents the deflection shortly after load application for the elastic case. It can be observed that the deformation shape in Abaqus displays a uniform displacement of the mid portion of the wall segment. As time elapses the deformation shape starts to resemble the assumed parabolic shape of the MDOF model. Since the maximum displacement correlates well between models, this discrepancy in the initial phase has a small impact when analysing maximum displacements.

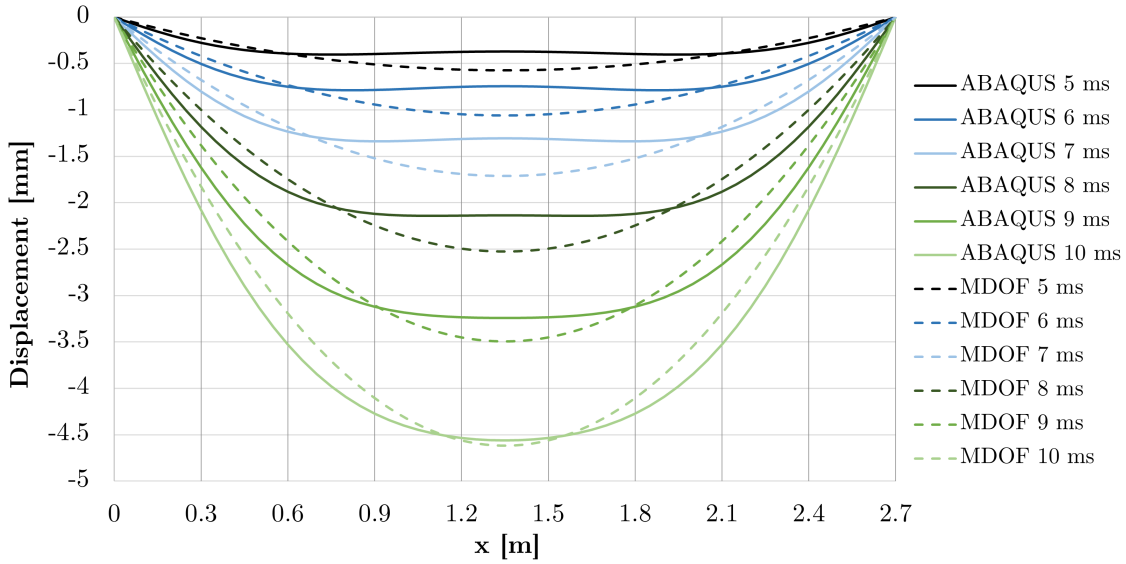

Figure 4.4: Elastic deformation shapes at different time steps, for the inner layer of Wall B subjected to load L1.

For an elastic-plastic response, the plastic transformation factor in Table 2.1 is utilized for the simplified models. This factor is based on the assumption of a triangular deformation shape. Hence, the shape of the initial elastic response is not represented accurately using the MDOF model when applying a plastic transformation factor. This is illustrated in Figure 4.5 when comparing the assumed deformation shape to the response obtained from the FE model. Abaqus can capture the transition from an elastic and parabolic shape to a triangular shape with a plastic hinge.

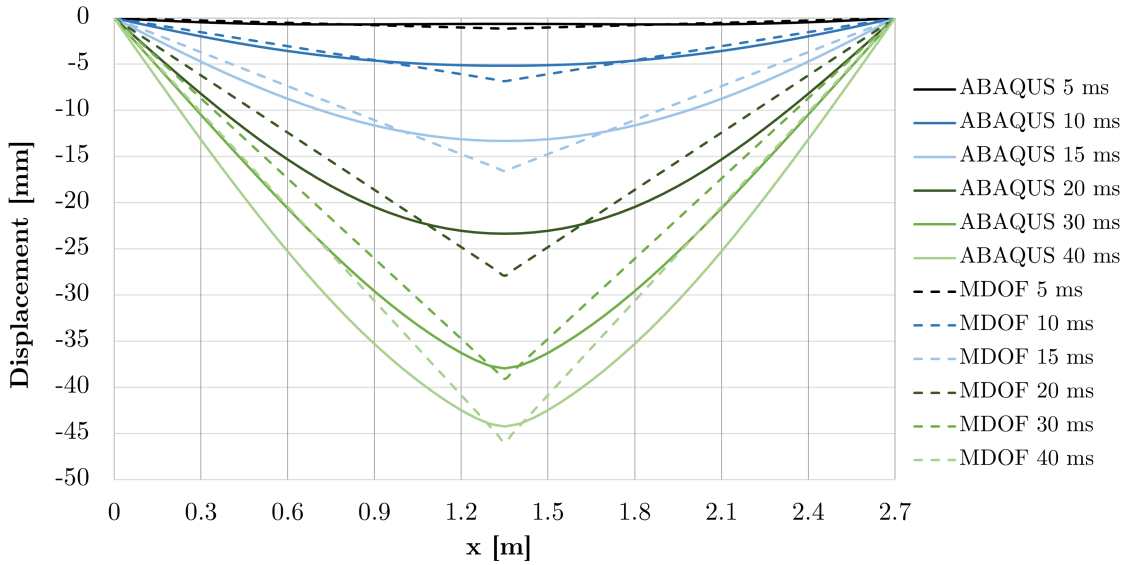

Figure 4.5: Plastic deformation shapes at different time steps, for the inner layer of Wall B subjected to load L2.

4.1.3 Insulation boundary cases

This section studies boundary cases of insulation properties in four cases: low and high stiffness combined with low and high compressive yield stress. The analysed cases do not necessarily reflect a real combination of properties. A high elastic modulus is expected to correlate to a high yield stress and vice versa. However, the aim is to evaluate how the models correlates with such a combination of insulation properties.

4.1.3.1 Low yield stress

Figure 4.6 illustrates the response when combining high and low elastic modulus with a low yield stress. The intermediate layer exhibits large plastic deformations as the load is applied. The influence of a varying elastic modulus is small since the deformation is mainly plastic. The models display a wide variety, where the SDOF model yields a large deflection compared to the MDOF and Abaqus models. The insulation layer cannot generate sufficient resistance to prevent the concrete layers from colliding. The collision occurs earlier in the MDOF model compared to the Abaqus model.

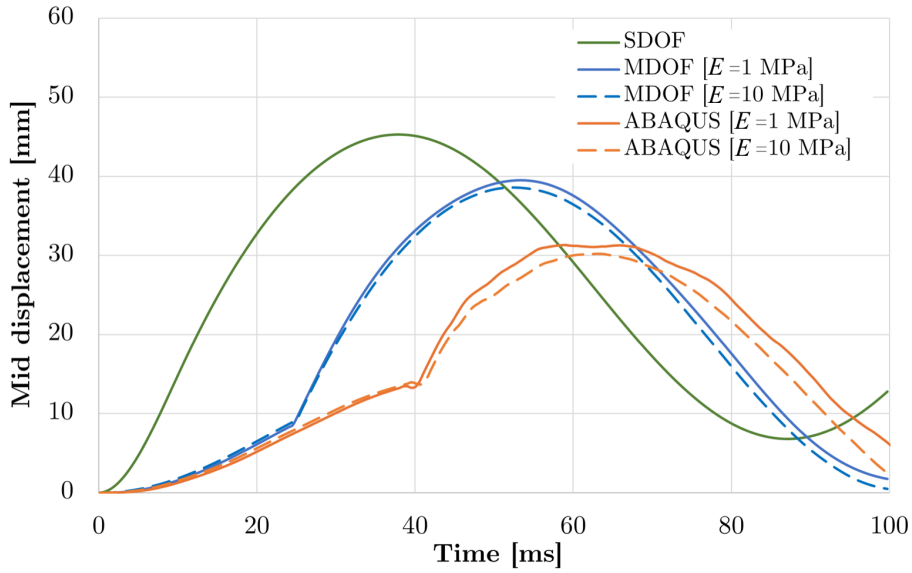

Figure 4.6: Mid displacement for varying elastic modulus and yield stress of 10 kPa for Wall B subjected to Load L2.

4.1.3.2 High yield stress

A high compressive yield stress is combined with boundary cases of the modulus of elasticity. The mid displacement of the inner concrete layer is presented in Figure 4.7. The stress in the insulation is within the elastic range. However, the figure indicates that the inner concrete layer experiences plastic deformations. The models display a larger difference for a low elastic modulus compared to the higher upper limit. The MDOF and Abaqus model share a similar response for the presented cases.

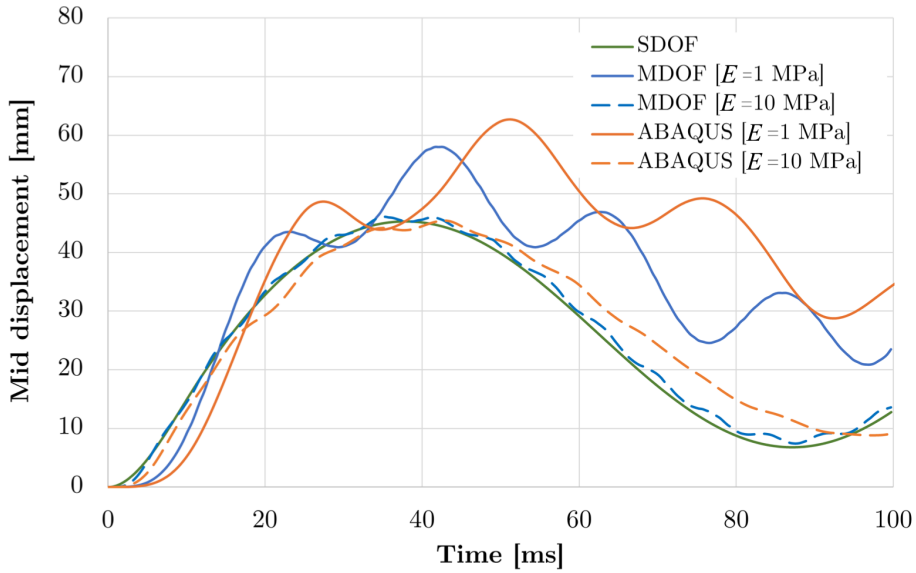

Figure 4.7: Mid displacement for varying elastic modulus and yield stress of 1000 kPa for Wall B subjected to Load L2.

The properties of the insulation layer influence the behaviour of the wall configuration. A lower yield stress does not generate sufficient resistance to keep the concrete layers from colliding, see Figure 4.6. In the elastic range, with a high yield limit, the modulus of elasticity considerably affects the behaviour of the wall. A low modulus of elasticity causes a large variety between models while increasing the modulus of elasticity increases the correlation between the models, illustrated in Figure 4.7.

4.1.4 Moment and Shear force

The sectional bending moments and shear forces of the inner layer are investigated for an elastic structural response. The sectional forces obtained from the MDOF model are compared to the Abaqus model. The response is illustrated shortly after the load application. Additionally, the force envelope, meaning the maximum value during all time steps, is compared.

4.1.4.1 Elastic Bending Moment

The bending moment of the initial portion of the response is shown in Figure 4.8. The bending moment calculated using Abaqus does not display the parabolic shape of the simplified models. The displacement shown in Figure 4.4 and the bending moment are closely related, where the moment is proportional to the curvature of the wall segment. The Abaqus model indicates two initial local maximums that merge into one, while the MDOF model always generates a parabolic moment distribution. This means that the moment deviates considerably in different parts along the wall.

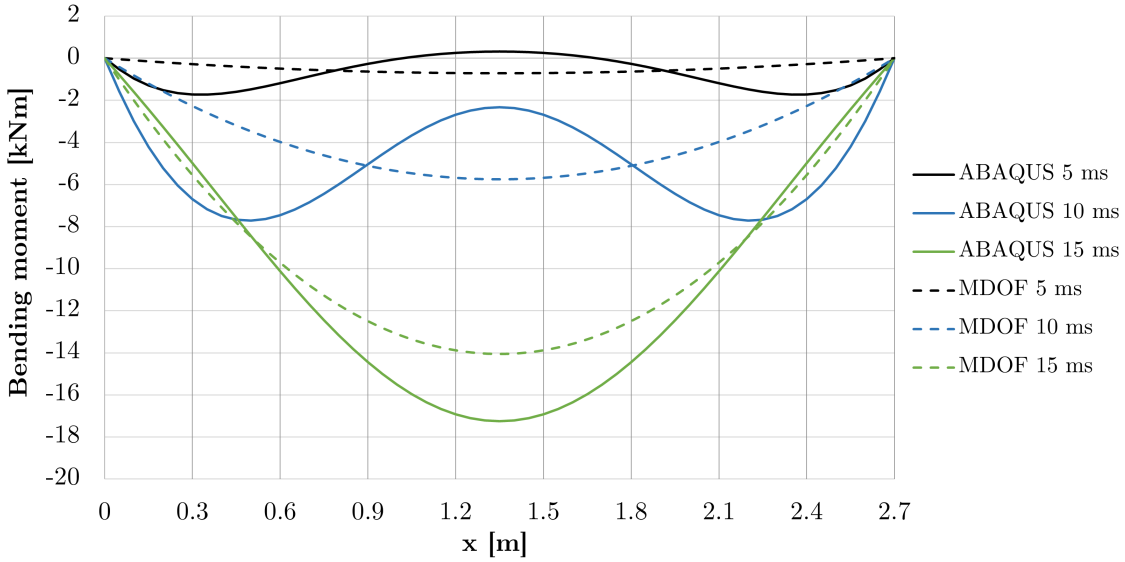

Figure 4.8: Elastic bending moment for the inner layer of Wall B subjected to L1.

The moment envelope is illustrated in Figure 4.9. All models yield similar results in the mid portion, whereas the simplified models display a lower moment close to the supports. This is caused by the deformation shape not being parabolic in the initial phase of the response for the FE analysis. This results in concentrated moments close to the supports.

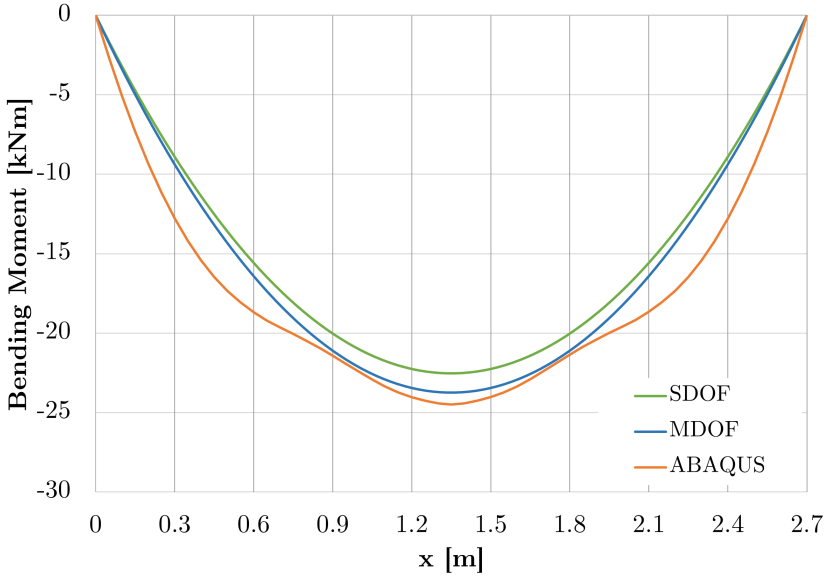

Figure 4.9: Elastic moment envelope of the inner layer of Wall B subjected to L1.

4.1.4.2 Elastic Shear Force

The shear force during the initial phase of the response is illustrated in Figure 4.10. The MDOF model underestimates the initial shear force compared to the finite element analysis. The Abaqus model indicates a concentration of shear force at the supports. The shear force is the derivative of the bending moment and is hence

also dependent on the deformation shape of the wall segment. Since the simplified models do not account for complex deformation shapes, the models can not capture the more complex behaviour seen in Abaqus.

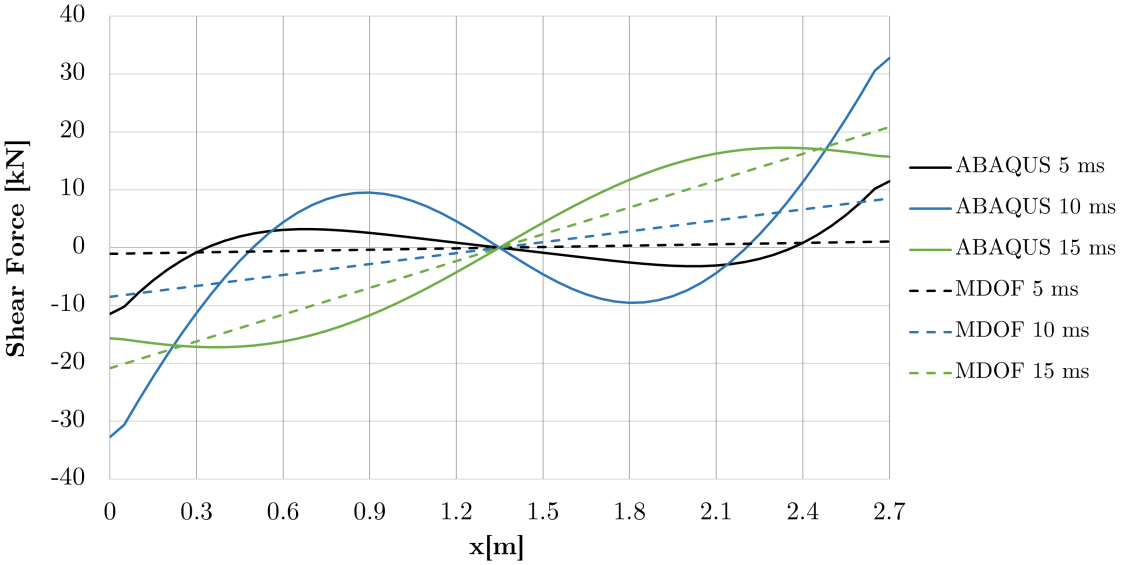

Figure 4.10: Elastic shear force for the inner layer of Wall B subjected to L1.

The envelope shear force is illustrated in Figure 4.11. The simplified models underestimate the shear force considerably when compared to the Abaqus model. Both SDOF and MDOF can not account for the more complex behaviour of the inner concrete layer. This seems to affect the displacement, bending moment and shear force along the beam. The discrepancy between the models is small when looking at displacements but is magnified when studying bending moments and shear forces.

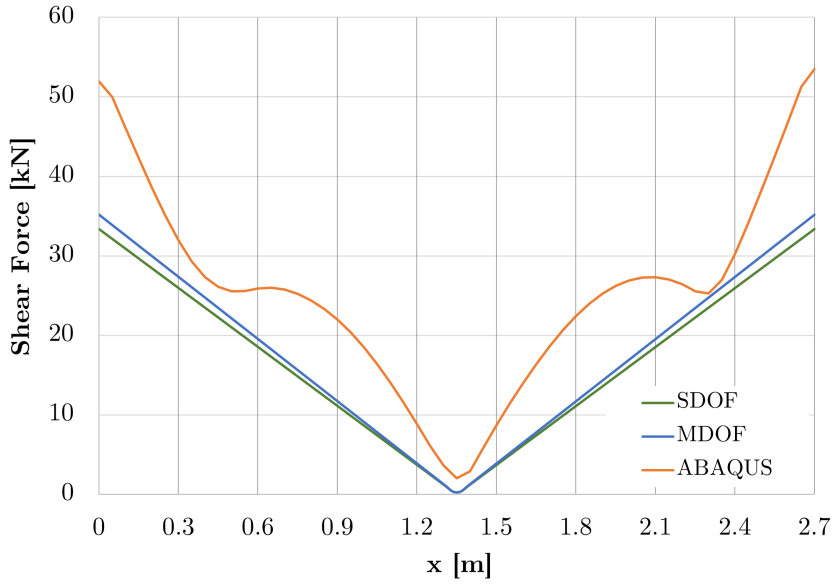

Figure 4.11: Elastic shear force envelope for the inner layer of Wall B subjected to L1.

4.2 Energy balance

The energy distribution for the two simplified models and the Abaqus model was investigated for wall configuration B subjected to load L2. The external and internal work of each model was analysed by studying the external and internal forces of the systems. This enabled the visualisation of how the internal energy distribution changes with time. The methodology is described in Section 3.5.2.

4.2.1 SDOF

Figure 4.12 presents the external and internal work of the SDOF system. The blue area in the figure corresponds to the external work that arises from the applied impulse. The red area is the internal work that is generated by the resistance of the structure. Energy balance is fulfilled as the areas for external and internal work are equal. The resisting force increases linearly until it reaches the elastic limit and is then constant.

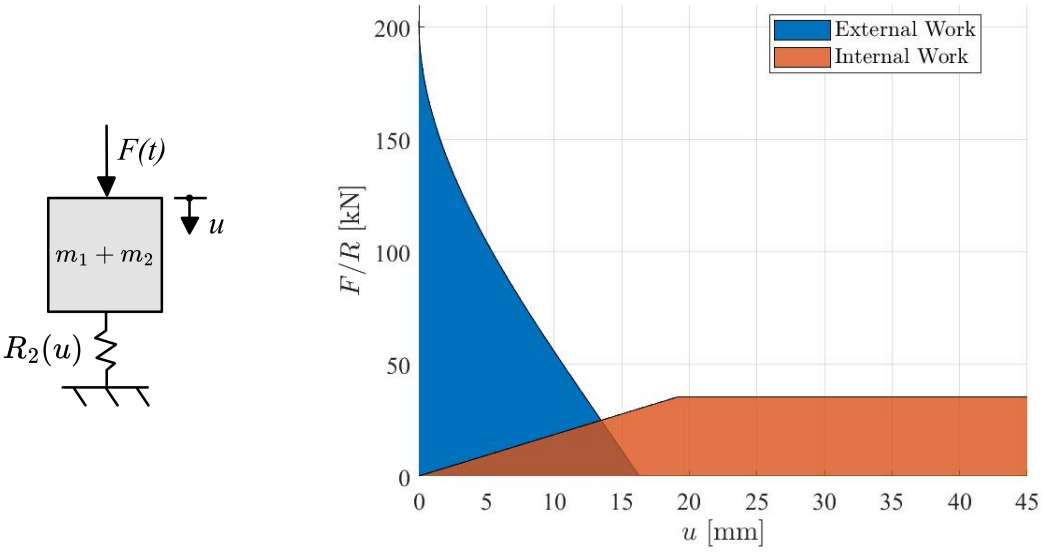

Figure 4.12: Energy balance for Wall B and load L2, utilizing SDOF model.

The displacement, velocity and energy distribution for the SDOF model are shown in Figure 4.13. Initially, the velocity increases rapidly as the load is applied to the mass. The high velocity of the mass causes high kinetic energy. During the first 10 ms of the response, kinetic energy dominates the energy distribution. Potential energy is introduced to the system as the mass starts to move. The potential energy corresponds to the internal strain energy caused by the elastic displacement of the mass. The potential energy increases until the spring exhibits its maximum resisting force and starts to yield.

The total external work reaches its limit as the load is removed from the model. The external work is balanced by kinetic, potential and dissipated energy. The initially

high kinetic energy is transformed into potential and dissipated energy as the mass moves. Elastic displacements cause potential energy while yielding of the spring causes dissipation through plastic deformations. The dissipation of energy stops as the maximum displacement of 45 mm is reached at a time of 38 ms. This occurs as the internal and external work in Figure 4.12 are equal. This means the external work is balanced by potential and dissipated energy at maximum displacement. Simultaneously, the velocity is zero and the mass starts to sway back. The elastic energy shifts between potential and kinetic energy as the mass oscillates.

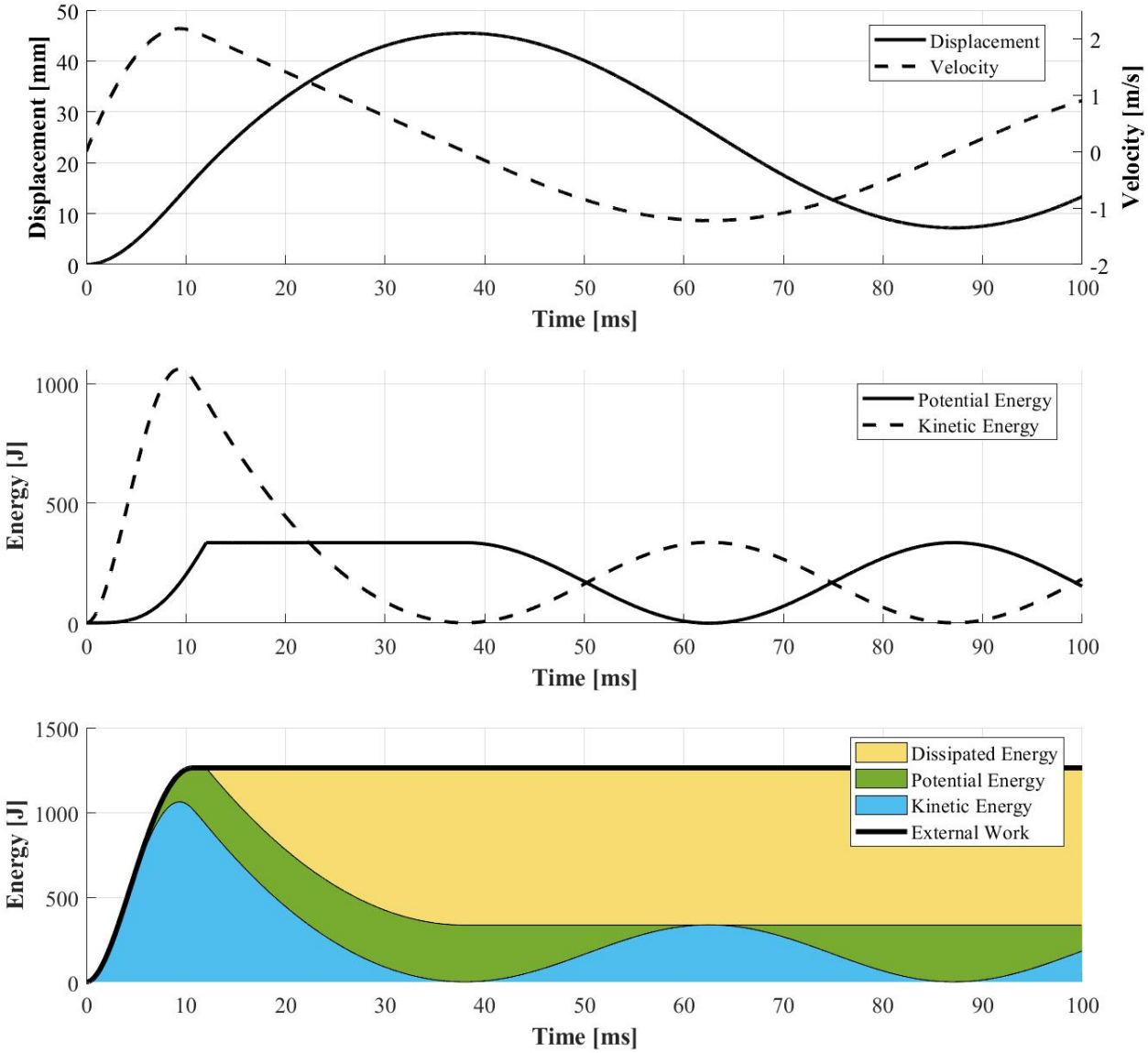

Figure 4.13: Displacement, velocity and energy distribution with combination of SDOF, Wall B and load L2.

4.2.2 MDOF

Figure 4.14 illustrates the energy balance using the MDOF model. The external force acting on the light outer concrete layer results in large displacements and more external work introduced into the system. Hence, the blue area in Figure 4.14 is larger compared to the SDOF model in Figure 4.12. The energy balance is achieved by the additional contribution of the insulation, where the external work equals the sum of the internal work. Since the response, R_2, is defined similarly for the SDOF and MDOF model, the internal work in Figure 4.12 and 4.14 have equal appearances.

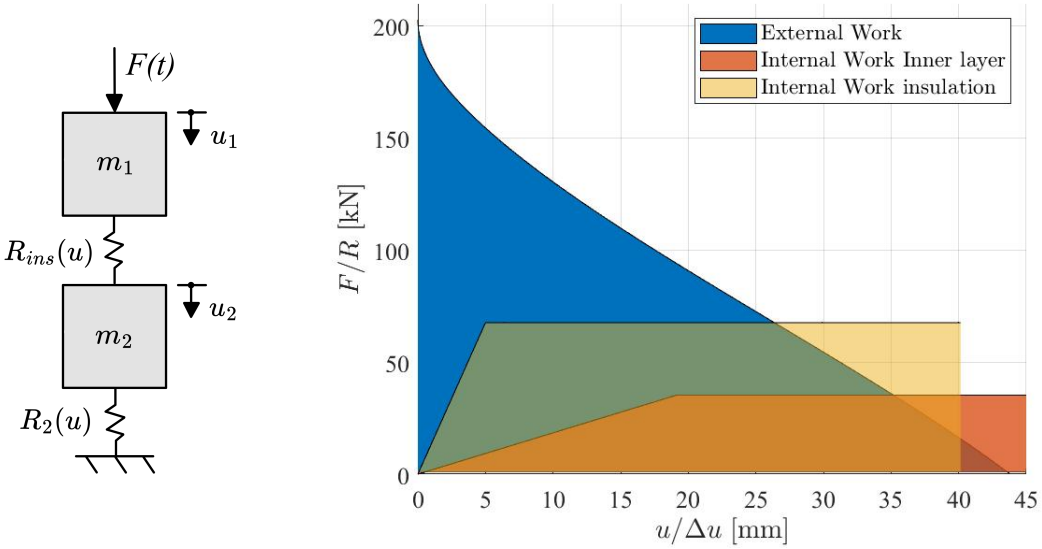

Figure 4.14: Energy balance for Wall B and load L2, utilizing MDOF model.

The energy balance of the MDOF model is summarized in Figure 4.15. There are pronounced differences compared to the SDOF model. The intermediate spring representing the intermediate layer causes a delay in displacement and velocity of the inner mass m_2. The mass representing the outer layer exhibits a high velocity and large displacement as the load is applied. In Figure 4.15, the kinetic energy of mass m_1 and dissipation in spring R_{ins}, dominates the energy distribution of the initial phase.

Movement of the heavier mass, m_2, is initiated as the load is transferred through the spring. The motion of the inner mass will similarly to the SDOF model cause kinetic, potential and dissipated energy. Dissipation of energy dominates the energy distribution as time elapses. The increased external work in the MDOF model is mostly dissipated through plastic deformation of the insulation layer. The remaining energy in the system shifts between the kinetic and potential energy of the masses in the system.

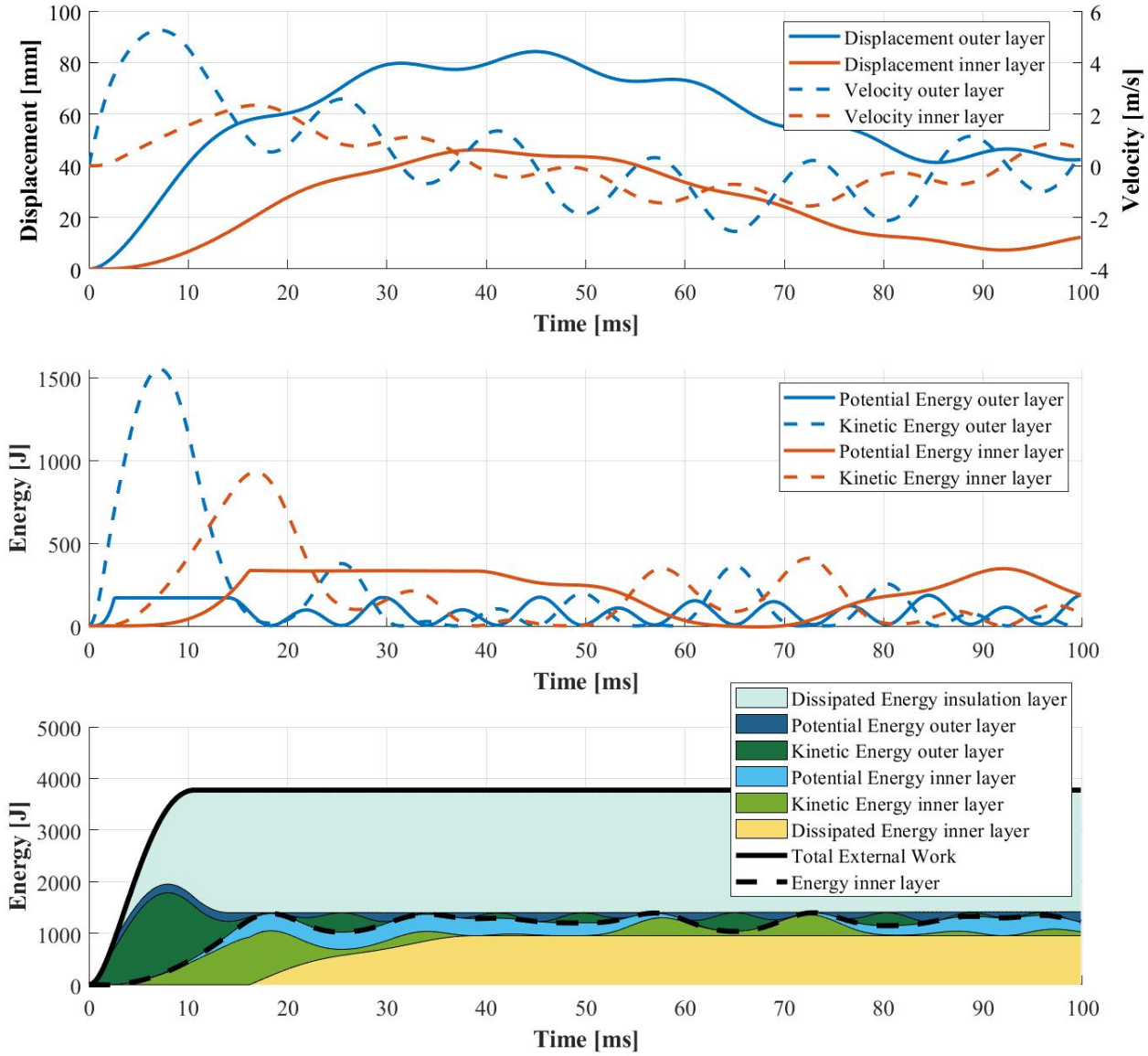

Figure 4.15: Displacement, velocity and energy distribution with a combination of MDOF, Wall B and load L2.

4.2.3 FEM

The energy distribution found using the FE model in Abaqus is illustrated in Figure 4.16. Abaqus display a similar response to the MDOF model. Both exhibit large external work compared to SDOF and the internal energy is dominated by dissipation in the insulation layer. However, Abaqus yield a larger total energy compared to MDOF. The Abaqus model has a similar distribution over time as the SDOF and MDOF models, where the kinetic energy is initially large and later transformed into dissipated energy and potential energy. The inner layer exhibits additional plastic deformation as the concrete layer sways backwards at approximately 78 ms.

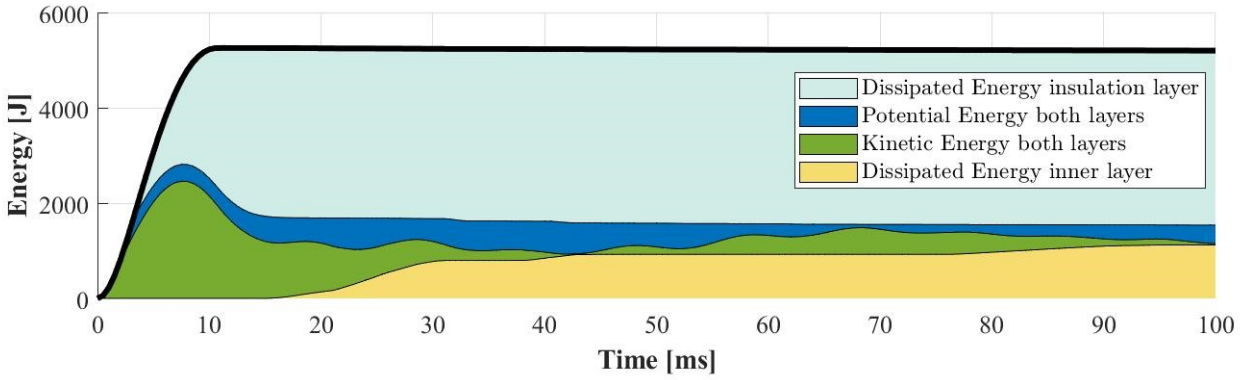

Figure 4.16: Energy distribution with combination of FEM, Wall B and load L2.

4.3 Transferred impulse

The propagation of load is analysed in the following section. The applied load is compared to the internal resisting forces in each model. The section also illustrates how the force characteristics change within the structure.

4.3.1 SDOF

The load is applied to the SDOF model as illustrated in Figure 4.17. This will cause a motion of the mass that compresses the spring and generates resisting forces. The motion is slow due to the high mass and its inertia effect. This causes the resisting force to increase gradually. The maximum resisting force is reached when the spring starts yielding, limiting the magnitude of the force to the supports.

The impulse is defined as the integral of the load-time function. It can be observed that the duration of the applied load is short compared to the required time for the response function to transfer the same impulse to the supports. The impulses are equal as the areas in Figure 4.17 are the same. This corresponds to the time of maximum displacement and when the load transferred to the support starts decreasing.

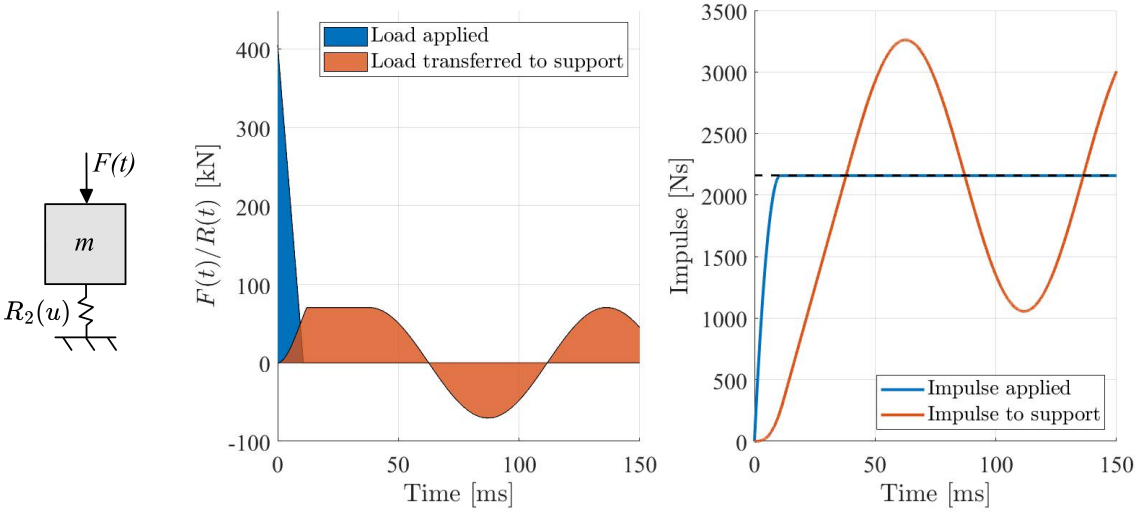

Figure 4.17: Load and impulse transfer using SDOF model.

The applied impulse and the impulse to support are equal as the lines intersect in the impulse-time graph in Figure 4.17. The same load is experienced in both directions meaning the mass is in equilibrium. At this time, the velocity of the mass is zero since the mass has no momentum. This is also seen in Figure 4.13, where the system's kinetic energy is zero at the time of maximum displacement.

4.3.2 MDOF

The MDOF model transfers the impulse through one additional layer, R_{ins}. The load is directly applied to the mass representing the outer concrete layer. The load is then transferred through the spring, R_{ins}, to the mass of the inner concrete layer. Lastly, the load reaches the supports through the resistance force of the spring R_2.

The inner layer represented by the mass m_2 and the response R_2 will be subjected to the force from R_{ins}, instead of the external force directly. The inner layer will therefore experience a load with a smaller magnitude but increased duration, compared to mass m_1 subjected to load $F(t)$. The load to the supports is similar to the SDOF model, with a more uneven appearance caused by the oscillating force in R_{ins}.

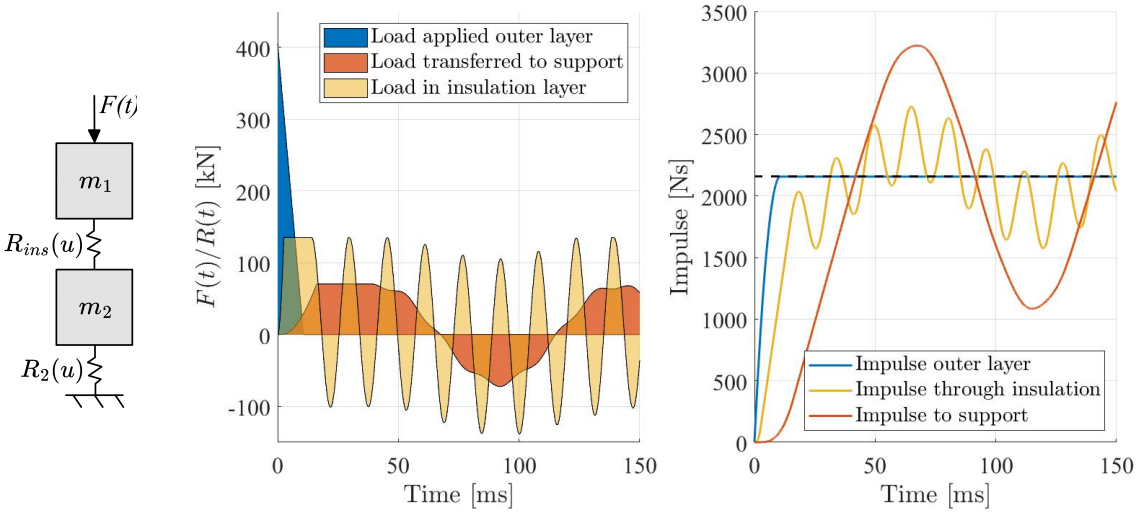

Figure 4.18: Load and impulse transfer using MDOF model.

Similarly to the SDOF model, the intersections of the impulse-time curve in Figure 4.18 are connected to the momentum and kinetic energy of each component. As the impulse through the insulation intersects the impulse on the outer layer, the velocity and kinetic energy of the mass m_1 is zero. Similarly, the inner layer has no velocity when the impulse through the insulation is equal to the impulse to the support.

4.3.3 FEM

Similar to the MDOF model, the FEM model transfers the applied impulse through multiple layers. The maximum magnitude of the transferred load in the intermediate layer and the general shape of the response function are similar to the MDOF model. The load transferred to the support undergoes a decrease after 30 ms. This decrease coincides with the tensile force in the insulation layer. The FE analysis considers the full section of the wall segment and is hence able to capture differences along the length of the element. The impulse might therefore be affected by the more complex movement, causing the different pattern of the impulse through the insulation layer in Figure 4.19. The transferred impulse to the supports has a more disturbed pattern compared to the response function of the MDOF model.

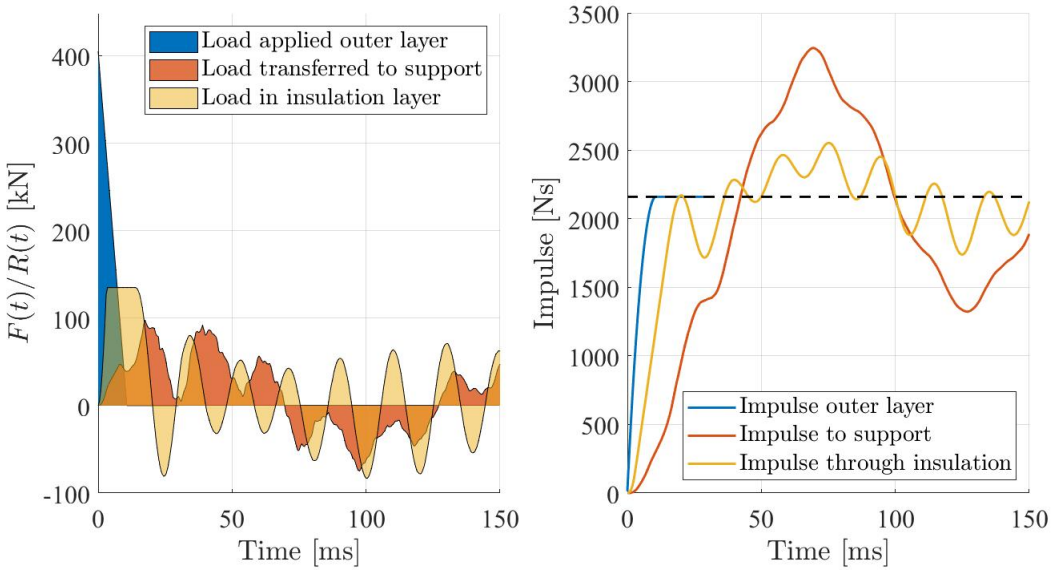

Figure 4.19: Load and impulse transfer using Abaqus.

4.4 Discussion

Comparing all three models displays an overall high correlation when studying mid-displacement and response of the wall configurations. The largest deviation in mid displacement was found when studying wall configuration C. For this case, the simplified models produced larger midpoint displacements compared to Abaqus. The difference can originate from the simplified models neglecting the stiffness of the outer concrete layer. For Wall C, the outer layer consists of a considerable portion of the total concrete thickness and neglecting the stiffness might be overly conservative. The MDOF and Abaqus model exhibit more similarities compared to the SDOF model. Both models can capture behaviours that the SDOF model cannot. For instance, the colliding of concrete layers and a delay in movement of the inner load-bearing layer.

The loads were chosen to get three levels of loading. This enabled the visualization of both an elastic and elasto-plastic response. Subjecting the structures to severe loading, L3, resulted in large deformations exceeding the plastic rotational capacity of the inner load-bearing layer. Therefore, failure can be expected for this load magnitude. According to Johansson & Laine (2012b), there are large discrepancies in rotational capacity when utilizing different calculation codes. Hence, it is difficult to assess when the structure will fail with regard to rotational capacity during impulse loading.

The difference between models gets more pronounced when analyzing boundary cases of insulation properties. When the insulating layer consists of a material with a low yield stress, MDOF and Abaqus display similar behaviour, where the intermediate material is too soft to resist the layers from colliding. The time of collision is different for the models. This can originate from the complexity of the respective model. In the MDOF model, the concrete layers are assumed to compress the insulation layer uniformly. This is not the case in Abaqus, where the shape of each layer is described separately. The load transfer between the concrete layers is more complex in Abaqus, leading to a slight difference in response. Additionally, the stiffness of the outer layer is accounted for in Abaqus. This can explain the delay in collision since the bending stiffness of this layer counteracts the compression of the insulation at the midpoint. In the case of a high yield limit, the insulation layer has a fully elastic response. A combination of high yield stress and low modulus of elasticity results in an increased mid displacement. However, this combination of material properties is not reasonable since a high yield stress is presumed to correlate with a high modulus of elasticity.

It was observed that the bending moment and shear along the wall element deviated between models. According to Johansson (2015), the number of eigenmodes is vital when describing moment and shear. For deflections, the first mode has a significant impact. Analysing moment and shear requires additional modes to get an accurate representation. Since the SDOF and MDOF models are based on the first eigenmode when deriving transformation factors, these models are best suited for describing deflection. If sectional forces are of interest, a FE model can describe a more complex behaviour since it can account for additional eigenmodes. Johansson (2015) also states that more intense impulses, with high peak pressure and short duration, magnify the significance of higher eigenmodes. A possible failure mode for an impulse-loaded wall is direct shear, caused by initial high shear forces at the supports. From the envelope shear distribution, see Figure 4.11, it is shown that the simplified models do not capture this effect and underestimate the shear force at the supports.

Section 4.2 displayed a difference in energy balance between SDOF, MDOF and Abaqus. The amount of external work depends on the mass on which the applied impulse acts. For the SDOF model, the load acts on the total mass, resulting in low external work induced into the system. For MDOF and Abaqus the applied load acts on the light outer layer. A low mass combined with soft insulation results in a large amount of induced energy through external work. For the studied case the increase is mostly consumed by plastic straining in the insulation layer. The inner layer is hence only experiencing a portion of the external work. Reducing the amount of energy that enters the inner layer can help minimize its deformation. This is further studied in Chapter 5.

The load transferred to the support is similar for SDOF and MDOF, while Abaqus display a more disturbed load transfer. This can originate from the effects of rapid loading. The simplified models are based on a deformation shape from static loading, while the actual deformation when subjected to impulse load can be different. Rapid loading might cause a complex deformation shape along the element, causing a more disturbed load transfer. Abaqus can capture this behaviour while SDOF and MDOF cannot. The Abaqus and MDOF models can reduce the peak of the transferred load by considering the maximum resistance of the insulation. The inner layer experiences a lower peak pressure for a longer duration, compared to the SDOF model where the load is directly applied to the mass. Additionally, the required time for the load to reach the support is slightly longer for MDOF and Abaqus. This is favourable since the maximum load level on the inner layer is reduced.

All models capture the overall behaviour similarly, where the MDOF and Abaqus models display a more detailed response. The models are based on simplifications and it is difficult to evaluate how well the models represent a real concrete sandwich wall. The models can describe the behaviour of a structure with varying mass and stiffness along its cross-section. Simplifying the wall not to include shear connectors will affect the response of the cross-section. They may provide composite action which would change the behaviour of the structure significantly. Additionally, the shear connectors are expected to strengthen the compressive resistance of the intermediate layer. A possible way to account for this strengthening could be to use an effective stiffness where the strength and stiffness of the shear connectors are included. This would further increase the complexity of the MDOF model and may introduce composite action when modelling shear connectors in Abaqus. The accuracy of the simplified models might therefore be affected since they do not account for the composite behaviour of the inner and outer concrete layers. Overall, each respective model has its strengths and weaknesses. A summary of the general advantages and disadvantages are presented in Table 4.3.

Table 4.3: Advantages and disadvantages of models.

Model	Advantages	Disadvantages
SDOF	• Simple • Mostly accurate	• Loss of accuracy for certain geometries • Neglects insulation effects • Underestimates sectional forces • Does not describe failure
MDOF	• More detailed than SDOF • Accounts for insulation effects • Quick and easy to adapt	• Loss of accuracy for certain geometries • Underestimates sectional forces • Does not describe failure
Abaqus	• 2D visualization of response • Accounts for more eigenmodes • Describes sectional forces more precisely • Complexity of model can be increased and adapted	• Can be hard to interpret • Small additional benefits compared to MDOF • Computationally less efficient

5

Parametric Study

The response using different insulation properties is investigated to find the parameters resulting in the most favourable structural response, indicated by minimized displacements. A parametric study including the effects of yield stress, elastic modulus and thickness of the intermediate layer is presented in this chapter. The material properties generating the most favourable effects are used to compare the optimized response to the unoptimized wall composition.

5.1 Effects of insulation yield stress

The different wall configurations display a similar behaviour when analysing a range of yield stresses. Each configuration has a pronounced reduction in mid displacement for a specific yield stress, see Figure 5.1. The optimized yield stress allows the inner and outer layers to compress the insulation to its maximum, without causing collision. A weaker insulation allows for an excessive movement of the outer layer, causing a collision of concrete layers. A high yield stress does not allow for plastic deformations and energy dissipation. Hence, the optimal yield stress corresponds to the yield limit allowing full compression of the intermediate layer without collision of the inner and outer concrete layer.

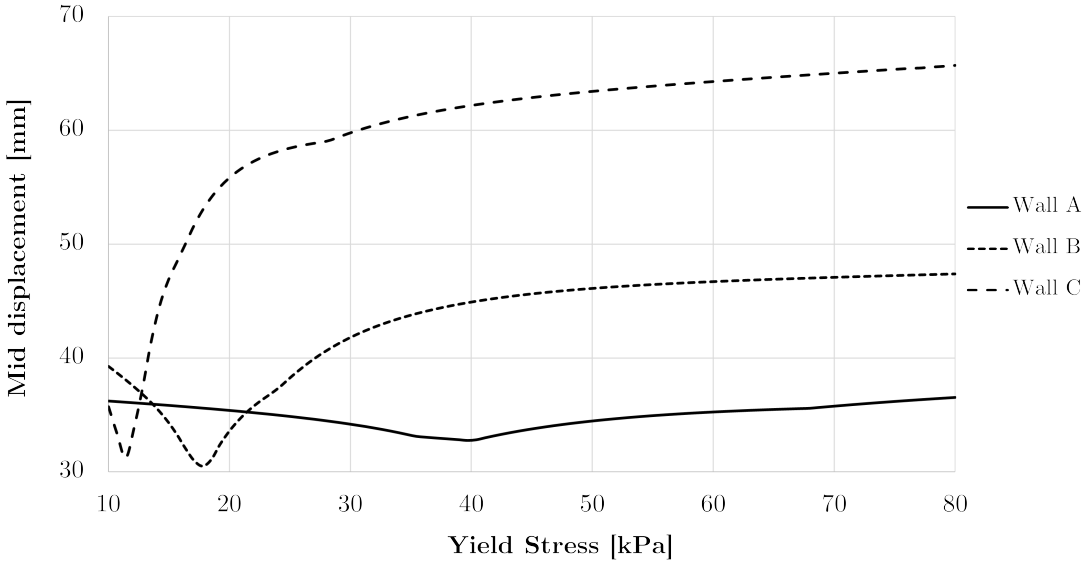

Figure 5.1: Mid displacement for varying insulation yield stress. The modulus of elasticity is assigned to 2 MPa, while the walls are subjected to load L2.

The deflections illustrated in Figure 5.1 display a large discrepancy between wall configurations for unoptimized yield stresses. However, they display similar mid-point displacement when equipped with their respective optimal yield stress. Wall B and C experience a slightly smaller mid displacement than Wall A, although the load-bearing inner layers are less stiff. The benefit of an optimized insulation layer is hence greater for wall configurations B and C compared to A. The result is case-specific, meaning other wall configurations have different optimized values for the same load. Hence, the optimal yield stress is sensitive to wall geometry and load magnitude.

The mid displacements with optimized values are presented in Table 5.1. The results from Abaqus are included to confirm the results, even with optimized values. Abaqus displays a similar reduction in mid displacement as the MDOF model. It is evident that a structure with a heavy outer layer, such as Wall C, experiences a greater reduction of maximum deflections. Compared to a structure with mass and stiffness concentrated at its inner layer, similar to Wall A.

Table 5.1: Displacements for the respective wall with optimized yield stress, subjected to load L2.

Mid Displacements [mm]			
	A	B	C
MDOF Unoptimized	34.4	46.0	63.0
MDOF Optimised	**32.8**	**30.5**	**31.2**
ABAQUS Unoptimised	35.6	45.6	54.1
ABAQUS Optimised	**33.5**	**31.5**	**32.0**

The magnitude of the load affects the optimal yield stress. This is visualised in Figure 5.2 where the optimal yield stress is plotted against impulse density. The impulse density is calculated for a fixed load duration of 10 ms, meaning the peak pressure is changed to obtain the presented impulse density. The optimal yield stresses displayed in Figure 5.1 can be observed in Figure 5.2 at 800 Pas, corresponding to load L2. It is observed that the optimal yield stress increases with increasing impulse density. Wall A has a significant spread in optimal yield stress, while Wall C displays a smaller spread. Worth noting is that the lower load densities have an optimal yield stress below the lower bound limit in Table 3.2. The effect of utilizing the optimal yield stress for varying impulse densities is further analysed in Section 5.4.1.

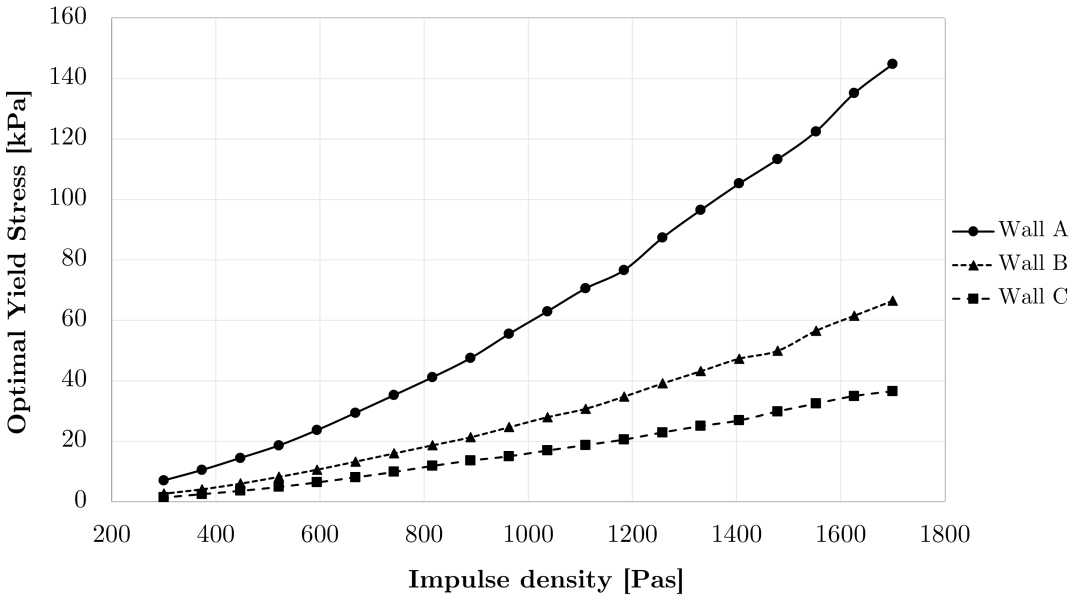

Figure 5.2: Optimal yield stress as a function of impulse density.

5.2 Effects of insulation Modulus of Elasticity

The midpoint displacement for varying modulus of elasticity is illustrated in Figure 5.3. All wall configurations indicate similar behaviour where a high stiffness results in smaller displacements. The effect of an optimized modulus of elasticity has less impact on the structural response compared to yield stress. The modulus of elasticity does not influence the plastic straining directly. Instead, it governs the elastic part of the response. A low modulus of elasticity allows larger deformations before yielding occurs in the insulation. The allowed elastic displacement before yielding is hence influenced.

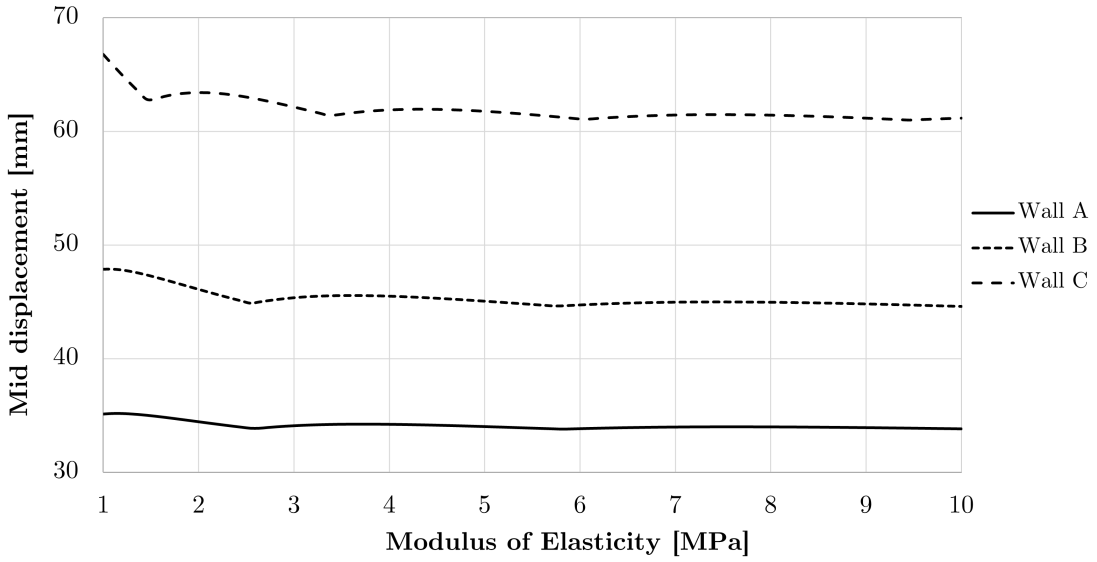

Figure 5.3: Mid displacement for varying insulation modulus of elasticity. The yield stress is assigned to 50 kPa, while the walls are subjected to load L2.

Figure 5.3 indicates a step-wise decrease of mid displacement as the modulus of elasticity increases. The local minimums coincide with the values where the global swaying of the structure is counteracted by the smaller oscillation caused by the interaction between the two concrete layers. The analysis shows that a stiff material is desirable to minimize the mid-point deflection. An intermediate layer with increased stiffness will reduce the allowed limit for elastic compression of the insulation. Plastic dissipation of energy will therefore occur for smaller deformations. This is considered a desirable trait when reducing the maximum mid displacement through plastic deformation of the intermediate layer.

5.3 Effects of insulation thickness

Increasing the insulation thickness allows for large compression and increased energy dissipation in the intermediate layer. Increasing the thickness will affect the optimal yield stress since the geometry allows for larger deformations. The effect of the optimal yield stress for a range of insulation thicknesses is illustrated in Figure 5.4. Wall A displays a larger variation in optimal yield stress for varying thicknesses, while the other wall configurations display a smaller spread. This is similar to the studied case in Figure 5.2 where the optimal yield stress is compared for different impulse densities.

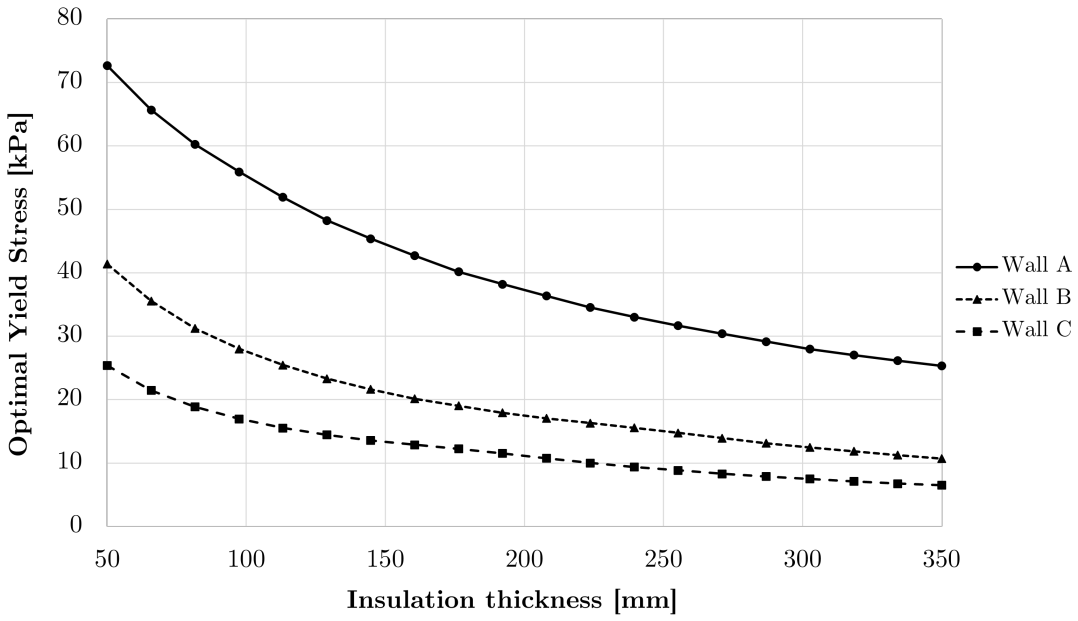

Figure 5.4: Optimized yield stress for varying insulation thickness. The modulus of elasticity is assigned to 2 MPa, while the walls are subjected to load L2.

An increased insulation thickness can reduce the mid deflections. Wall A is less sensitive to the insulation thickness, while Wall C experiences a large reduction in displacements for an increasing thickness. The mid deflection for different insulation thicknesses is illustrated in Figure 5.5. The gradients in the figure are large for intermediate thicknesses, while smaller for thin and thick insulation. This is especially pronounced for Walls B and C. The positive effect is hence not linearly increasing. Additionally, the effect is limited to the material parameters, where the optimal yield stress is low for large insulation thicknesses.

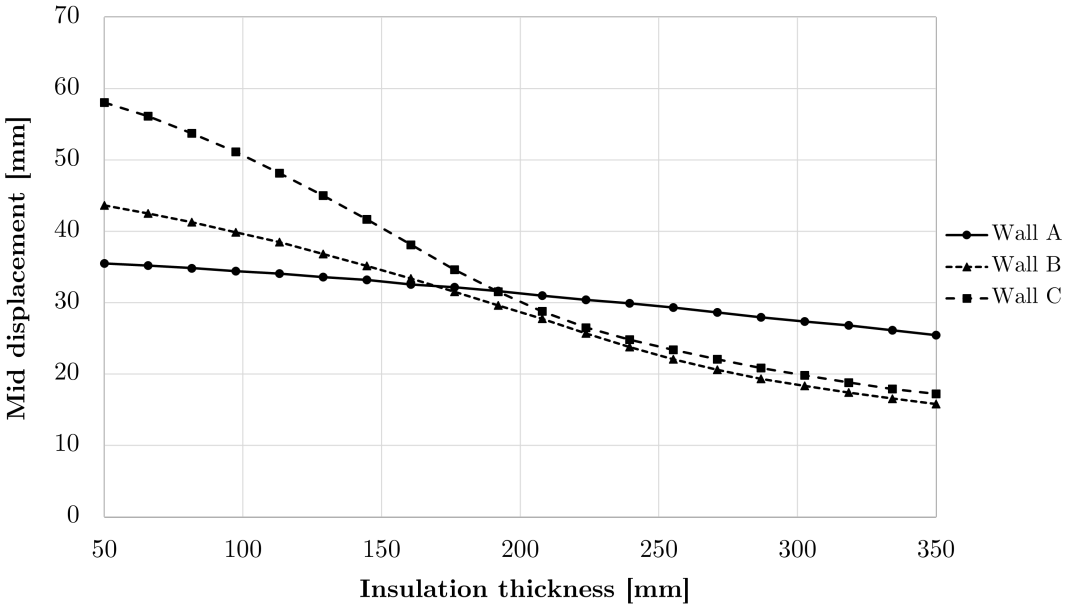

Figure 5.5: Mid displacement for varying insulation thickness. The modulus of elasticity is assigned to 2 MPa, while the walls are subjected to load L2.

An increased insulation thickness allows for lower yield limits of the insulation layer. This is desirable since a greater amount of energy can be dissipated through plastic straining of the material. The optimal insulation thickness is therefore connected to the yield limit of the insulation material. It is not beneficial to increase the insulation thickness if the yield limit cannot be decreased to allow for additional plastic deformation.

5.4 Effects of optimized material properties

Wall B is reanalysed using the optimized material properties presented in Section 5.1 and 5.2. The results from the comparison in Chapter 4 are used to show how optimizing the intermediate layer influences the response of the structure. The mid displacement, energy distribution and transferred impulse are studied in the following sections. The insulation thickness is not modified.

5.4.1 Mid displacement

The response with optimized properties is presented in Figure 5.6. Table 4.1 shows a maximum deflection of 46 mm for the same load and geometry. Utilizing the optimized properties is, for this case, able to reduce the maximum deflection by 33 %. The MDOF and Abaqus models display similar effects when changing the material properties. In Figure 5.6 it is observed that the maximum deflection is both reduced and delayed. Previously the maximum deflection occurred at approximately 38 ms and is now delayed to 50 ms for both the MDOF and Abaqus model.

The load transfer and the time of maximum deflection are further described in Section 5.4.3.

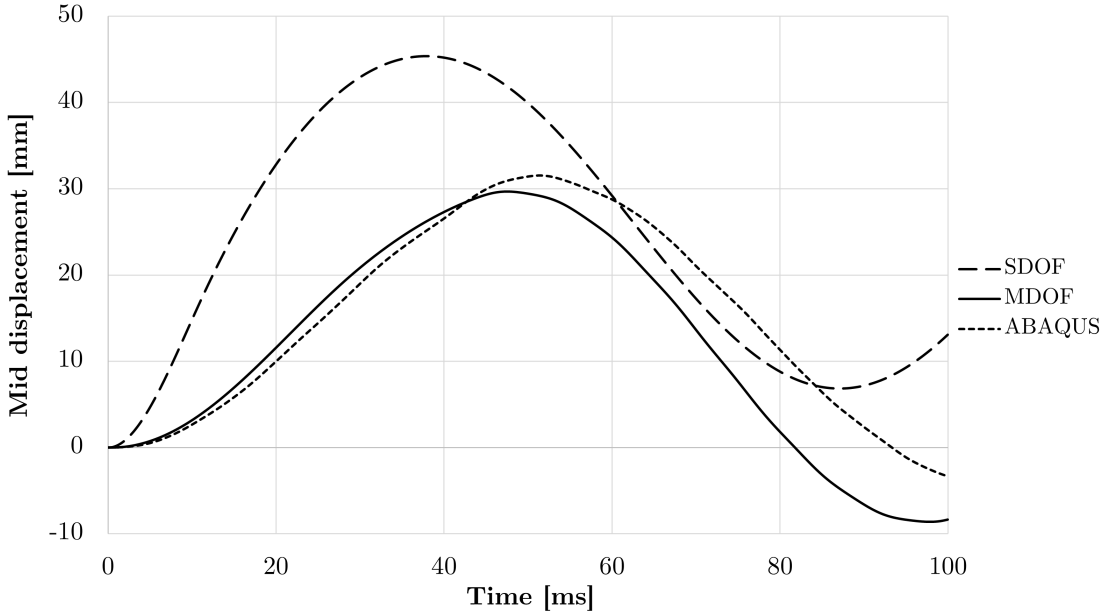

Figure 5.6: Effects of optimized yield stress for Wall B subjected to Load L2.

The unoptimized and optimized response for different load intensities is illustrated in Figure 5.7 and 5.8 respectively. For the unoptimized case, wall configuration A displays the lowest displacements. After optimization, all wall configurations experience a reduction in displacement. For low impulse densities, the structures display similar displacement. Wall B and C are hence reduced more compared to wall configuration A. The optimized yield limits used in Figure 5.8 are shown in Figure 5.2.

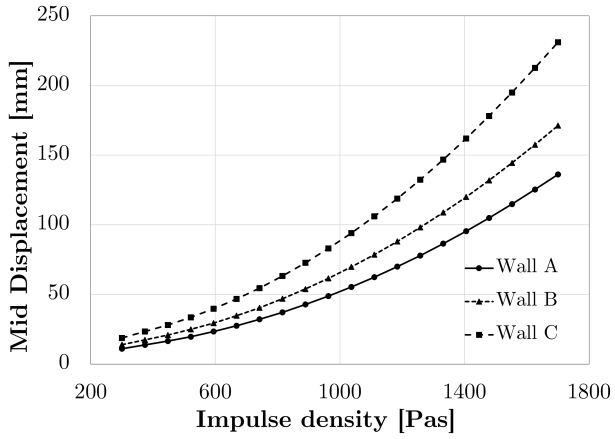

Figure 5.7: Unoptimized displacement using SDOF model.

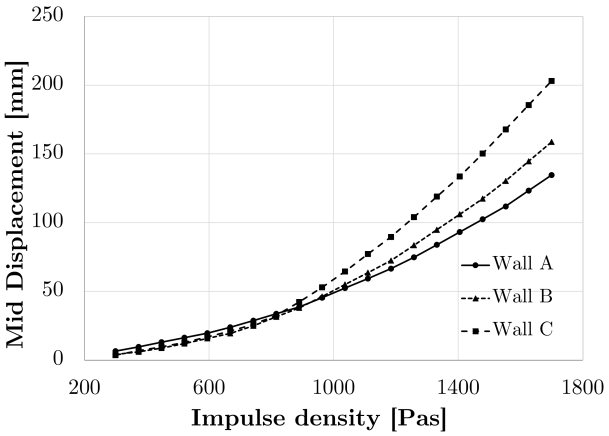

Figure 5.8: Optimized displacement using MDOF model.

Figure 5.9 illustrates the favourable effects for varying load intensities and wall configurations. The reduction is determined by comparing the response of the optimized MDOF model to the SDOF model. It is shown that the favourable effect is most evident at low load magnitudes for structures with a mass concentration in the facade layer. Wall configuration C, when subjected to low load intensities, can reduce the maximum mid-deflection up to 80 % by accounting for the optimized insulation layer. The favourable effect is less prominent at higher load intensities. Wall A, with most of its mass located at the inner load-bearing layer, is less sensitive to the properties of the intermediate layer.

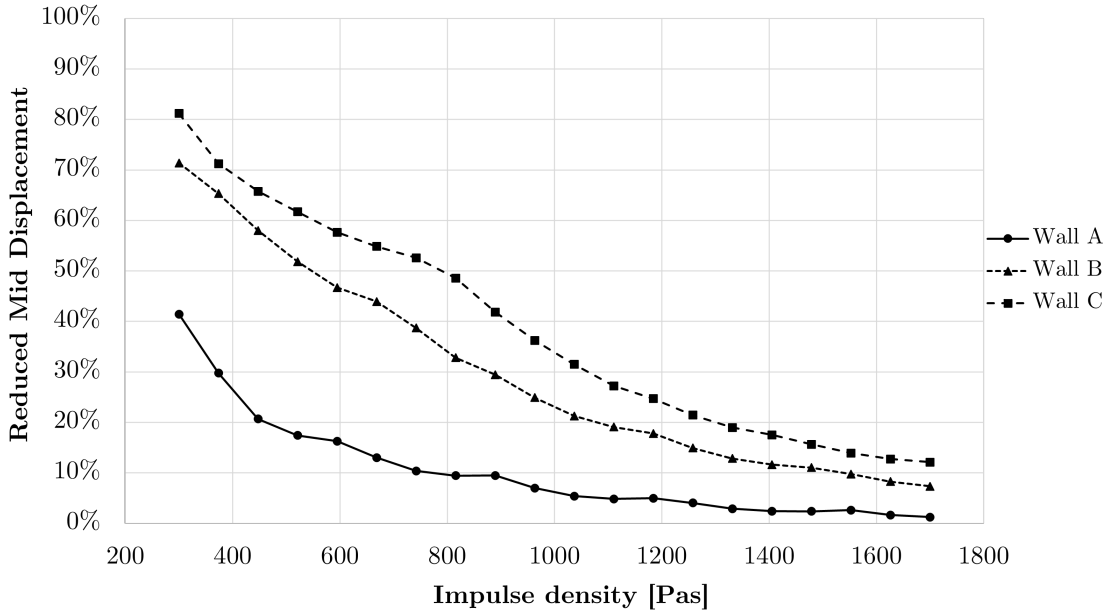

Figure 5.9: Reduction when optimizing yield limit and modulus of elasticity, MDOF compared to SDOF.

5.4.2 Energy distribution

The optimized energy distribution of wall configuration B subjected to load L2 is presented in Figure 5.10. The original unoptimized distribution is illustrated in Figure 4.15. The external work and the dissipated energy in the intermediate layer are increased. On the other hand, the energy content in the inner load bearing concrete layer is decreased. For the optimized structure, the outer and inner concrete layers almost collide. This is seen in Figure 5.10, where the difference in displacement of the outer and inner layer is just below the limit for collision described in Section 3.3.2.1.

The amount of kinetic energy in the outer layer is almost doubled in the initial phase of the response, compared to the unoptimized analysis. This is explained by the reduced yield stress, causing a lower resisting force acting on the outer mass. Similarly the potential energy of the outer layer is low since the insulation has a reduced ability to generate large forces. Instead of storing potential energy, it is dissipated through plastic deformations in the intermediate layer.

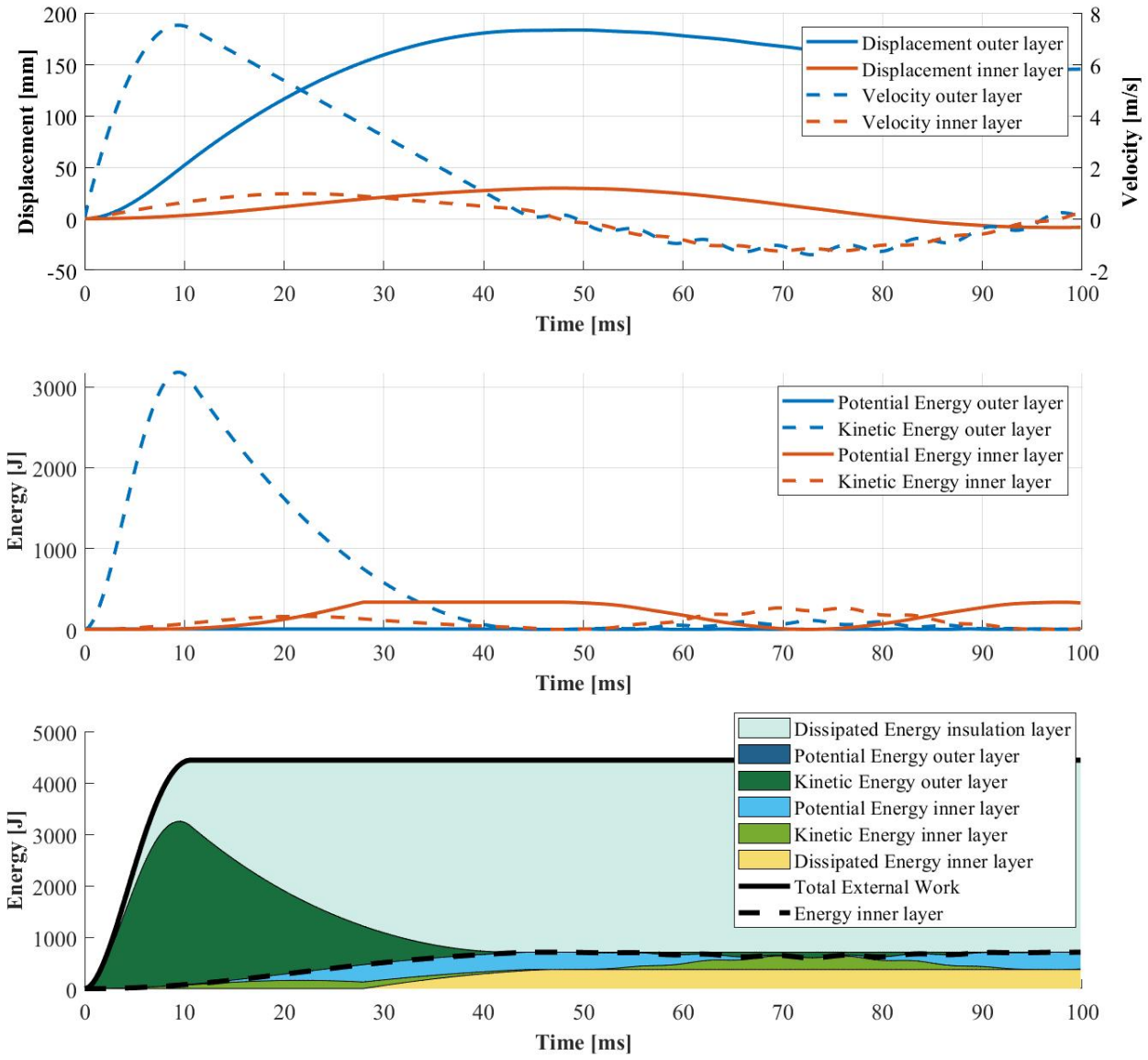

Figure 5.10: Optimized displacement, velocity and energy distribution with a combination of MDOF, Wall B and load L2.

5.4.3 Transferred Impulse

The transferred impulse of Wall B subjected to load L2 with optimized insulation properties is presented in Figure 5.11. The low yield stress results in small internal resistance forces of the insulation. This optimization reduces extreme force peaks transferred through the structure. The load on the inner layer is hence lower in magnitude but extends over a longer period, compared to the unoptimized response in Figure 4.18. The insulation exhibits compression until maximum deflection. This was not the case for the unoptimized wall, where the insulation experienced compression and tension before maximum deflection.

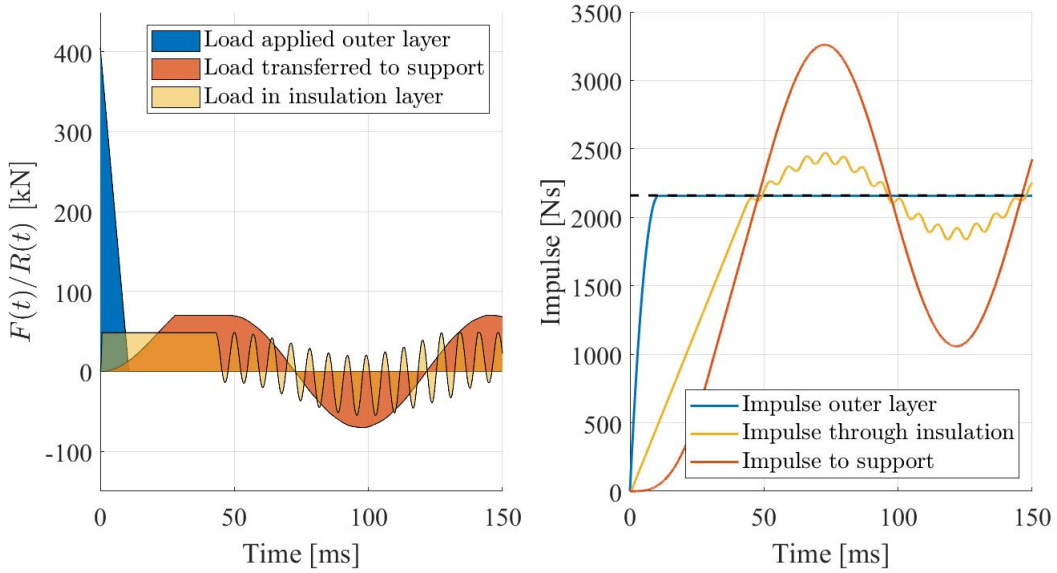

Figure 5.11: Load and impulse transfer with optimized insulation properties.

The low yield stress reduces the magnitude of the resisting force acting on the load-bearing layer. The magnitude of the load acting on the inner layer is much lower than the applied external force. The high modulus of elasticity increases the frequency of the oscillating behaviour in the insulation. The impulse-time graph shows that the load transferred to the support is delayed. A material with higher strength would transfer the impulse more quickly, similar to the case in Figure 4.18, while softer insulation would result in a collision, also causing rapid load transfer.

5.5 Discussion

When analysing the results from the parametric study, there was a noticeable trend, where Wall A was less affected by a change in the parameters of the intermediate insulation layer. This was true for the yield limit, modulus of elasticity and thickness. Wall C experienced a large favourable effect. Adapting and utilizing optimal parameters meant a large reduction in displacement. The total deflection was reduced to the same range as the much stiffer and stronger wall configurations.

The yield limit, modulus of elasticity and thickness of the intermediate layer all displayed different effects on the response. The favourable yielding required maximal compression to allow for dissipation while preventing the concrete layers from colliding. The insulation layer was modelled as elastic-plastic with an upper limit for collision. This way of modelling the plastic range is simplified and a gradual increase is expected during the densification of the polymeric foam, see Figure 2.11. Implementing a more detailed response to the material could increase the positive effect of the insulation further. The densification of the insulation could avoid collision of the layers and instead provide a smooth load transfer without a hard impact.

The modulus of elasticity and the thickness of the intermediate layer do not have a specific value where the response is most favourable, instead the parameters are favoured as high as possible. The elastic stiffness and the yield stress are presumed to correlate where a material with a low yield stress is expected to have a lower modulus of elasticity. There might therefore be a contradiction where both variables can not be optimized due to material limitations. Increasing the thickness of the layer is also limited to material parameters, where there is no additional benefit in increasing the layer thickness if the yield stress can not be decreased further.

The more pronounced reduction experienced by Wall C is partly explained by the energy distribution and the load transfer. The external work is low since the outer layer has a high mass. The dissipation through the insulation can hence account for a larger portion of the energy in the system. Wall C additionally has lower optimal insulation yield stress compared to Wall A. A low yield stress will prolong the load transfer and reduce the load peaks. This is shown to have a favourable effect.

According to Krundaeva et al. (2016), the strain rate highly influences the material response of the insulation. High strain rates result in higher stiffness as well as yielding limits. This means the static mechanical properties increase when the material is exposed to blast loads. The densification also occurs earlier, meaning the assumed maximum compression of 80 % may be less if the strain rate was considered. The optimized parameters may thus have to be adjusted, to accurately describe the dynamic mechanical properties.

A parameter that has not been covered is the thermal aspects of the intermediate layer. The insulation is used to reduce heat transfer and is thus chosen to do this most efficiently. This thesis does not analyse parameters such as thermal conductiv-

ity, which determines the insulating capabilities. The presented optimized insulation properties concerning blast mitigation, may not align with optimal thermal properties.

From the parametric study it is evident that many parameters influence the response of the structure and the positive effect of the insulation layer is therefore difficult to evaluate. The mass distribution of the cross-section has an essential impact, where a heavy outer layer magnifies the effect of the insulation. For a structure with a lighter layer the effects are not as pronounced. Considering and utilizing the effect might therefore be of importance when analysing a structure with a heavy outer layer, for instance a heavy concrete or brick facade. On the other hand, it might not be of importance to consider the insulation for a wall with a thin, light, metal sheet facade.

The optimal yield stress is for the analysed structures and load intensities found in the lower portion of the range in which EPS and XPS are produced. The low required yield stress of the intermediate layer might therefore be difficult to reach, especially if the shear connectors further increase the compressive strength of the layer.

6
Conclusion

This thesis aimed to describe the structural behaviour of a concrete sandwich wall subjected to impulse loading. The intermediate insulation layer was studied to find the properties resulting in the most favourable response. Allowing large plastic straining in the insulation, without collision of concrete layers, provides a desirable response. The MDOF and the Abaqus model correlated well and were able to account for the insulation effects, unlike the SDOF model.

The developed models display different advantages and disadvantages. The simpler SDOF model captures the overall behaviour but cannot account for the effects of the insulation. The MDOF model captures these effects, which is important to optimise the response. Utilizing simplified models is useful when analysing deflections, energy distribution and load transfer. However, these models do not capture and describe sectional forces as accurately as a finite element program.

The parametric study emphasises the benefit of an intermediate layer with optimized properties. Not considering the insulation might be an overly conservative approach for certain combinations of properties and loads. The benefit of the insulation has a larger impact on structures with a heavier outer layer subjected to lower load magnitudes. An intermediate layer with properties adapted to the geometry and load magnitude can reduce the deflection of the element by a considerable amount.

Utilizing the benefit of the insulation requires an accurate prediction of the load characteristics. Loads outside the span used in design will not experience the same beneficial effects. The optimal yield stress of the studied wall configurations is low, oftentimes below the material properties of EPS and XPS. Therefore, it could be suitable to utilize other materials or modified versions of polymeric foams with desired properties.

The analysis did not include shear connectors, which are expected to affect the cross-section's stress distribution and the intermediate layer's stiffness. Further studies including the effects of different combinations of shear connectors and the impact of composite action are of great importance to utilize the findings in this study. It is additionally of interest to validate the behaviour and the beneficial effects described in this study by experiments.

References

Abrahamsson, T. (2019). *Structural Dynamics and Linear Systems*. Chalmers University of Technology.

Al-Emrani, M., Engström, B., Johansson, M., & Johansson, P. (2019). *Bärande konstruktioner Del 1*. Chalmers University of Technology.

Anand, A., & Singhal, V. (2023). *Structural Behaviour of Precast Concrete Sandwich Panel: A Review*. Department of Civil and Environmental Engineering, IIT Patna, Patna, India. Springer Science; Business Media Deutschland GmbH.

Biggs, J. M. (1964). *Introduction to Structural Dynamics*. McGraw-Hill Book Company.

Bischoff, P. H., & Perry, S. H. (1991). Compressive behaviour of concrete at high strain rates. In *Materials and structures* (pp. 425–450, Vol. 24). Springer.

Cimellaro, G. P., & Marasco, S. (2018). *Introduction to Dynamics of Structures and Earthquake Engineering* (Vol. 45). Springer International Publishing.

Ekengren, B., Johansson, M., Leppänen, J., & Laine, L. (2005). *Dynamisk lastpåverkan Referensbok*. Räddningsverket.

Huang, Q., Hamed, E., & Gilbert, R. I. (2020). Behavior of Concrete Sandwich Panels under Eccentric Axial Compression—Testing and Finite Element Analysis. *ACI Structural Journal*, *117*(3), 235–247.

International Federation for Structural Concrete. (2013). *fib Model Code for Concrete Structures 2010*. Wilhelm Ernst & Sohn.

Johansson, M. (2000). *Structural Behaviour in Concrete Frame Corners of Civil Defence Shelters*. Chalmers University of Technology.

Johansson, M. (2015). *Beräkning av impulsbelastad konstruktion*. MSB.

Johansson, M., & Laine, L. (2012a). *Bebyggelsens motståndsförmåga mot extrem dynamisk belastning Del 1: Last av luftstötvåg*. MSB.

Johansson, M., & Laine, L. (2012b). *Bebyggelsens motståndsförmåga mot extrem dynamisk belastning Del 3: Kapacitet hos byggnader*. MSB.

Johansson, M., & Laine, L. (2019). Simulation of Concrete Wall Subjected to Airblast by Developing an Elastoplastic Spring Model in Modelica Modelling Language. *International Journal of Architectural and Environmental Engineering*, *13*(2).

Krundaeva, A., De Bruyne, G., Gagliardi, F., & Van Paepegem, W. (2016). Dynamic compressive strength and crushing properties of expanded polystyrene foam for different strain rates and different temperatures. *Polymer Testing*.

Mehta, P. K. (K., & Monteiro, P. J. M. (2014). *Concrete : Microstructure, Properties, and Materials*. McGraw-Hill Education.

Mlakar, P. F., & Barker, D. (2010). Blast Phenomena. In *Handbook for blast resistant design of buildings* (p. 161). John Wiley & Sons.

Munther, M., & Runebrant, J. (2018). *Structural Response of Concrete Beams Subjected to Drop Weight Impact*. Chalmers University of Technology.

Rahimidehgolan, F., & Altenhof, W. (2023). Compressive behavior and deformation mechanisms of rigid polymeric foams: A review. *Composites Part B: Engineering*, *253*.

Runesson, K., & Larsson, R. (n.d.). *CONSTITUTIVE MODELING OF ENGINEERING MATERIALS-THEORY AND COMPUTATION*. Chalmers University of Technology.

Sfer, D., Carol, I., Gettu, R., & Etse, G. (2002). Study of the Behavior of Concrete under Triaxial Compression. *Journal of Engineering Mechanics*, *128*(2), 156–163.

Simulia. (2006). ABAQUS Analysis User's Manual. https://classes.engineering.wustl.edu/2009/spring/mase5513/abaqus/docs/v6.6/books/usb/default.htm?startat=pt03ch06s03at07.html

Smilowitz, R., & Tennant, D. (2010). Structural Systems Design. In *Handbook for blast resistant design of buildings*. John Wiley & Sons.

Sundolitt. (2019, September). Produktguide. https://www.sundolitt.com/globalassets/inriver/resources/sundolitt-produktguide-sept-2019.pdf

Tawil, H., Tan, C. G., Sulong, N. H. R., Nazri, F. M., Sherif, M. M., & El-Shafie, A. (2022). Mechanical and Thermal Properties of Composite Precast Concrete Sandwich Panels: A Review. *Buildings*, *12*.

Zielinski, J. A. (1982). *Fracture of Concrete and Mortar under Uniaxial Impact Tensile Loading*. Delft University of Technology.

Appendix A: Load characteristics

The appendix contains the calculation of load L1, L2 and L3. The peak pressure and scaled impulse density are calculated following the material presented by Johansson & Laine (2012a). The fictitious time duration is calculated assuming the simplified impulse curve presented in Section 2.3.3.

Calculation of load L1:

$r := 25\ \boldsymbol{m}$ — Distance

$W := 75\ \boldsymbol{kg}$ — Charge weight (TNT)

$\alpha := 2$ — Reflection factor

$W_{mod} := \alpha \cdot W = 150\ \boldsymbol{kg}$ — Reflected charge weight

$$Z := \frac{r}{W_{mod}^{\left(\frac{1}{3}\right)}} = 4.7\ \frac{\boldsymbol{m}}{\boldsymbol{kg}^{\frac{1}{3}}}$$ — Scaled distance

$P := 80\ \boldsymbol{kPa}$ — Peak pressure (Johansson & Laine, 2012a)

$$i_{scaled} := 80\ \frac{\boldsymbol{Pa \cdot s}}{\boldsymbol{kg}^{\frac{1}{3}}}$$ — Scaled impulse density

$i := i_{scaled} \cdot W_{mod}^{\left(\frac{1}{3}\right)} = 425\ \boldsymbol{Pa \cdot s}$ — Impulse density

$t_r := \frac{2 \cdot i}{P} = 10.6\ \boldsymbol{ms}$ — Fictitious time duration

Calculation of load L2:

$r := 25\ \boldsymbol{m}$ — Distance

$W := 150\ \boldsymbol{kg}$ — Charge weight (TNT)

$\alpha := 2$ — Reflection factor

$W_{mod} := \alpha \cdot W = 300\ \boldsymbol{kg}$ — Reflected charge weight

$Z := \frac{r}{W^{\left(\frac{1}{3}\right)}} = 4.7\ \frac{\boldsymbol{m}}{\boldsymbol{kg}^{\frac{1}{3}}}$ — Scaled distance

$P := 150\ \boldsymbol{kPa}$ — Peak pressure (Johansson & Laine, 2012a)

$i_{scaled} := 120\ \frac{\boldsymbol{Pa \cdot s}}{\boldsymbol{kg}^{\frac{1}{3}}}$ — Scaled impulse density

$i := i_{scaled} \cdot W_{mod}^{\left(\frac{1}{3}\right)} = 803\ \boldsymbol{Pa \cdot s}$ — Impulse density

$t_r := \frac{2 \cdot i}{P} = 10.7\ \boldsymbol{ms}$ — Fictitious time duration

Calculation of load L3:

$r := 25\ \boldsymbol{m}$ Distance

$W := 400\ \boldsymbol{kg}$ Charge weight (TNT)

$\alpha := 2$ Reflection factor

$W_{mod} := \alpha \cdot W = 800\ \boldsymbol{kg}$ Reflected charge weight

$$Z := \frac{r}{W_{mod}^{\left(\frac{1}{3}\right)}} = 2.7\ \frac{\boldsymbol{m}}{\boldsymbol{kg}^{\frac{1}{3}}}$$ Scaled distance

$P := 300\ \boldsymbol{kPa}$ Peak pressure
(Johansson & Laine, 2012a)

$$i_{scaled} := 160\ \frac{\boldsymbol{Pa \cdot s}}{\boldsymbol{kg}^{\frac{1}{3}}}$$ Scaled impulse density

$i := i_{scaled} \cdot W_{mod}^{\left(\frac{1}{3}\right)} = 1485\ \boldsymbol{Pa \cdot s}$ Impulse density

$i := 1500\ \boldsymbol{Pa \cdot s}$

$t_r := \frac{2 \cdot i}{P} = 10\ \boldsymbol{ms}$ Fictitious time duration

Appendix B: Abaqus input data

B.1 Calculations of concrete properties

Calculation of equivalent modulus of elasticity and yield stress for wall B. The same procedure applies to wall configurations A and C. Equal reinforcement amounts have been assumed for the respective wall, meaning the ultimate capacity varies. The same geometry and material data have been used as presented in Appendix C. A summary of the values for each wall and concrete layer is presented in Table 3.4.

Equivalent Modulus of Elasticity: Inner RC layer

$I_{FEM} := \frac{b \cdot {t_2}^3}{12} = (2.813 \cdot 10^8)\ mm^4$ Moment of inertia ABAQUS

$x_{II} := 22.8\ mm$ Initial guess

$x_{II} := \mathbf{root}\left({x_{II}}^2 + \frac{2 \cdot \alpha \cdot A_s}{b} \cdot (x_{II} - d), x_{II}\right)$

$x_{II} = 22.8\ mm$ Neutral axis stadium II

$I_{II} := \frac{b \cdot {x_{II}}^3}{3} + \alpha \cdot A_s \cdot (d - x_{II})^2$ Neglecting compressive reinf.

$I_{II} = (3.041 \cdot 10^7)\ mm^4$ Moment of inertia stadium II

$E_{eq} := E_{cm} \cdot \frac{I_{II}}{I_{FEM}} = 3.352\ GPa$ Equivalent Modulus of Elasticity

Yield stress: Inner RC layer

$\alpha_R := 0.81$

$\beta_R := 0.416$

$x := \frac{f_{yk} \cdot A_s}{\alpha_R \cdot f_{ck} \cdot b} = 9.7\ \boldsymbol{mm}$ Height of compressive zone

$\varepsilon_{sy} := \frac{f_{yk}}{E_s} = 0.003$ Yielding strain steel

$\varepsilon_{cu} := 3.5 \cdot 10^{-3}$ Ultimate strain concrete

$\varepsilon_s := \varepsilon_{cu} \cdot \frac{(d-x)}{x} = 0.042 \quad > \quad \varepsilon_{sy}$ Ok, yielding as assumed

$M_{Rd} := \alpha_R \cdot f_{ck} \cdot b \cdot x \cdot (d - \beta_R \cdot x) = 23.75\ \boldsymbol{kN \cdot m}$ Ultimate Moment Capacity

$W_{el} := \frac{b \cdot t_2^{\,2}}{6} = 0.004\ \boldsymbol{m^3}$ Section modulus
(3 integration points)

$W_{pl} := \frac{b \cdot t_2^{\,2}}{4} = 0.006\ \boldsymbol{m^3}$ Section modulus
(5 or more integration points)

$f_y := \frac{M_{Rd}}{W_{pl}} = 4.223\ \boldsymbol{MPa}$ Fictitious yield stress

Equivalent Modulus of Elasticity: Outer RC layer

$d := \frac{t_1}{2} = 25\ mm$ Effective depth

$I_{FEM} := \frac{b \cdot {t_1}^3}{12} = \left(1.042 \cdot 10^7\right)\ mm^4$ Moment of inertia ABAQUS

$x_{II} := 8.8\ mm$ Initial guess

$x_{II} := \mathbf{root}\left({x_{II}}^2 + \frac{2 \cdot \alpha \cdot A_s}{b} \cdot \left(x_{II} - d\right), x_{II}\right)$

$x_{II} = 8.8\ mm$ Neutral axis stadium II

$I_{II} := \frac{b \cdot {x_{II}}^3}{3} + \alpha \cdot A_s \cdot \left(d - x_{II}\right)^2$ Neglecting compressive reinf.

$I_{II} = \left(8.92 \cdot 10^5\right)\ mm^4$ Moment of inertia stadium II

$E_{eq} := E_{cm} \cdot \frac{I_{II}}{I_{FEM}} = 2.655\ GPa$ Equivalent Modulus of Elasticity

Yield stress: Outer RC layer

$M_{Rd} := \alpha_R \cdot f_{ck} \cdot b \cdot x \cdot \left(d - \beta_R \cdot x\right) = 4.1 \ \boldsymbol{kN \cdot m}$ — Ultimate Moment Capacity

$W_{el} := \frac{b \cdot t_1^{\,2}}{6} = \left(4.167 \cdot 10^{-4}\right) \ \boldsymbol{m}^3$ — Section modulus (3 integration points)

$W_{pl} := \frac{b \cdot t_1^{\,2}}{4} = \left(6.25 \cdot 10^{-4}\right) \ \boldsymbol{m}^3$ — Section modulus (5 or more integration points)

$f_y := \frac{M_{Rd}}{W_{pl}} = 6.587 \ \boldsymbol{MPa}$ — Fictitious yield stress

$q_{Rd} := M_{Rd} \cdot \frac{8}{l^2} = 4.5 \ \frac{\boldsymbol{kN}}{\boldsymbol{m}}$ — Plastic Ultimate Load

B.2 Calculations of insulation properties

The insulation's elastic stiffness and yielding force are presented for the input data used in Section 4.1.1. The same procedure applies to other choices of modulus of elasticity, lengths and yield stresses. The outermost springs (or connectors) have half the effective area, leading to half the stiffness and yielding force.

$b := 1000\ \boldsymbol{mm}$ Section width

$l_{element} := 50\ \boldsymbol{mm}$ Element length

$E := 2\ \boldsymbol{MPa}$ Modulus of Elasticity

$A := b \cdot l_{element} = \left(5 \cdot 10^4\right)\ \boldsymbol{mm}^2$ Area

$L := 200\ \boldsymbol{mm}$ Spring length / insulation thickness

$k := \frac{E \cdot A}{L} = 500000\ \frac{\boldsymbol{N}}{\boldsymbol{m}}$ Elastic spring stiffness

$f_y := 50\ \boldsymbol{kPa}$ Yield stress for insulation

$F_y := f_y \cdot A = 2500\ \boldsymbol{N}$ Yield force for insulation

$u_{el} := \frac{F_y}{k} = 5\ \boldsymbol{mm}$ Elastic displacement

Outermost (end) springs have half the stiffness & half the yielding force

Appendix C: Model verification

The appendix contains hand calculations for the model verification presented in Section 3.4.5. The calculations are made for the inner layer of wall configuration B.

$q := 15\ \frac{kN}{m}$ Static load

Geometry wall B

$l := 2.7\ m$ Span length

$t_1 := 50\ mm$ Section height (outer layer)

$t_2 := 150\ mm$ Section height (inner layer)

$b := 1000\ mm$ Section width

$t_c := 25\ mm$ Concrete cover thickness

$d := t_2 - t_c = 125\ mm$ Distance to tensile reinforcement

$d_{prim} := t_c$ Distance to compressive reinforcement

$s_r := 200\ mm$ Rebar spacing

$\phi := 10\ mm$ Rebar dimension

$A_{si} := \frac{\pi}{4} \cdot \phi^2 = 78.5\ mm^2$ Area one rebar

$A_s := \frac{b}{s_r} \cdot A_{si} = 392.7\ mm^2$ Area all rebars in layer

Material data

$f_{ck} := 25\ \boldsymbol{MPa}$ $\qquad$ $f_{yk} := 500\ \boldsymbol{MPa}$

$E_{cm} := 31\ \boldsymbol{GPa}$ $\qquad$ $E_s := 200\ \boldsymbol{GPa}$

$f_{cm} := f_{ck} + 8\ \boldsymbol{MPa} = 33\ \boldsymbol{MPa}$

$\rho_c := 2500\ \frac{\boldsymbol{kg}}{\boldsymbol{m}^3}$ $\qquad$ $\alpha := \frac{E_s}{E_{cm}} = 6.452$

Inner RC Layer

$x_{II} := 0.022\ \boldsymbol{m}$ $\qquad$ Initial guess

$x_{II} := \mathbf{root}\left({x_{II}}^2 + \frac{2 \cdot \alpha \cdot A_s}{b} \cdot \left\langle x_{II} - d \right\rangle, x_{II} \right)$ $\qquad$ Neutral axis (pure bending)

$x_{II} = 22.8\ \boldsymbol{mm}$ $\qquad$ Neutral axis stadium II

$I_{II} := \frac{b \cdot {x_{II}}^3}{3} + \alpha \cdot A_s \cdot \left\langle d - x_{II} \right\rangle^2$ $\qquad$ Neglecting compressive reinf.

$I_{II} = \left(3.041 \cdot 10^{-5}\right)\ \boldsymbol{m}^4$ $\qquad$ Moment of inertia stadium II

Static Response: Ultimate Load

$\alpha_R := 0.81$ $\qquad$ $\beta_R := 0.416$

$x := \frac{f_{yk} \cdot A_s}{\alpha_R \cdot f_{ck} \cdot b} = 9.7\ \boldsymbol{mm}$ $\qquad$ Height of compressive zone

$\varepsilon_{sy} := \frac{f_{yk}}{E_s} = 0.003$ $\qquad$ Yielding strain steel

$\varepsilon_{cu} := 3.5 \cdot 10^{-3}$ $\qquad$ Ultimate strain concrete

$\varepsilon_s := \varepsilon_{cu} \cdot \frac{(d - x)}{x} = 0.042$ $\quad > \quad$ ε_{sy} $\qquad$ Ok, yielding as assumed

$M_{Rd} := \alpha_R \cdot f_{ck} \cdot b \cdot x \cdot \left(d - \beta_R \cdot x\right) = 23.75\ \boldsymbol{kN \cdot m}$ Ultimate Moment Capacity

$q_{Rd} := M_{Rd} \cdot \frac{8}{l^2} = 26.1\ \frac{\boldsymbol{kN}}{\boldsymbol{m}}$ Plastic Ultimate Load

$q_{Rd\_FEM} := 26.5\ \frac{\boldsymbol{kN}}{\boldsymbol{m}}$ Ultimate load Abaqus

$correlation := \frac{q_{Rd}}{q_{Rd\_FEM}} = 98.4\%$

Static Response: Elastic Displacement

$EI_{II} := E_{cm} \cdot I_{II} = 0.943\ \boldsymbol{MN \cdot m^2}$

$u := \frac{5 \cdot q \cdot l^4}{384 \cdot EI_{II}} = 11\ \boldsymbol{mm}$ Elastic displacement

$u_{abaqus} := 11.1\ \boldsymbol{mm}$ Deflection Abaqus

$correlation := \frac{u}{u_{abaqus}} = 99.2\%$

Dynamic Response: Elastic Displacement

$i := 800\ \boldsymbol{Pa \cdot s}$ Impulse density

$\kappa_{mF} := 0.787$ Elastic factor

$I_k := b \cdot l \cdot i = 2160\ \boldsymbol{N \cdot s}$ Impulse

$m_c := \kappa_{mF} \cdot t_2 \cdot b \cdot l \cdot \rho_c = 797\ \boldsymbol{kg}$ Transformed elastic mass

$k_{II} := \frac{384 \cdot E_{cm} \cdot I_{II}}{5 \cdot l^3} = \left(3.7 \cdot 10^6\right)\ \frac{\boldsymbol{N}}{\boldsymbol{m}}$ Stiffness stadium II

$u_{el} := \frac{I_k}{m_c} \cdot \sqrt{\frac{m_c}{k_{II}}} = 39.9\ \boldsymbol{mm}$ Elastic displacement

$u_{abaqus} := 39.2\ \boldsymbol{mm}$ Deflection Abaqus

$correlation := \frac{u_{abaqus}}{u_{el}} = 98.3\%$

Dynamic Response: Elastic-plastic Displacement

$\kappa_{mF} := 0.667$ Plastic factor

$m_c := \kappa_{mF} \cdot t_2 \cdot b \cdot l \cdot \rho_c = 675\ \boldsymbol{kg}$ Transformed plastic mass

$R_m := \frac{8 \cdot M_{Rd}}{l} = 70.4\ \boldsymbol{kN}$ Maximum resistance

$u_{el} := \frac{R_m}{k_{II}} = 19.1\ \boldsymbol{mm}$ Elastic displacement

$u_{tot} := \frac{{I_k}^2}{2 \cdot m_c \cdot R_m} + \frac{u_{el}}{2} = 58.6\ \boldsymbol{mm}$ Total displacement

$u_{abaqus} := 57.0\ \boldsymbol{mm}$ Deflection Abaqus

$correlation := \frac{u_{abaqus}}{u_{tot}} = 97.2\%$

Appendix D: Plastic rotational capacity

Calculations according to Eurocode 2:

$l := 2.7\ m$ Wall length

$x := 9.7\ mm$ Height of compressive zone

$d := 125\ mm$ Effective depth (wall B)

$\frac{x}{d} = 0.08$

$l_0 := \frac{l}{2}$ Distance between the point where the moment is zero and plastic hinge

$\lambda := \frac{l_0}{d} = 10.8$

$k_\lambda := \sqrt{\frac{\lambda}{3}} = 1.897$

$\theta_{pl\_B} := 11 \cdot 10^{-3}$ B500B (rad)

$\theta_{pl\_B\_allowed} := k_\lambda \cdot \theta_{pl\_B} = 0.021$ rad

$\theta_{pl\_C} := 33 \cdot 10^{-3}$ B500C (rad)

$\theta_{pl\_C\_allowed} := k_\lambda \cdot \theta_{pl\_C} = 0.063$ rad

Allowed deformation in field:

$u_{rd} := \frac{\theta_{pl\_B\_allowed} \cdot l}{2} = 28.2\ mm$ B500B

$u_{rd} := \frac{\theta_{pl\_C\_allowed} \cdot l}{2} = 84.5\ mm$ B500C

Appendix E: Matlab Code

This appendix contains all Matlab code, including the SDOF and MDOF models.

Matlab variable description

The following vectors/matrices are used in the Matlab script. Vectors are used in the SDOF (containing one column), while matrices are introduced for the MDOF (containing two columns). Vectors and matrices that are not commented follow the same structure as matrix u.

$u(:, 1 \text{ or } 2)$ Matrix containing displacements. The first column describes the outer layer while the second column describes the inner layer. The matrix has the same number of rows as time steps in the analysis.

$a(:, 1 \text{ or } 2)$ Matrix containing accelerations. Same structure as $u(:, 1 \text{ or } 2)$.

$v(:, 1 \text{ or } 2)$ Matrix containing velocities. Same structure as $u(:, 1 \text{ or } 2)$.

$R(:, 1 \text{ or } 2)$ Response functions of springs. The first column describes the response of the inner layer while the second column describes the response of the insulation.

$k(1, 1 \text{ or } 2)$ Secant stiffness. Same structure as $R(:, 1 \text{ or } 2)$.

E.1 SDOF

```
clc
clear
clf

time_span=100;          % Analysis duration [ms]

%----------------Load characteristics-------------------------------------

P_rp=150*10^3;          % Peak pressure [Pa]
i_rp=800;               % Impulse density [Pas]

%----------------Section Geometry-----------------------------------------

t1=0.05;                % Outer layer thickness     [m]
t2=0.15;                % Inner layer thickness     [m]
```

```
t_ins=0.20;             % Insulation thickness      [m]
t_c=0.025;              % Re-bar cover thickness    [m]
b=1;                    % Segment width             [m]
phi=10/1000;            % Rebar dimension           [m]
s=0.2;                  % Rebar spacing             [m]
l=2.7;                  % Wall length               [m]
d=t2-t_c;               % Top surface to re-bar     [m]

%k_mF=0.787;            % Transformation factor elastic
k_mF=0.667;             % Transformation factor plastic

%----------------Material properties---------------------------------------

% Concrete material properties

E_c=31*10^9;                % Concrete modulus of elasticity     [Pa]
f_ck=25*10^6;               % Concrete compressive strength      [Pa]
rho=2500;                   % Doncrete density                   [kg/m^3]
eps_cu=3.5*10^-3;           % Concrete ultimate strain           [-]

% Steel material properties
E_s=200*10^9;               % Steel modulus of elasticity        [Pa]
f_yk=500*10^6;              % Steel compressive strength         [Pa]

% Ratio of MOE:S
alpha=E_s/E_c;
alpha_R=0.810;
Beta_R=0.416;

%----------------Calculating properties------------------------------------

A_si=phi^2*pi/4;                % Area/rebar                 [m^2]
A_s=b/s*A_si;                   % Reinforcement/layer        [m^2]

% Second moment of area stage II
fun=@(x) x^2+(2*alpha*A_s)*(x-d)/b;
x_II=fzero(fun,0.025)                       % Neutral Axis StageII
I_II=(b*x_II^3)/3+alpha*A_s*(d-x_II)^2;     % Moment of inertia StageII

% Stiffness and capacity of cross section
x=f_yk*A_s/(alpha_R*f_ck*b)                 % Neutral axis maximum capacity
eps_sy=f_yk/E_s;
eps_s=eps_cu*(d-x)/x;
if(eps_s<eps_sy)
    disp('not ok')
end
```

```
M_Rd=f_yk*A_s*(d-Beta_R*x);                % Bending resistance of CS
R_m=8*M_Rd/l;                              % Maximum resisting force
k_el=384*E_c*I_II/(5*l^3);                 % Stiffness w.r.t. mid point
u_el=R_m/k_el;                             % Elastic limit

m_b=rho*b*(t1+t2)*l;                       % Total mass of layer
m=m_b*k_mF;                                % Translated mass of layer

%----------------Applied impulse load-------------------------------------

t_1=2*i_rp/P_rp;                           % Load duration
f_1=b*l*P_rp;                              % Peak load
I_1=b*l*i_rp;                              % Impulse

% Time steps and load vector
dt=t_1/100;                                % Time step
t_end=time_span/1000;                      % End time
x_axis=[0:dt:t_end]';

% Creating load vector. from f to 0 at t=0 to t=t_1
f=zeros(length(x_axis),1);

for i=1:length(x_axis)                     % Assigning load to load vector
    if x_axis(i)<t_1
        f(i)= f_1*(t_1-x_axis(i))/t_1;
    else
        f(i)=0;
    end
end

%----------------Creating vectors for analysis----------------------------
u=zeros(size(f));               % Displacement vector for each time step
v=zeros(size(f));               % Velocity vector for each time step
a=zeros(size(f));               % Acceleration vector for each time step
u_max=zeros(length(f),1);       % Max displacement for each time step
du_pl=zeros(length(f),1);       % Plastic increase for each time step
u_pl_tot=zeros(length(f),1);    % Total plastic displacemtn each time step

%----------------Newmark itterations method-------------------------------

M=m;                            % Mass matrix
V=0;                            % No damping
k=k_el;                         % Initial stiffness

% Initial conditions:
```

```
u_0=0;     u(1)=u_0;
v_0=0;     v(1)=v_0;
a_0=M\f(1);  a(1,:)=a_0;
gam=1/2;
B=1/4;

for i=2:length(x_axis)              % Solving for u,v,a for each time step

    K=k;                            % Updating stiffness
    M_bar=M+gam*dt*V+B*dt^2*K;      % Updating M_bar-matrix

    % Using Newmark equations.
    a(i)=(M_bar\(f(i)'-V*(v(i-1)'+(1-gam)*dt*a(i-1)')-K*(u(i-1)'+...
        dt*v(i-1)'+(1/2-B)*dt^2*a(i-1)')))';
    u(i)=(u(i-1)'+dt*v(i-1)'+(1/2-B)*dt^2*a(i-1)'+B*dt^2*a(i)')';
    v(i)=(v(i-1)'+(1-gam)*dt*a(i-1)'+gam*dt*a(i)')';

    % Comparing max displacement to elastic limit to determine if the
    % deflections are in the plastic range.

    u_max(i)=max(u(1:i));   % Maximum displacement up to current time step
        if (u(i)>u_el && u(i)>u_max(i-1))
                du_pl(i)=u(i)-max(u_el,u_max(i-1));    % Plastic increase
        else
                du_pl(i)=0;
        end
        u_pl_tot(i)=sum(du_pl(1:i));          % Current plastic deformation
        R=k_el*(u(:)-u_pl_tot);               % Update response function

        if R(i)>R_m
            R(i)=R_m;           % Maximum resisting force reached
        end
        k=R(i)/u(i);            % Secant stiffness used in next iteration
end
```

E.2 MDOF

```
clc
clear
clf

time_span=100;          % Analysis duration [ms]

%----------------Load characteristics-------------------------------------

P_rp=150*10^3;           % Peak pressure [Pa]
i_rp=800;                % Impulse density [Pas]

%----------------Section Geometry-----------------------------------------

t1=0.05;                % Outer layer thickness     [m]
t2=0.15;                % Inner layer thickness     [m]
t_c=0.025;              % Re-bar cover thickness    [m]
b=1;                    % Segment width             [m]
phi=10/1000;            % Rebar dimension           [m]
s=0.2;                  % Rebar spacing             [m]
l=2.7;                  % Wall length               [m]
d=t2-t_c;               % Top surface to re-bar     [m]
d_ins=0.2;              % Insulation thickness      [m]

%k_mF=0.787;            % Transformation factor elstic
k_mF=0.667;             % Transformation factor plastic
%----------------Material properties--------------------------------------

% Concrete material properties
E_c=31*10^9;            % Concrete modulus of elasticity     [Pa]
f_ck=25*10^6;           % Concrete compressive strength      [Pa]
rho=2500;               % Doncrete density                   [kg/m^3]
eps_cu=3.5*10^-3;       % concrete ultimate strain           [-]

% Steel material properties
E_s=200*10^9;           % Steel modulus of elasticity        [Pa]
f_yk=500*10^6;          % Steel compressive strength         [Pa]
% Insulation material properties
E_ins=  2*10^6;           % Insulation modulus of elasticity      [Pa]
f_yins= 50*10^3;          % Insulation compressive strength       [Pa]
C_ins=  0;                % Insulation damping

% Rati0 of MOE:S
alpha=E_s/E_c;
```

```
alpha_R=0.810;
Beta_R=0.416;

%----------------Calculating properties-----------------------------------

A_ins=l*b;                      % Insulation area
A_si=phi^2*pi/4;                % Area/rebar                  [m^2]
A_s=b/s*A_si;                   % Reinforcement/layer         [m^2]

% Second moment of area stage II for inner layer

fun=@(x) x^2+(2*alpha*A_s)*(x-d)/b;
x_II=fzero(fun,0.025)                       % Neutral Axis StageII
I_II=(b*x_II^3)/3+alpha*A_s*(d-x_II)^2;     % Moment of inertia StageII

% Stiffness and capacity of cross section
x=f_yk*A_s/(alpha_R*f_ck*b);                % Neutral axis maximum capacity
eps_sy=f_yk/E_s;
eps_s=eps_cu*(d-x)/x;

if(eps_s<eps_sy)
    disp('not ok')
end
% Elastic stiffness and maximum resisting forces, Concrete
M_Rd=f_yk*A_s*(d-Beta_R*x);                 % Bending resistance of CS
R_m=8*M_Rd/l;                               % Maximum resisting force
k_el=384*E_c*I_II/(5*l^3);                  % Stiffness v.r.t mid point
u_el=R_m/k_el;                              % Elastic limit

% Elastic stiffness and maximum resisting forces, Insulation
k_el_ins=E_ins*A_ins/d_ins;                 % Elastic stiffness
R_m_ins=f_yins*A_ins;                       % Maximum resisting force
u_el_ins=R_m_ins/k_el_ins;

% Mass of each layer
m_b1=rho*b*(t1)*l;                          % Total mass of outer layer
m_b2=rho*b*(t2)*l;                          % Total mass of inner layer
m1=m_b1*k_mF;                               % Applying factor
m2=m_b2*k_mF;                               % Applying factor

%----------------Applied impulse load-------------------------------------
t_1=2*i_rp/P_rp;                            % Load duration
f_1=b*l*P_rp;                               % Peak load
I_1=b*l*i_rp;                               % Impulse
```

```
% Step 12. Creating apporpriate time steps.
dt=t_1/1000;                    % Time step
t_end=time_span/1000;           % End time
n=t_end/dt;
x_axis=[0:dt:t_end]';

% Creating load vector. from F_1 to 0 at t=0 to t=t_1
F1=zeros(length(x_axis),1);

for i=1:length(x_axis)        % Assigning load to load vector
    if x_axis(i)<t_1
        F1(i)= f_1*(t_1-x_axis(i))/t_1;
    else
        F1(i)=0;
    end
end

%----------------Creating vectors for analysis-----------------------------

u=zeros(length(x_axis),2);      % Displacement vector for each time step
v=zeros(size(u));               % Velocity vector for each time step
a=zeros(size(u));               % Acceleration vector for each time step
R=zeros(size(u));               % Response function
u_max=zeros(size(u));           % Max displacement for each time step
du_pl=zeros(size(u));           % Plastic increase for each time step
u_pl_tot=zeros(size(u));        % Total plastic displacement each time step
impact=1;
%----------------Newmark itterations method--------------------------------
% Assembly of initial K-matrix
K_ins=k_el_ins* [1 -1;-1 1];
K_l2=k_el*[0 0;0 1];
K=K_ins+K_l2;
% Assembly of M-matrix
M_l1=m1*[1 0;0 0];
M_l2=m2*[0 0;0 1];
M=M_l1+M_l2;

V=C_ins*[1 0;0 1];              % No damping

% Assembly of load vector;
F2=zeros(length(F1),1);         % No external force on inner layer
f=[F1 F2];                      % Load vectors.

% Initial condicitons:
u_0=[0 0]';     u(1,:)=u_0;
v_0=[0 0]';     v(1,:)=v_0;
```

```
a_0=M\f(1,:)';  a(1,:)=a_0;

gam=1/2;
B=1/4;

k=[k_el k_el_ins];       % Initail stiffnesses of inner layer and insulation

for i=2:length(x_axis)

    K_l2=k(1)*[0 0; 0 1];               % Update stiffness of inner layer
    K_ins=k(2)*[1 -1;-1 1];             % Update stiffness of Insulation layer
    K=K_ins+K_l2;

    M_bar=M+gam*dt*V+B*dt^2*K;          % Updating M_bar-matrix

    % Using Newmark equations
    a(i,:)=(M_bar\(f(i,:)'-V*(v(i-1,:)'+...
        (1-gam)*dt*a(i-1,:)')-K*(u(i-1,:)'+dt*v(i-1,:)'+...
        (1/2-B)*dt^2*a(i-1,:)')))';
    u(i,:)=(u(i-1,:)'+dt*v(i-1,:)'+(1/2-B)*dt^2*a(i-1,:)'+B*dt^2*a(i,:)')';
    v(i,:)=(v(i-1,:)'+(1-gam)*dt*a(i-1,:)'+gam*dt*a(i,:)')';

    % Comparing max displacement to elastic limit to deremine if the
    % Deflection is in the plastic range.

        % Plasticity of inner concrete layer
        u_max(i,1)=max(u(1:i,2));
        if (abs(u(i,2))>u_el && u(i,2)>u_max(i-1,1))
                du_pl(i,1)=u(i,2)-max(u_el,u_max(i-1,1));
        else
                du_pl(i,1)=0;
        end
        u_pl_tot(i,1)=sum(du_pl(1:i,1))% Update current plastic displacement
        R(:,1)=k_el*(u(:,2)-u_pl_tot(:,1));
        if R(i,1)>R_m                  % Does the response exceed the limit
            R(i,1)=R_m;
        end
        k(1)=R(i,1)/u(i,2);             % Update secant stiffness


        % Plasticity of insulation layer
        u_max(i,2)=max(u(1:i,1)-u(1:i,2));  % Maxium displacement difference
        if ((u(i,1)-u(i,2))>u_el_ins && (u(i,1)-u(i,2))>u_max(i-1,2))
                du_pl(i,2)=(u(i,1)-u(i,2))-max(u_el_ins,u_max(i-1,2));
        else
                du_pl(i,2)=0;
```

```
        end
        u_pl_tot(i,2)=sum(du_pl(1:i,2));     % Current plastic displacement
        R(:,2)=k_el_ins*((u(:,1)-u(:,2))-u_pl_tot(:,2));
        if R(i,2)>R_m_ins
            R(i,2)=R_m_ins;
        end

    if(u(i,1)-u(i,2)> d_ins*0.8 && impact==1)
        v(i,2)=(v(i,2)*m2+v(i,1)*m1)/(m2+m1);% Velocity after impact
        v(i,1)=v(i,2);
        impact=0
    else
       k(2)=R(i,2)/(u(i,1)-u(i,2));          % Update secant stiffness
    end

end
```